Factorization of double parton scattering: The double Drell-Yan process

DISSERTATION
ZUR ERLANGUNG DES DOKTORGRADS
DER NATURWISSENSCHAFTEN (DR. RER. NAT.)
DER FAKULTÄT FÜR PHYSIK

DER UNIVERSITÄT REGENSBURG

vorgelegt von

Daniel Ostermeier

aus

Rotthalmünster

im Jahr 2016

Promotionsgesuch eingereicht am:	27.11.2015
Die Arbeit wurde angeleitet von:	Prof. Dr. Andreas Schäfer
Prüfungsausschuss:	
Vorsitzender:	Prof. Dr. K. Rincke
1. Gutachter:	Prof. Dr. A. Schäfer
2. Gutachter:	Dr. M. Diehl
weiterer Prüfer:	Prof. Dr. F. Evers
Termin Promotionskolloquium:	25.04.2016

Abstract

With the center of mass energy of particle colliders becoming higher and higher multiparton interactions (MPIs) become ever more import and are highly relevant for the LHC. The basis for reliably describing these events based on first principles is built by extending the QCD factorization formalism to multiparton interactions. One of the most important tasks is to show that contributions due to exchange of Glauber gluons cancel in the sum over all diagrams. In this work we make a contribution to this effort by proving cancellation of Glauber gluon exchange at the one gluon exchange level for the double Drell-Yan process. In doing so, we also review some of the progress made in establishing factorization for MPIs in the last years and indicate how this proof can be extended to all orders in perturbation theory.

Contents

To my parents
Waltraud and Albert Ostermeier
with gratitude

1. Introduction

With the discovery of the Higgs boson [1, 2], the LHC has provided the last missing piece for eventually verifying the Standard Model. In spite of this great success, the expectations of the physics community were disappointed, because there is still no distinct signal from physics beyond the Standard Model (BSM). Although ATLAS and CMS both might have found first signs of such physics, which they announced in their talks given at CERN on the 15th of December 2015, these signals at around 750 GeV are still very preliminary and could easily be mere statistical fluctuations. BSM physics has to exist, and with run 2 having started at the LHC after its energy upgrade such signals might be discovered soon. At the same time it becomes clearer and clearer that these signals will be rather subtle and that a detailed understanding of the Standard Model background will be indispensable in order to isolate the signals for new physics.

One of the key techniques needed to reliably calculate the QCD background are the so-called QCD factorization theorems, which greatly enhance the predictive power of perturbative QCD (pQCD) [3]. Within the framework of hard scattering factorization, cross sections are calculated as a convolution of parton distribution functions, hard scattering cross sections at the parton level and, in the case of transverse momentum dependent (TMD) factorization, soft factors. There has been lots of effort to prove these factorization theorems to all orders in the strong coupling in pQCD, see e.g. [3, 4, 5]. Some of the approximations used in these studies to arrive at the factorized form of the cross sections are not valid for soft gluon exchange when the gluon momentum is in the so-called Glauber region. Therefore, to validate these proofs it is essential to show that the effects of these Glauber gluon exchanges cancel in the sum over all possible diagrams.

The standard factorization formalism of pQCD is only valid for one hard interaction per hadron-hadron collision. However, with increasing energy the Bjorken x values of partons contributing to reactions with some given $\hat{s} = x_1 x_2 s$ decrease and as the PDFs grow rapidly for small x multiple hard interactions become ever more important. At Tevatron they reached already sizeable levels for specific reactions like outgoing (3 jets + γ) or (4 jets), see [6], and for the LHC they are nearly omnipresent, see e.g. [7, 8]. Basically, while multiparton interactions (MPIs) are power suppressed for total cross sections, this is not the case for differential ones, see [9].

Many discovery channels for BSM physics require multiple hard particles in the final state, so they fall in the group of processes especially prone to MPI backgrounds. Obviously theory is called to arms to describe these events reliably, such that pure QCD backgrounds can be subtracted with only small systematic errors. This requires, however, a far reaching extension of present day techniques, and substantial progress has already been made [9, 10, 11].

As we are interested in differential cross sections, in particular as functions of transverse momenta, one has to develop a multiparton version of TMDs, which by themselves are still faced with open factorization issues. Already for single hard scattering factorization might get broken if hadronic initial and final state interactions occure, like in $p+p \to 2$ jets$+X$ [12]. Thus, there is presently absolutely no guarantee that MPIs can be brought under complete theoretical control with all implications this has for the discovery potential of the LHC.

Not to be faced with all of these complications at once, we study in this contribution only the double Drell-Yan process, which is the theoretically cleanest case and does not have any hadronic final state interactions. This process is under complete control in the single scattering case and allows for a generalization to multiparton scattering, serving as a testing ground for developing the theory of multiparton interactions.

As already mentioned, one of the most crucial steps in establishing factorization is to show that contributions due to the exchange of Glauber gluons cancels. In this work, we study the exchange of Glauber gluons in the double Drell-Yan process at the one gluon exchange level. Our conlusion is that there is no contribution from the Glauber region. We will review some of the progress made in establishing factorization for MPIs [9, 11, 13] on the way.

This work is organized as follows: In chapters 2 and 3 we will give a brief account of the basic concepts of QCD and the hard scattering factorization framework. In chapter 4 we review how the concept of TMDs can be generalized to double parton scattering, how the factorized form of the cross section of double Drell-Yan can be derived at tree level and what the current state of the art of implementing MPIs into the analysis of experimental data is [9]. In the case of perturbatively large transverse momenta, one can calculate splitting contributions to the dTMDs, which we will do in chapter 5. As we will see, these splitting contributions have important consequences for the theory of multiparton interactions, as they lead to conceptual issues regarding the consistent separation of single and double parton scattering. A review of the steps needed to establish factorization of double Drell-Yan beyond leading order is given in chapter 6. In chapter 7 we will then prove the cancellation of Glauber gluon exchange in double Drell-Yan at the one gluon exchange level for two particular toy models and also in general. We then give some example calculations of $\mathcal{O}(\alpha_S)$ corrections to dTMDs and the hard scattering part in chapter 8. Finally, we will give the main ideas behind the proof of cancellation of Glauber gluon exchange in the double Drell-Yan process to all orders in chapter 9 [13]. We conclude in chapter 10.

2. Quantum Chromodynamics

The known microscopic interactions can be classified into electromagnetic, weak, strong and gravitational. Quantum Chromodynamics (QCD) is a relativistic, non Abelian quantum field theory that describes the strong interaction. In QCD there are two types of fundamental fields, namely the fermionic quark fields and the bosonic gluon field. Unlike in the quantum field theory of the electromagnetic interaction, Quantum Electrodynamics (QED), where the fundamental fields correspond to actually observable particles (e.g. electrons and photons), one cannot observe isolated single particles states of quarks or gluons. Instead they always form composite particles, the so-called hadrons, with the quarks being the basic constituents and the gluons transmitting the strong force, binding them together.

An important property of QCD is that while the coupling is strong at typical hadronic scales ($\sim 10^{-15}$m), it goes to zero for vanishing distances. This property is called asymptotic freedom and has some important consequences: While one can employ small coupling perturbation theory familiar from QED for small distances, this is not the case for hadronic ones. That means that the bound states of QCD are intrinsically non-perturbative. Thus one cannot make predictions from first principles based on perturbation theory alone, but rather has to employ additional techniques like lattice QCD.

QCD gives rise to an overwhelming amount of phenomena, and we will give a short overview of its formulation and its most important properties in the following. The contents of the next sections can be found in any standard textbook or lecture on QCD and quantum field theories, see e.g. [5, 14, 15, 16].

2.1. The QCD Lagrangian

In spite of the rich phenomenology QCD provides, the Lagrangian describing the whole theory can be written down in only two lines, and in the gauge $\partial_\mu A^{a,\mu} = 0$ it reads

$$\begin{aligned}\mathcal{L}_{\mathrm{QCD}} = &\sum_f \bar{\psi}_f(x)\left(i\not{D} - m_f\right)\psi_f(x) - \frac{1}{4}G^a_{\mu\nu}G^{a,\mu\nu} \\ &- \frac{c}{2}\left(\partial_\mu A^{a,\mu}\right)\left(\partial_\nu A^{a,\nu}\right) - \bar{\xi}^a(x)\partial_\mu\partial^\mu\xi^a(x) + g f^{abc}\bar{\xi}^a(x)\partial^\mu\left(A^c_\mu(x)\xi^b(x)\right) \ . \end{aligned} \tag{2.1}$$

The first term of the Lagrangian in eq. (2.1) is the fermionic part, where the sum over f indicates the sum over the six known quark flavors of the Dirac spinors ψ_f (up, down, charm, strange, top, bottom). $D_\mu = (\partial_\mu + igt^a A^a_\mu)$ is the covariant derivative, with t^a ($a = 1, \ldots, 8$) being the generators of the SU(3) color group. They are related to the Gell-Mann matrices λ^a by $t^a = \lambda^a/2$. As is well known, the generators of SU(3) do not commute, which makes

QCD a non Abelian theory. They obey the relation

$$[t^a, t^b] = if^{abc}t^c \ . \tag{2.2}$$

Note that we have omitted the color indices $i, j = 1, \ldots, 3$ on the quark fields as well as on the covariant derivative and summing over color indices is tacitly assumed. Some important identities for the groups SU(N) that will be relevant for the calculations in this work are given in appendix B. The second term in (2.1) is the gluonic part, where the gluon field strength tensor $G^a_{\mu\nu}$ is given by

$$G^a_{\mu\nu} = \partial_\mu A^a_\nu - \partial_\nu A^a_\mu - gf^{abc}A^b_\mu A^c_\nu \ . \tag{2.3}$$

The last term in eq. (2.3) emerges due to the SU(3) group being non Abelian and it leads to three gluon and four gluon vertices, which have no counterpart in QED. It is these additional terms that add some more complications to the quantization of QCD. In particular, the three gluon vertex breaks gauge invariance if not accounted for correctly.

The terms in the second line of (2.1) are the so-called gauge fixing and gauge compensating terms, and they appear due to the following reason: In the path integral formulation of QCD, Green functions (vacuum expectation values of time ordered products of fields) are given by a functional integral

$$\langle 0|\mathrm{T}f[A, \psi, \bar{\psi}]|0\rangle = \mathcal{N}\int \mathcal{D}A\mathcal{D}\psi\mathcal{D}\bar{\psi}\, e^{iS[A,\psi,\bar{\psi}]} f[A, \psi, \bar{\psi}] \ . \tag{2.4}$$

On the l.h.s. the fields are the quantum fields of QCD while on the r.h.s. the fields are the corresponding classical fields, where ψ and $\bar{\psi}$ are Grassmann-valued. The problem with this formulation is that the path integral sums over all possible solutions related by gauge symmetry instead of selecting one of them. In order to solve this overcounting problem and to be able to use the same methods to derive e.g. Green functions from the path integral formulation as in QED, one has to add a gauge fixing term to the Lagrangian and introduce so-called Fadeev-Popov ghost fields ξ^a, which are unphysical scalar fields that obey the Fermi statistics and are constructed such that they always cancel the unwanted terms corresponding to contributions from unphysical gluon polarizations. These additional terms are given in the second line of (2.1). The Feynman rules of QCD, which are needed for perturbative calculations, can then be derived from the Lagrangian (2.1) and they are given in appendix A.

Note that after the Fadeev-Popov method has been used for gauge fixing, the Lagrangian (2.1) is not gauge invariant, i.e. it is not invariant under the following simultaneous local SU(3) transformations:

$$\begin{aligned} \psi_{i,f}(x) &\Rightarrow [e^{-ig\omega^a(x)t^a}]_{ij}\psi_{j,f}(x)\,, \\ A^a_\mu(x)t^a &\Rightarrow \frac{-i}{g}e^{-ig\omega^b(x)t^b}D_\mu e^{ig\omega^c(x)t^c} \ . \end{aligned} \tag{2.5}$$

This makes the derivation and formulation of generalized Ward identities, which are needed for the derivation of factorization theorems, much more complicated. The corresponding identities for non Abelian gauge theories are called Slavnov-Taylor identities [17, 18]. The La-

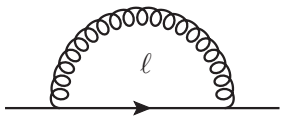

Figure 2.1.: Quark self energy graph.

grangian (2.1) possesses a different symmetry, namely the so-called BRST symmetry [19, 20]. Regarding the quark and gluon fields, the BRST transformations are just gauge transformations as given in eq. (2.5), and therefore any given gauge invariant operator is also BRST invariant.

2.2. Regularization and renormalization

Just like in QED, ultra-violet (UV) divergences appear when calculating diagrams that contain loops. A simple example is given by the quark self energy diagram depicted in figure 2.1. Calculating this graph, one sees that it is divergent due to contributions from large loop momenta ℓ, i.e. from regions where the two interaction vertices are very close to each other. These divergences appear due to the fact that QCD does not remain valid up to arbitrary energies, but rather has to be seen as an effective theory which is only valid in an energy regime far away from the Planck scale ($\sim 10^{19}$GeV). There, the gravitational interaction and the strong interaction are of comparable strength and thus the assumptions made to construct the quantum field theory formulation of QCD (flat Minkowski space and simple Lorentz transformations) are no longer valid.
Gauge theories like QED and QCD have the crucial property that they are renormalizable, i.e. the occuring UV divergences are at most logarithmic and the theory decouples from the physics at the Planck scale. This can be seen from the observation, that in QCD calculations the logarithmic divergences in the ultraviolet scale Λ_{UV} always appear together with physical quantities of much lower scale $\Lambda_i \ll \Lambda_{\mathrm{UV}}$. The potentially divergent part of the difference in the measurement of this physical quantitiy at two different scales is then given by

$$\log \frac{\Lambda_i^2}{\Lambda_{\mathrm{UV}}^2} - \log \frac{\Lambda_j^2}{\Lambda_{\mathrm{UV}}^2} = \log \frac{\Lambda_i^2}{\Lambda_j^2}\,, \tag{2.6}$$

where the divergence has cancelled between the two terms. Generally speaking, in renormalizable theories like QCD the divergences can be removed by the following procedure:

Regularization of the theory: As a first step, one has to introduce a regulator that renders the theory finite. This can e.g. be done by imposing a cutoff on the loop momenta, but this kind of regularization breaks Lorentz invariance and is rather unsuitable for most calculations. The most convenient way of regularizing QCD for the purpose of perturbative calculations is the so-called dimensional regularization. Given that the renormalizability of QCD is already proven, one introduces an operation called "d-dimensional integration" with the following properties:

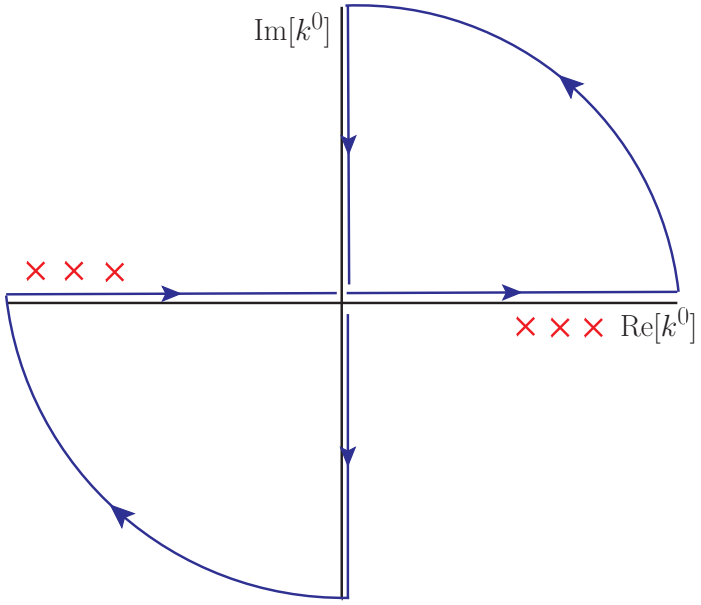

Figure 2.2.: Wick rotation of the integration contour in eq. (2.10). When all external momenta are spacelike, the poles in Green functions lie in the 2nd and 4th quadrant and the Wick rotation can be performed.

1. Linearity

$$\int \mathrm{d}^d k_E \left[a f(k_E) + b g(k_E) \right] = a \int \mathrm{d}^d k_E f(k_E) + b \int \mathrm{d}^d k_E g(k_E) \tag{2.7}$$

2. Translation invariance

$$\int \mathrm{d}^d k_E f(k_E + p_E) = \int \mathrm{d}^d k_E f(k_E) \quad \text{for arbitrary finite } p_E \tag{2.8}$$

3. Scaling law

$$\int \mathrm{d}^d k_E f(\lambda k_E) = \lambda^{-d} \int \mathrm{d}^d k_E f(k_E) \quad \text{for } \lambda \in \mathbb{R} \tag{2.9}$$

4. For all integrands that give at most a logarithmic divergence, the d-dimensional integration reproduces the result of the Riemann integral in the limit $d \to 4$.

Note that all the properties listed above are for Euclidian vectors with $k_E^2 = k_1^2 + \ldots + k_d^2$. The usual Lorentz-invariant square of a 4-vector can be related to this via a so-called Wick rotation, which is depicted in figure 2.2. For integrals that are at most logarithmically divergent, the contribution of the arcs vanishes and one can replace

$$\int_{-\infty}^{\infty} \mathrm{d}k^0 \ldots = - \int_{i\infty}^{-i\infty} \mathrm{d}k^0 \ldots = \int_{-\infty}^{\infty} \mathrm{d}k^4 \ldots \,, \tag{2.10}$$

which implies $k^0 \to ik^4$ and $k^2 \to -k_E^2$. In general, such a rotation is only possible for suitable external momenta. One can show that all poles (the red crosses in figure 2.2) of the integrand are in the 2nd and 4th quadrant and thus the Wick rotation can be performed for the case where all external momenta are spacelike. The resulting integral can then conveniently be performed using the master formula

$$\int \mathrm{d}^d k_E \frac{(k_E^2)^\alpha}{(k_E^2+M^2)^\beta} = \pi^{d/2}(M^2)^{\alpha-\beta+d/2}\frac{\Gamma(\alpha+d/2)\Gamma(\beta-\alpha-d/2)}{\Gamma(d/2)\Gamma(\beta)} \,. \tag{2.11}$$

Note that the corresponding results for external momenta which are not all spacelike are then uniquely defined by analytic continuation. When going from 4 to $d = 4 - 2\varepsilon$ dimensions, one introduces an (arbitrary) additional parameter μ and replaces the coupling g by $g\mu^\varepsilon$. This new parameter is often called renormalization scale. An important property of the d-dimensional integration is that all power divergent intergals, i.e. integrals that diverge stronger than logarithmically, vanish. One can therefore use dimensional regularization only for theories for which such divergences are already known to be absent, as for QCD.

Redefinition of theory parameters: A crucial point is to realize that the parameters (the coupling, the masses of the fields and the field normalizations) appearing in the Lagrangian (2.1) do not correspond to measurable, physical quantities and we will refer to them as "bare" parameters indicated by a subscript "(0)" in the following. We can use the freedom to redefine the field normalization in the Lagrangian (2.1) as

$$\psi_{(0),f} = Z_2^{1/2}\psi_f \,, \quad A^\mu_{(0)} = Z_3^{1/2}A^\mu \quad \xi_{(0)} = \tilde{Z}^{1/2}\xi \,, \tag{2.12}$$

where Z_2, Z_3 and $\tilde{Z}$ are the wave function renormalization factors for the quark fields, the gluon fields and the ghost fields, respectively. One can then absorb the dependence on the ultra-violet cutoff into the bare parameters and the wave function renormalization such that the bare parameters are functions of the physical parameters and the cutoff. In order to obtain finite Green functions (only the Green functions of renormalized fields have to be finite), appropriate counterterms have to be added to the Lagrangian. These counterterms are designed such that they exactly cancel the appearing UV divergences in one-particle-irreducible graphs like in figure 2.1. As the requirement that the divergent parts cancel does only determine the divergent but not the finite part of the counterterms, there is still some freedom of choice. Rules for determining the finite part are called renormalization prescriptions. For calculations in perturbative QCD in many cases the modified minimal subtraction ($\overline{\mathrm{MS}}$) scheme is used, where one essentially subtracts the term proportional to [5, 21]

$$\frac{1}{\varepsilon}S_\varepsilon = \frac{1}{\varepsilon}\frac{(4\pi)^\varepsilon}{\Gamma(1-\varepsilon)} = \frac{1}{\varepsilon} + \log(4\pi) - \gamma_E + \mathcal{O}(\varepsilon) \,. \tag{2.13}$$

The physical limit: Now that the UV divergences have canceled, one can take the limit $\varepsilon \to 0$. Note that in doing so, the bare parameters become singular such that the physical parameters remain finite, though with a dependence on the renormalization scale μ.

2.3. Running coupling, asymptotic freedom and confinement

An important property of quantum field theories like QED and QCD is that the physical parameters, in particular the coupling "constants" e and g, are not constant but rather depend on the scale at which they are measured. In QCD, this leads to the two famous effects called asymptotic freedom and confinement.
This so-called running of the coupling can be obtained in next-to-leading order by calculating all one loop corrections to the quark-gluon vertex. When the quarks are taken to be massless, the result for the sum over all diagrams is

$$g = g_{(0)} \left[1 + \frac{g_{(0)}^2}{16\pi^2} \left(\frac{1}{\varepsilon} + \log \frac{\mu^2}{-k^2} \right) \left(\frac{11}{6} N - \frac{1}{3} N_f \right) \right] , \tag{2.14}$$

where k is the momentum of the gluon, N is the number of colors and N_f is the number of quark flavors with mass squared much smaller than $-k^2$. Using that the difference between the bare coupling and the renormalized coupling is of order $g_{(0)}^3$, one obtains the following differential equation for g:

$$\frac{\mathrm{d}g(k^2)}{\mathrm{d}\log(-k^2)} = -\frac{g^2}{16\pi^2} \left(\frac{11}{6} N - \frac{1}{3} N_f \right) + \mathcal{O}(g^5) . \tag{2.15}$$

This differential equation is solved by

$$g(k^2) = \frac{g(\tilde{\mu}^2)}{1 + \frac{g(\tilde{\mu}^2)}{16\pi^2} \left(\frac{11}{3} N - \frac{2}{3} N_f \right) \log \left(\frac{-k^2}{\tilde{\mu}^2} \right)} , \tag{2.16}$$

where $\tilde{\mu}^2$ and $g(\tilde{\mu}^2)$ are integration constants. Using the condition

$$\frac{g(\tilde{\mu}^2)}{16\pi^2} \left(\frac{11}{3} N - \frac{2}{3} N_f \right) \log \left(\frac{\Lambda_{\mathrm{QCD}}^2}{\tilde{\mu}^2} \right) = -1 \tag{2.17}$$

these two integration constants can be absorbed into one and the final result for the running coupling $\alpha_S = g^2/4\pi$ then reads

$$\alpha_S(k^2) = \frac{4\pi}{\left(\frac{11}{3} N - \frac{2}{3} N_f \right) \log \left(\frac{-k^2}{\Lambda_{\mathrm{QCD}}^2} \right)} . \tag{2.18}$$

So Λ_{QCD} obviously is the physical scale where the strong coupling becomes singular, and its value is around $200 - 250\,\mathrm{MeV}$. The final expression for the running coupling (2.18) has some remarkable implications. On one hand, this result has been calculated using massless quarks and yet one arrives at an expression containing a physical dimensionful parameter Λ_{QCD}. This implies, that the conformal symmetry, i.e. the symmetry under scale transformations, is broken even in massless QCD. On the other hand, one can see already from eq. (2.15) that the coupling decreases with increasing absolute value of transferred momentum squared. This implicates that, at high enough scales, the coupling becomes small enough for perturbation theory to be applied. In this regime the quarks and antiquarks can be treated as quasi-free particles. At the same time the coupling becomes large for distances of hadronic size. This

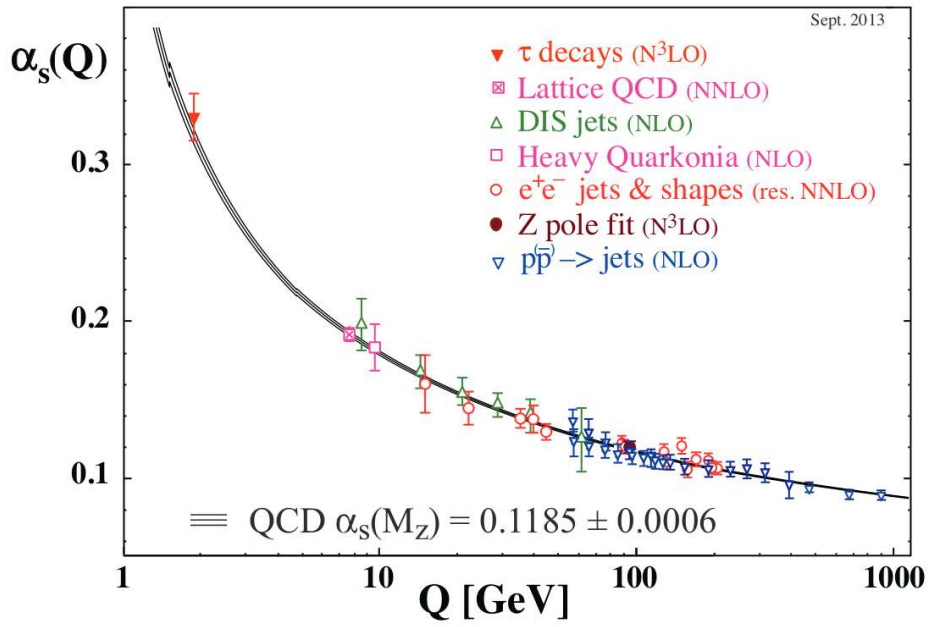

Figure 2.3.: Summary of measurements of α_S as a function of the energy scale Q. The respective degree of QCD perturbation theory used in the extraction of α_S is indicated in brackets (NLO: next-to-leading order; NNLO: next-to-next-to leading order; res. NNLO: NNLO matched with resummed next-to-leading logs; N^{3}LO: next-to-NNLO). This plot is taken from [22, chapter 9].

leads to the effect often referred to as confinement: One cannot observe free quarks or gluons, because when trying to separate them the interaction energy becomes large enough to create new quark-antiquark pairs, leading to the formation of new hadrons.

Eq. (2.18) is only the expression for the running coupling at one loop. One can, of course, also calculate higher order corrections. Defining the so-called β-function, the differential equation for the running coupling then reads

$$\beta = \frac{\mathrm{d}}{\mathrm{d}\log\mu^2}\alpha_S(\mu^2) = -\frac{\beta_0}{4\pi}\alpha_S^2 - \frac{\beta_1}{8\pi^2}\alpha_S^3 - \frac{\beta_2}{128\pi^3}\alpha_S^4 + \dots \tag{2.19}$$

with coefficients

$$\beta_0 = 11 - \frac{2}{3}N_f\,, \quad \beta_1 = 51 - \frac{19}{3}N_f\,, \quad \beta_2 = 2857 - \frac{5039}{9}N_f + \frac{325}{27}N_f^2\,, \tag{2.20}$$

which are given for the number of colors $N = 3$ and β_2 is given in the $\overline{\mathrm{MS}}$-scheme. One can now compare the predictions of these calculations with various experimental measurements of α_S, and this leads to the famous plot of the running coupling of QCD given in figure 2.3. The growth of α_S at small Q implies that perturbative calculations are only viable above a scale of $\mu^2 \sim 4\mathrm{GeV}^2$. Below this scale, different techniques like lattice QCD have to be applied.

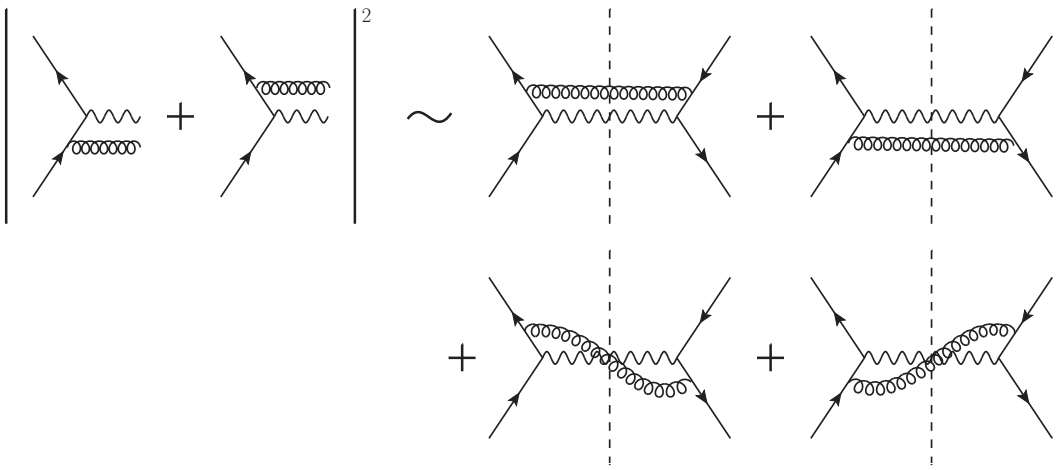

Figure 2.4.: Diagrammatic representation of the Cutkosky cutting rules (2.23). The dashed line denotes the final state cut.

2.4. Cut diagrams

For practical calculations it is often useful to not calculate amplitudes but to organize them in terms of cut diagrams. Due to the unitarity of the S-matrix $S = 1 + iT$ it holds

$$T^\dagger T = -i(T - T^\dagger)\,. \tag{2.21}$$

The Cutkosky cutting rules [23] state, that this is equal to the sum over all internal cuts, i.e.

$$T^\dagger T = -i(T - T^\dagger) = -\sum_C T_C\,. \tag{2.22}$$

A squared amplitude can then be calculated as

$$\sum_X \langle i|T^\dagger|X\rangle\langle X|T|i\rangle = \langle i|T^\dagger T|i\rangle = \langle i| - \sum_C T_C|i\rangle\,. \tag{2.23}$$

Taking the single gluon emission correction to the Drell-Yan production of a muon pair at the parton level as an example, the diagrammatic identity corresponding to the Cutkosky rule (2.23) is given in figure 2.4. In order to obtain the complete result for the $\mathcal{O}(\alpha_S)$ correction to the cross section, one has to add further diagrams corresponding to no gluon emission, i.e. self energy diagrams and vertex corrections. In calculations the usual Feynman rules given in appendix A are to be applied to the left of the final state cut. The corresponding Feynman rules for lines to the right of the final state cut are obtained by complex conjugation.

3. Hard scattering factorization

As we have explained in the previous chapter, the strong coupling is only small at sufficiently high energies, or, equivalently, at sufficiently small distances. However, when calculating cross sections of, e.g., proton-proton scattering, there are contributions from both small distances and large distances of hadronic size. This means that these cross sections cannot be calculated completely using only perturbation theory. A way out of this dilemma is given by the so-called factorization theorems, which we will explain for the example of a simple QCD process, namely the Drell-Yan production of a muon pair $pp \to \mu^+\mu^- X$ depicted in figure 3.1(a). Given that we will treat the individual steps of the derivation of the factorization theorem for the double Drell-Yan process in quite some detail in the following chapters, we will only outline the main ideas behind the factorization theorems here.

3.1. Collinear factorization

We first look at the case where only the longitudinal momenta $q^\pm = \frac{1}{\sqrt{2}}(q^0 \pm q^3)$ of the produced muon pair are measured. The momenta of the beam remnants as well as the transverse momentum $\boldsymbol{q} = (q^1, q^2)$ are not measured, i.e. they are integrated over. When the $\mu^+\mu^-$ pair has high invariant mass, the production of the photon can be described by the interaction of one constituent (parton) out of each proton. At leading order in the strong coupling, this is just the quark-antiquark annihilation depicted in figure 3.1(a).
The basic idea behind the factorization approach now is to seperate the whole process into two parts: A nonperturbative part that describes the long-distance dynamics of the process (red circle) and a parton level hard scattering part that depends on the short distance dynamics of the process and that can be calculated in perturbation theory (blue circle). It has been proven that, if the process is sufficiently inclusive, the cross section can approximately be written as [3]

$$\frac{\mathrm{d}\sigma}{\mathrm{d}Q^2\mathrm{d}y} = \sum_{i,j} \int_0^1 \mathrm{d}x_1 \int_0^1 \mathrm{d}x_2 f_i(x_1,\mu^2) f_j(x_2,\mu^2) \frac{\mathrm{d}\hat{\sigma}(x_1,x_2,i,j,\mu^2)}{\mathrm{d}Q^2\mathrm{d}y}\,, \tag{3.1}$$

where $y = \frac{1}{2}\log\frac{q^+}{q^-}$ is the rapidity of the produced muon pair and Q is its invariant mass. Corrections to the cross section (3.1) are suppressed by powers of Λ/Q, where Λ is a typical hadronic mass scale.
The parton distribution functions (PDFs) $f_i(x_n,\mu^2)$ represent the long distance dynamics of the process and are inherently non-perturbative objects. They only depend on the fraction of large longitudinal momentum x_n carried by the respective parton and the factorization scale μ, while the dependence on the transverse momenta and the other longitudinal momentum is integrated out. The PDFs represent the probability of finding a parton of species i with a momentum fraction x_n inside of the target and they are independent of the process under consideration, i.e. they are universal. The partonic cross section $\mathrm{d}\hat{\sigma}(x_1,x_2,i,j,\mu^2)/(\mathrm{d}Q^2\mathrm{d}y)$,

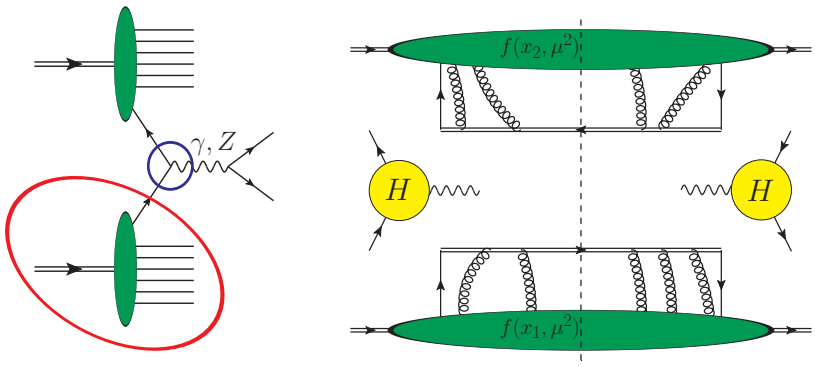

Figure 3.1.: Drell-Yan production of an electroweak gauge boson: (a) full diagram; (b) factorized form of the cross section in the framework of collinear factorization.

by contrast, depends on the process under consideration and can be calculated in perturbation theory. The factorized form of the cross section (3.1) is illustrated in figure 3.1(b).

At tree level, the parton distribution of an unpolarized quark inside the right-moving proton is then defined by the matrix element [5]

$$f_i(x_1) = \int \frac{\mathrm{d}b^-}{2\pi} e^{-ix_1 p^+ b^-} \langle p|\bar{\psi}_i(0, b^-, \mathbf{0}) \frac{\gamma^+}{2} \psi_i(0)|p\rangle \,, \tag{3.2}$$

where p is the momentum of the right-moving proton. We note that this definition is not gauge invariant and is to be amended with suitable so-called Wilson lines (the double lines in figure 3.1(b)) once QCD corrections are taken into account.

Once factorization theorems like (3.1) are proven, this adds a tremendous amount of predictive power to perturbative QCD. One can determine the parton distribution functions from a suitable process like Deep Inelastic Scattering (DIS) and can then use these results for any other process that has been proven to be factorizing. One only has to calculate the hard part, i.e. the parton level cross section, of the process under consideration and obtains a prediction for the cross section.

3.2. TMD factorization

There are many cases where the collinear factorization formalism outlined in the previous section cannot be applied, in particular when details of the final state such as transverse momenta are measured. For these cases, the formalism has to be extended to parton distribution functions where the dependence on the intrinsic transverse momenta of the partons is not integrated out, so called tranverse momentum dependent parton distribution functions (TMDs).

An intuitive definition of a TMD for an unpolarized quark of flavor i inside of a right-moving proton is obtained by keeping the transverse momentum dependence of the usual PDFs defined in eq. (3.2),

$$f_i(x,\mathbf{k},\mu^2) \stackrel{?}{=} \int \frac{db^-}{(2\pi)} e^{-ixp^+b^-} \int \frac{d^2\mathbf{b}}{(2\pi)^2} e^{i\mathbf{k}\cdot\mathbf{b}} \langle p|\bar{\psi}_i(0,b^-,\mathbf{b})\frac{\gamma^+}{2}\psi_i(0)|p\rangle\,, \tag{3.3}$$

where the "?" indicates that this will not be the final definition [5]. The corresponding factorization theorem at tree level reads

$$\begin{aligned}\frac{d\sigma}{dx_1 dx_2 d^2\mathbf{q}} = \frac{1}{2q^2}\sum_{i,j}\int d^2\mathbf{k}_1 d^2\mathbf{k}_2 \delta^{(2)}(\mathbf{q}-\mathbf{k}_1-\mathbf{k}_2)\times \\ \times f_i(x_1,\mathbf{k}_1,\mu^2) f_j(x_2,\mathbf{k}_2,\mu^2) H_{ij}(x_1x_2s,\mu^2)\,,\end{aligned} \tag{3.4}$$

where H describes the hard scattering at parton level. Indeed, the definition (3.3) and the factorization formula (3.4) are sufficient at tree level, but they are not sufficient for a treatment of the process in full QCD. On one hand, the operator in (3.3) contains two quark fields at different positions. As is well known, such operators are not gauge invariant unless the two quark fields are joined by a gauge link, a so-called Wilson line. On the other hand, one has to allow for additional gluon exchange, which will lead to major changes in the definition (3.3) and the factorization formula (3.4). We will not discuss all these issues here, but will treat them in the context of double Drell-Yan in chapter 6.

4. Double Drell-Yan: Lowest order analysis

As already mentioned in chapter 1, with center of mass collision energies becoming higher and higher, an ever smaller value of Bjorken x of the partons inside a proton is enough to contribute to reactions at a specific scale $Q^2 = x_1 x_2 s$. As the PDFs and TMDs grow rapidly for small x, the probability for two or more hard interactions rises dramatically. A theoretically sound understanding of these multiple interactions is indispensable in order to be able to calculate and subtract the QCD background when searching for signals from BSM physics. This requires substantial extension of the techniques used for the calculation of cross sections within the single parton scattering framework, and especially of the collinear and TMD factorization procedure. Given that there are substantial difficulties with proving factorization theorems and even explicit violations of TMD factorization in processes with hadrons in both the initial and final state, see e.g. [12], we will restrict our analysis to the most simple case of double parton scattering, namely the double Drell-Yan process depicted in figure 4.1. This process serves as an ideal starting point for the development of the theory of multiple interactions, as its single parton scattering counterpart is completely understood.

In this chapter we will derive the factorized form of the cross section of the double Drell-Yan process in lowest order of the strong coupling. We will restrict ourselves to cross sections differential in transverse momenta. Similar derivations for cross sections integrated over transverse momenta have been given in the past, cf. [24, 25].
In section 4.1 we give the definitions of the double parton distributions, paying special attention to the color and spin structure. In section 4.3 we derive the factorized form of the cross section at lowest order and compare the cross sections of single and double parton scattering with power counting methods. We conclude this chapter with a brief account of the current state of the art of implementing double parton scattering into the analysis of experimental data in section 4.4. Throughout this chapter, we will closely follow the nomenclature, derivations and reasoning of [9].

4.1. Definition of two-parton distributions

We start with defining the two-parton distributions that will appear in the cross section of the double Drell-Yan process depicted in figure 4.1. Note that the following definitions are only valid at lowest order in the strong coupling. At higher orders, these definitions have to be supplemented with appropriate Wilson lines that ensure gauge invariance, and the resulting cross sections contain additional so-called soft factors. We will deal with these complications in chapter 6.

4.1.1. Scalar distributions

We will first give the definition of a two-parton distribution for (hypothetical) scalar partons described by a Hermitian field ϕ. In this case one doesn't have to deal with the complications

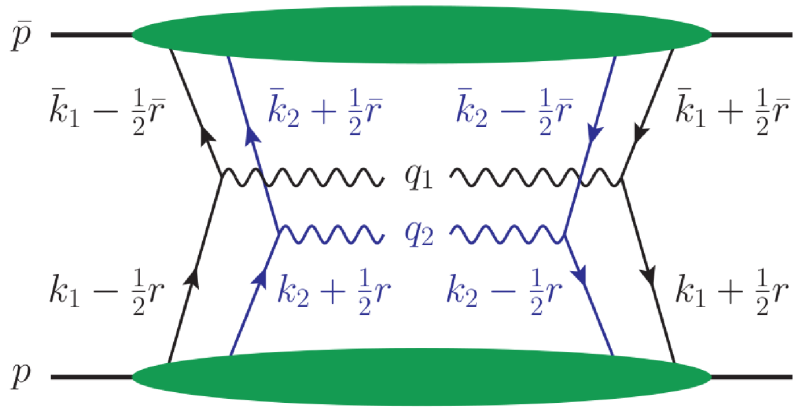

Figure 4.1.: Momentum assignement for the double Drell-Yan process at lowest order in the strong coupling.

that arise due to the parton spin of quarks and gluons in QCD. The starting point for the derivation of the scalar distributions is the two-parton correlation function, which describes the emission of two partons in the scattering amplitude and the absorption of two partons in its conjugate. The definition reads

$$\Phi(l_i, l_i') = \int \frac{d^4\xi_1}{(2\pi)^4} \frac{d^4\xi_1'}{(2\pi)^4} e^{i\xi_1 l_1 - i\xi_1' l_1'} \int \frac{d^4\xi_2}{(2\pi)^4} e^{i\xi_2 l_2} \langle p|\bar{T}\Big[\phi(0)\phi(\xi_1')\Big] T\Big[\phi(\xi_1)\phi(\xi_2)\Big]|p\rangle\,, \quad (4.1)$$

where T and $\bar{T}$ denote time-ordering and anti-time-ordering of the fields, respectively. Due to momentum conservation, the parton momenta have to fulfill the condition $l_1 + l_2 = l_1' + l_2'$. Switching to symmetric variables, the structure of the cross section becomes more clear. We first use translational invariance to shift all field positions by $-\frac{1}{2}\xi_2$ and then replace

$$l_i = k_i - \tfrac{1}{2}r\,, \quad l_i' = k_i + \tfrac{1}{2}r \quad (4.2)$$

for the momentum variables and

$$y + \tfrac{1}{2}z_1 = \xi_1 - \tfrac{1}{2}\xi_2\,, \quad y - \tfrac{1}{2}z_1 = \xi_1' - \tfrac{1}{2}\xi_2\,, \quad z_2 = \xi_2 \quad (4.3)$$

for position variables. The resulting expression for the two parton correlation function is

$$\begin{aligned}\Phi(k_i, r) = &\left[\prod_{i=1}^{2} \int \frac{d^4 z_i}{(2\pi)^4} e^{i z_i k_i}\right] \int \frac{d^4 y}{(2\pi)^4} e^{-iyr} \\ &\times \langle p|\bar{T}\Big[\phi\big(-\frac{1}{2}z_2\big)\phi\big(y - \frac{1}{2}z_1\big)\Big] T\Big[\phi\big(\frac{1}{2}z_2\big)\phi\big(y + \frac{1}{2}z_1\big)\Big]|p\rangle\,. \end{aligned} \quad (4.4)$$

We now define the transverse momentum dependent two-parton distribution function (dTMD) as

$$F(x_i, \boldsymbol{k}_i, \boldsymbol{r}) = \left[\prod_{i=1}^{2} k_i^+ \int dk_i^-\right] (2\pi)^3\, 2p^+ \int dr^-\, \Phi(k_i, r)\Big|_{k_i^+ = x_i p^+,\, r^+ = 0}\,, \tag{4.5}$$

which can be rewritten as

$$\begin{aligned} F(x_i, \mathbf{k}_i, \mathbf{r}) = \left[\prod_{i=1}^{2} \int \frac{dz_i^-}{2\pi} e^{i x_i z_i^- p^+} \int \frac{d^2\mathbf{z}_i}{(2\pi)^2} e^{-i\mathbf{z}_i\cdot\mathbf{k}_i}\right] 2p^+ \int dy^- d^2\mathbf{y} e^{i\mathbf{y}\cdot\mathbf{r}} \\ \times \langle p|\mathcal{O}(0, z_2)\mathcal{O}(y, z_1)|p\rangle \end{aligned} \tag{4.6}$$

with the abbreviation

$$\mathcal{O}(y, z_i) = \phi\left(y - \tfrac{1}{2}z_i\right) \frac{i}{2}\left(\overrightarrow{\partial} - \overleftarrow{\partial}\right)^+ \phi\left(y + \tfrac{1}{2}z_i\right)\Big|_{z_i^+ = y^+ = 0}\,. \tag{4.7}$$

Note that in (4.6) we have replaced the time-ordered and anti-time-ordered products by usual products. This can be done, because the position arguments of the fields have a plus-component that is zero. The fields therefore have spacelike seperation and commute because of causality.

4.1.2. Quarks

The starting point for the definition of the two-quark parton distribution is the correlation function for two quarks entering the hard scattering, which is defined by

$$\begin{aligned} \Phi_{\alpha_1\beta_1\alpha_2\beta_2}(k_i, r) = \left[\prod_{i=1}^{2} \int \frac{d^4 z_i}{(2\pi)^4} e^{i z_i k_i}\right] \int \frac{d^4 y}{(2\pi)^4} e^{-iyr} \\ \times \langle p|\bar{T}\left[\bar{q}_{\beta_1}(y - \tfrac{1}{2}z_1)\bar{q}_{\beta_2}(-\tfrac{1}{2}z_2)\right] T\left[q_{\alpha_2}(\tfrac{1}{2}z_2) q_{\alpha_1}(y + \tfrac{1}{2}z_1)\right]|p\rangle\,, \end{aligned} \tag{4.8}$$

where α_i and β_j are Dirac indices and T denotes time-ordering whereas $\bar{T}$ denotes anti-time-ordering, as is appropriate for the quark fields in the amplitude and its conjugate, respectively. Moreover, we only consider unpolarized hadrons and therefore averaging over the proton spin is tacitly assumed in (4.8). Integrating the correlation function over the parton minus-momenta, we can omit the anti-time and time-ordering due to the spacelike separation of the fields. Thus we can bring them into the following order by an even permutation yielding no change of sign:

$$\bar{q}_{\beta_1}(y - \tfrac{1}{2}z_1) q_{\alpha_1}(y + \tfrac{1}{2}z_1) \bar{q}_{\beta_2}(-\tfrac{1}{2}z_2) q_{\alpha_2}(\tfrac{1}{2}z_2)\,. \tag{4.9}$$

The Dirac indices of the correlation function are contracted with the indices of the hard scattering matrices $H_{1,\beta_1\alpha_1}$ and $H_{2,\beta_2\alpha_2}$. The next step is to expand the hard scattering matrices in a Clifford basis:

$$\begin{aligned} H_{i,\beta\alpha} = \tfrac{1}{2}\delta_{\beta\alpha}\mathrm{tr}\left(\tfrac{1}{2}H_i\right) + \tfrac{1}{2}(\gamma_5)_{\beta\alpha}\mathrm{tr}\left(\tfrac{1}{2}\gamma_5 H_i\right) + \tfrac{1}{2}(\gamma^\mu)_{\beta\alpha}\mathrm{tr}\left(\tfrac{1}{2}\gamma_\mu H_i\right) \\ + \tfrac{1}{2}(\gamma^\mu\gamma_5)_{\beta\alpha}\mathrm{tr}\left(\tfrac{1}{2}\gamma_\mu\gamma_5 H_i\right) + \tfrac{1}{2}i(\sigma^{\mu\nu}\gamma_5)_{\beta\alpha}\mathrm{tr}\left(\tfrac{1}{4}i\sigma_{\mu\nu}\gamma_5 H_i\right)\,. \end{aligned} \tag{4.10}$$

The product of Φ and H_i is, dominated only by three terms on the r.h.s. of eq. (4.10) whose product with Φ is proportional to the large scale $p^+ \sim Q$, namely by the terms proportional to $\frac{1}{2}\gamma^+$, $\frac{1}{2}\gamma^+\gamma_5$ and $\frac{1}{2}i\sigma^{+j}\gamma_5$, where $j = 1, 2$, see [9]. Integrating over the parton minus-momenta, we are then left with the following definition for two-quark distributions:

$$\begin{aligned} F_{a_1a_2}(x_i, \boldsymbol{z}_i, \boldsymbol{y}) &= \langle\langle(\bar{q}_3\Gamma_{a_2}q_2)(\bar{q}_4\Gamma_{a_1}q_1)\rangle\rangle \\ &= \left[\prod_{i=1}^{2}\int \frac{dz_i^-}{(2\pi)} e^{ix_i z_i^- p^+}\right] 2p^+ \int dy^- \\ &\quad \times \langle p|\left(\bar{q}(-\tfrac{1}{2}z_2)\Gamma_{a_2}q(\tfrac{1}{2}z_2)\right)\left(\bar{q}(y-\tfrac{1}{2}z_1)\Gamma_{a_1}q(y+\tfrac{1}{2}z_1)\right)\Big|_{z_1^+=z_2^+=y^+=0} \end{aligned} \tag{4.11}$$

Here, $a_i = q, \Delta q, \delta q$ labels the polarization of the corresponding quark. As is already known from single parton scattering, we have

$$\Gamma_q = \tfrac{1}{2}\gamma^+ \ , \qquad \Gamma_{\Delta q} = \tfrac{1}{2}\gamma^+\gamma_5 \ , \qquad \Gamma^j_{\delta q} = \tfrac{1}{2}i\sigma^{j+}\gamma_5 \tag{4.12}$$

for unpolarized, longitudinally polarized and transversely polarized quarks, respectively. The indices of the quarks fields on the r.h.s. of the first line of eq. (4.11) label the position argument and plus-momentum fraction of the particular parton, cf. figure 4.2. In detail we have

$$q_1 = q(x_1, y + \tfrac{1}{2}z_1) \ , \quad q_2 = q(x_2, \tfrac{1}{2}z_2) \ , \quad \bar{q}_3 = \bar{q}(x_2, -\tfrac{1}{2}z_2) \ , \quad \bar{q}_4 = \bar{q}(x_1, y - \tfrac{1}{2}z_1) \, . \tag{4.13}$$

We also define distributions that depend on transverse momenta instead of transverse positions:

$$\begin{aligned} F_{a_1a_2}(x_i, \boldsymbol{k}_i, \boldsymbol{y}) &= \left[\prod_{i=1}^{2}\int \frac{d^2\boldsymbol{z}_i}{(2\pi)^2} e^{-i\boldsymbol{z}_i\boldsymbol{k}_i}\right] F_{a_1a_2}(x_i, \boldsymbol{z}_i, \boldsymbol{y}) \, , \\ F_{a_1a_2}(x_i, \boldsymbol{k}_i, \boldsymbol{r}) &= \int \frac{d^2\boldsymbol{y}}{(2\pi)^2} e^{-i\boldsymbol{y}\boldsymbol{r}} F_{a_1a_2}(x_i, \boldsymbol{k}_i, \boldsymbol{y}) \, . \end{aligned} \tag{4.14}$$

In momentum space, we then have

$$\begin{aligned} q_1 &= q(x_1, \boldsymbol{k}_1 - \tfrac{1}{2}\boldsymbol{r}) \, , \quad q_2 = q(x_2, \boldsymbol{k}_2 + \tfrac{1}{2}\boldsymbol{r}) \, , \\ \bar{q}_3 &= \bar{q}(x_2, \boldsymbol{k}_2 - \tfrac{1}{2}\boldsymbol{r}) \, , \quad \bar{q}_4 = \bar{q}(x_1, \boldsymbol{k}_1 + \tfrac{1}{2}\boldsymbol{r}) \, . \end{aligned} \tag{4.15}$$

$F_{a_1a_2}(x_i, \boldsymbol{k}_i, \boldsymbol{y})$ does not admit a probability interpretation as one cannot measure transverse momentum and position simultaneously. However, the transverse momentum or transverse position integrated quantities

$$\begin{aligned} F_{a_1a_2}(x_i, \boldsymbol{y}) &= \left[\prod_{i=1}^{2}\int d^2\boldsymbol{k}_i\right] F_{a_1a_2}(x_i, \boldsymbol{k}_i, \boldsymbol{y}) = F_{a_1a_2}(x_i, \boldsymbol{z}_i = \boldsymbol{0}, \boldsymbol{y}) \\ F_{a_1a_2}(x_i, \boldsymbol{k}_i, \boldsymbol{r} = \boldsymbol{0}) &= \int d^2\boldsymbol{y} F_{a_1a_2}(x_i, \boldsymbol{k}_i, \boldsymbol{y}) \end{aligned} \tag{4.16}$$

do have a probability interpretation, i.e. $F_{a_1a_2}(x_i, \boldsymbol{k}_i, \boldsymbol{y})$ has the structure of a Wigner distribution: The integral over transverse momentum yields the probabilty for finding two partons

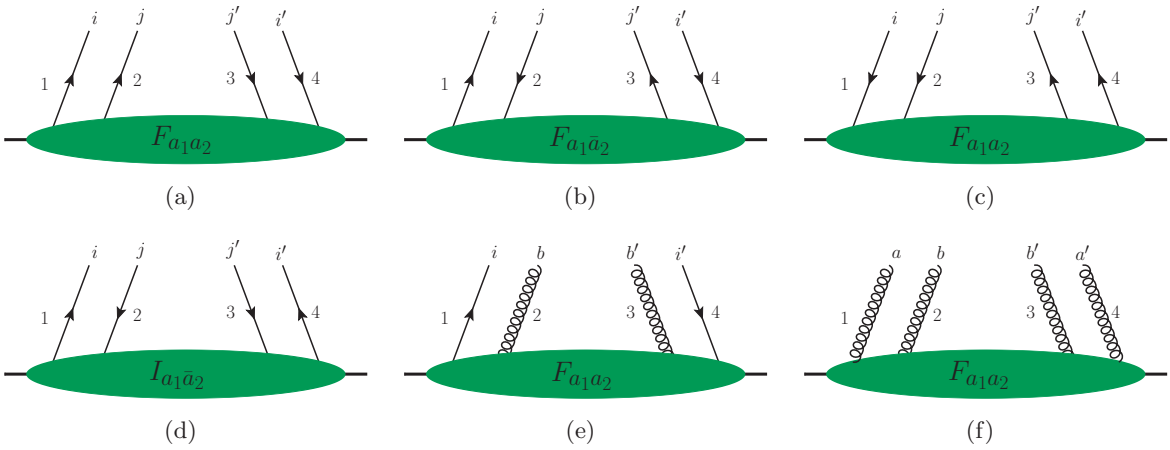

Figure 4.2.: Momentum assignement for two-parton distributions as given in eq. 4.15: (a) two quarks; (b) quark and antiquark; (c) two antiquarks; (d) interference distribution; (e) quark and gluon; (f) two gluons; The indices i, j, a and b label the color and will be discussed in section 4.2.

with plus-momentum fractions x_1 and x_2 with transverse separation $\boldsymbol{y}$, while the integral over transverse position gives the probability to find two partons with plus-momentum fractions x_1 and x_2 and transverse momenta $\boldsymbol{k}_1$ and $\boldsymbol{k}_2$. The same holds for the scalar distribution defined in eq. (4.6).

4.1.3. Antiquarks

The distribution for a quark and an antiquark or two antiquarks can be derived completely in the same way. The definitions are

$$\begin{aligned} F_{a_1\bar{a}_2}(x_i, \boldsymbol{k}_i, \boldsymbol{y}) &= \langle\langle (\bar{q}_2 \Gamma_{\bar{a}_2} q_3)(\bar{q}_4 \Gamma_{a_1} q_1) \rangle\rangle \,, \\ F_{\bar{a}_1\bar{a}_2}(x_i, \boldsymbol{k}_i, \boldsymbol{y}) &= \langle\langle (\bar{q}_2 \Gamma_{\bar{a}_2} q_3)(\bar{q}_1 \Gamma_{\bar{a}_1} q_4) \rangle\rangle \,, \end{aligned} \tag{4.17}$$

with

$$\Gamma_{\bar{q}} = \Gamma_q \,, \qquad \Gamma_{\Delta\bar{q}} = -\Gamma_{\Delta q} \,, \qquad \Gamma^j_{\delta\bar{q}} = \Gamma^j_{\delta\bar{q}} \,. \tag{4.18}$$

Just like in the single parton scattering case [26], the distributions of quarks and antiquarks are related to each other by

$$F_{\bar{a}_1\bar{a}_2}(x_i, \boldsymbol{k}_i, \boldsymbol{y}) = \sigma_{a_1}\sigma_{a_2} F_{a_1a_2}(-x_i, -\boldsymbol{k}_i, \boldsymbol{y}) \tag{4.19}$$

with sign factors $\sigma_q = \sigma_{\delta q} = 1$ and $\sigma_{\Delta q} = -1$.

4.1.4. Interference distribution

There is another type of two-parton distributions not discussed so far that do not admit a probability interpretation as they represent interference terms. Their appearance is a completely new feature compared to single hard scattering processes, where these terms are forbidden by fermion number and/or quark flavor conservation. Typical interference terms in fermion

number are

$$I_{a_1\bar{a}_2}(x_i, \boldsymbol{k}_i, \boldsymbol{y}) = \langle\langle (\bar{q}_2 \Gamma_{\bar{a}_2} q_4)\, (\bar{q}_3 \Gamma_{a_1} q_1) \rangle\rangle\,,$$
$$I_{\bar{a}_1 a_2}(x_i, \boldsymbol{k}_i, \boldsymbol{y}) = \langle\langle (\bar{q}_4 \Gamma_{a_2} q_2)\, (\bar{q}_1 \Gamma_{\bar{a}_1} q_3) \rangle\rangle\,, \tag{4.20}$$

where the first one is displayed in figure 4.2 (d), from which can be seen that the quark in the amplitude is an antiquark in the conjugate and vice versa. Additionally, there are interference terms in quark flavor, e.g.

$$I_{a_1 a_2}(x_i, \boldsymbol{k}_i, \boldsymbol{y}) = \langle\langle (\bar{u}_3 \Gamma_{a_2} d_2)\, \left(\bar{d}_4 \Gamma_{a_1} u_1\right) \rangle\rangle\,, \tag{4.21}$$

displayed in figure 4.3. In that case, the quark that is an up quark in the amplitude is a down quark in the conjugate and vice versa.

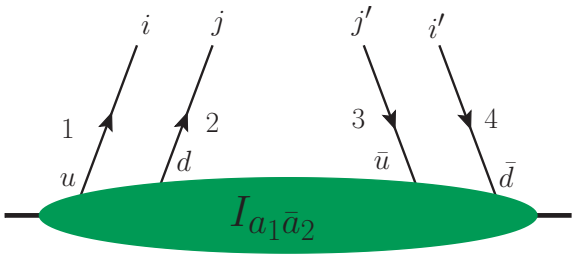

Figure 4.3.: Example for an interference distribution in quark flavor. The quark line that represents an up quark in the amplitude represents a down quark in its conjugate and vice versa.

4.1.5. Gluons

The starting point for the definition of the double gluon TMD is the two-gluon correlator

$$\Phi^{j_1 j_1' j_2 j_2'}(k_i, r) = \left[\prod_{i=1}^{2} \int \frac{d^4 z_i}{(2\pi)^4} e^{i z_i k_i}\right] \int \frac{d^4 y}{(2\pi)^4} e^{-iyr}$$
$$\times \langle p | \bar{T}\left[A^{j_2'}(-\tfrac{1}{2} z_2) A^{j_1'}(y - \tfrac{1}{2} z_1)\right] T\left[A^{j_2}(\tfrac{1}{2} z_2) A^{j_1}(y + \tfrac{1}{2} z_1)\right] | p \rangle\,. \tag{4.22}$$

Working in light-cone gauge, $A^+ = 0$, the leading contribution to the cross section originates from gluons with transverse polarization, i.e. $j_i, j_i' = 1, 2$, but one then has to be careful about effects from Wilson lines at spacetime infinity, as the gluon potential does not vanish at infinity in light-cone gauge. Working in covariant gauges, e.g. Feynman gauge, the attachement of gluons with polarization A^+ for the right-moving proton and of gluons with polarization A^- for the left-moving proton is not power suppresses and these gluons have to be resummed into appropriate Wilson lines, which we will discuss in chapter 6. After this step is taken the leading contribution to the cross section once again comes from gluons with transverse polarization and we will define the two-gluon distributions for these gluons.
For this purpose we need a decomposition of the two-gluon correlator (4.22). Any tensor depending only on two transverse indices j, j' can be decomposed into three parts, namely

the trace, an antisymmetric and a symmetric traceless part:

$$\begin{aligned} T^{jj'} &= \frac{1}{2}\left(\delta^{jj'}\delta^{kk'} + \varepsilon^{jj'}\varepsilon^{kk'} + \tau^{jj',kk'}\right) T^{kk'} \\ &= \delta^{jj'}\left(\frac{1}{2}\delta^{kk'}T^{kk'}\right) - i\varepsilon^{jj'}\left(\frac{1}{2}i\varepsilon^{kk'}T^{kk'}\right) + \tau^{jj',ll'}\left(\tau^{ll',kk'}T^{kk'}\right) \end{aligned} \tag{4.23}$$

where $\tau^{ii',jj'} = \frac{1}{2}(\delta^{ij}\delta^{i'j'} + \delta^{ij'}\delta^{i'j} - \delta^{ii'}\delta^{jj'})$. In light cone gauge, it holds $G^{+j} = \partial^+ A^j$, and we use this relation to replace the gluon potentials by gluon field strength operators. Including a factor k_i^+ for each gluon i, we obtain the following definition for the two-gluon distributions:

$$\begin{aligned} F_{a_1a_2}(x_i, \boldsymbol{k}_i, \boldsymbol{y}) = &\left[\prod_{i=1}^{2}\frac{1}{x_i p^+}\int\frac{dz_i^-}{2\pi}e^{ix_ip^+z_i^-}\int\frac{d^2\boldsymbol{z}_i}{(2\pi)^2}e^{-i\boldsymbol{z}_i\boldsymbol{k}_i}\right] 2p^+\int dy^- \\ &\times\langle p|\left(\Pi_{a_2}^{j_2j_2'}G^{+j_2'}(-\tfrac{1}{2}z_2)G^{+j_2}(\tfrac{1}{2}z_2)\right)\left(\Pi_{a_1}^{j_1j_1'}G^{+j_1'}(y-\tfrac{1}{2}z_1)G^{+j_1}(y+\tfrac{1}{2}z_1)\right)|p\rangle \\ = &(x_1p^+)^{-1}(x_2p^+)^{-1}\left\langle\left\langle\left(\Pi_{a_2}^{j_2j_2'}G_3^{+j_2'}G_2^{+j_2}\right)\left(\Pi_{a_1}^{j_1j_1'}G_4^{+j_1'}G_1^{+j_1}\right)\right\rangle\right\rangle \end{aligned} \tag{4.24}$$

Here, the a_i denote the polarization of the gluons and we have

$$\Pi_g^{jj'} = \delta^{jj'}\ , \qquad \Pi_{\Delta g}^{jj'} = i\varepsilon^{jj'}\ , \qquad \left(\Pi_{\delta g}^{ll'}\right)^{jj'} = \tau^{jj',ll'}\ , \tag{4.25}$$

where the first and second projector describe unpolarized and longitudinally polarized gluons, respectively, while the third one describes the interference of two gluons with helicities that differ by two units.

4.1.6. Mixed distributions

The definition for mixed distributions involving both quarks and gluons is easily written down and reads

$$F_{a_1a_2}(x_i, \boldsymbol{k}_i, \boldsymbol{y}) = (x_2p^+)^{-1}\left\langle\left\langle(\bar{q}_3\Gamma_{a_1}q_2)\left(\Pi_{a_2}^{jj'}G_4^{+j'}G_1^{+j}\right)\right\rangle\right\rangle\ , \tag{4.26}$$

with an analogous expression for antiquark-gluon distributions.

4.2. Color structure

4.2.1. Quarks

Single parton distributions have a trivial color structure, as the quarks and gluon fields always couple to a color singlet. In contrast to that, two-parton distributions have a nontrivial color structure (four open color indices, cf. figure 4.2) and we will give a possible color decomposition of the distributions in the following. We start with the two-quark distributions, which can be decomposed according to (we will not display the polarization labels, if not necessary, for better legibility)

$$F_{ii',jj'} = \frac{1}{N^2}\left[{}^1F\delta_{ii'}\delta_{jj'} + \frac{2N}{\sqrt{N^2-1}}{}^8F t_{ii'}^a t_{jj'}^a\right]\ , \tag{4.27}$$

with i, i' and j, j' being color indices and N being the number of colors. The functions ${}^1F$ and ${}^8F$ are defined as

$$\begin{aligned} {}^1F &= \delta_{i'i}\delta_{j'j}F_{ii',jj'} = \langle\langle(\bar{q}_{3,j}\Gamma_{a_2}q_{2,j})(\bar{q}_{4,i}\Gamma_{a_1}q_{1,i})\rangle\rangle \,, \\ {}^8F &= \frac{2N}{\sqrt{N^2-1}}t^a_{i'i}t^a_{j'j}F_{ii',jj'} = \langle\langle(\bar{q}_{3,j'}\Gamma_{a_2}t^a_{j'j}q_{2,j})(\bar{q}_{4,i'}\Gamma_{a_1}t^a_{i'i}q_{1,i})\rangle\rangle \,. \end{aligned} \tag{4.28}$$

The prefactors in (4.27) have been chosen such that the color singlet and color octet distributions enter the cross section with equal weight:

$$\frac{d\sigma}{\prod_{i=1}^2 dx_i d\bar{x}_i d^2\boldsymbol{q}_i} \sim \frac{{}^1F{}^1F + {}^8F{}^8F}{N^2} \,. \tag{4.29}$$

The overall normalization factors in (4.27) are given by the inverse of the color projectors times their complex conjugate, i.e.

$$\begin{aligned} (\delta_{ii'}\delta_{jj'}\delta_{i'i}\delta_{j'j})^{-1} &= \frac{1}{N^2} \,, \\ \left(t^a_{ii'}t^a_{jj'}(t^b_{ii'})^*(t^b_{jj'})^*\right)^{-1} &= \left(t^a_{ii'}t^a_{jj'}t^b_{i'i}t^b_{j'j}\right)^{-1} = \left(\frac{\delta^{ab}\delta^{ab}}{4}\right)^{-1} = \frac{4}{N^2-1} \,, \end{aligned} \tag{4.30}$$

where in the second line we have used that the generators are Hermitian. One can easily see that in ${}^1F$ and ${}^8F$ the lines carrying the same longitudinal momentum fractions couple to color singlets and octets for $N = 3$, respectively. The color decomposition of quark-antiquark (two-antiquark) distributions can be done in the same way, with appropriate exchange of the color indices j, j' (and i, i') on the r.h.s of eq. (4.27).
The decomposition for the interference distribution $I_{a_1\bar{a}_2}$ is given by (cf. figure 4.2(d))

$$I_{ii',jj'} = \langle\langle\left(\bar{q}_{2,j}\Gamma_{\bar{a}_2}q_{4,i'}\right)\left(\bar{q}_{3,j'}\Gamma_{a_1}q_{1,i}\right)\rangle\rangle = \frac{1}{N^2}\left[{}^1I\delta_{ij'}\delta_{i'j} + \frac{2N}{\sqrt{N^2-1}}{}^8I t^a_{ij'}t^a_{i'j}\right] . \tag{4.31}$$

4.2.2. Gluons

We will now come to the color decomposition for the two-gluon distributions, which is more complicated than the one for quarks and antiquarks. The three lowest dimensional irreducible representations, the color singlet and symmetric and antisymmetric octet, can be written down for any number of colors N and read

$$\begin{aligned} F^{aa',bb'} &= (x_1p^+)^{-1}(x_2p^+)^{-1}\langle\langle\left(\Pi_{a_2}G^{b'}_3G^b_2\right)\left(\Pi_{a_1}G^{a'}_4G^a_1\right)\rangle\rangle \\ &= \frac{1}{(N^2-1)^2}\left[{}^1F\delta^{aa'}\delta^{bb'} - \frac{\sqrt{N^2-1}}{N}{}^AF f^{aa'c}f^{bb'c} + \frac{N\sqrt{N^2-1}}{N^2-4}{}^SF d^{aa'c}d^{bb'c} + \dots\right] , \end{aligned} \tag{4.32}$$

where we have omitted Lorentz indices for better legibility. The overall normalization factors are, like above, given by the inverse of the color projectors times their complex conjugate:

$$\begin{aligned}\left(\delta^{aa'}\delta^{bb'}\delta^{a'a}\delta^{b'b}\right)^{-1} &= \frac{1}{(N^2-1)^2}\,,\\ \left(if^{aa'c}if^{bb'c}(-i)f^{aa'd}(-i)f^{bb'd}\right)^{-1} &= \frac{1}{N^2(N^2-1)}\,,\\ \left(d^{aa'c}d^{bb'c}d^{aa'd}d^{bb'd}\right)^{-1} &= \frac{N^2}{(N^2-1)(N^2-4)^2}\,.\end{aligned} \tag{4.33}$$

For $N=3$ the higher irreducible representations are $10, \overline{10}$ and 27 and the decomposition is given by

$$\begin{aligned}F^{aa',bb'} = \frac{1}{64}\Bigg[&{}^1F\delta^{aa'}\delta^{bb'} - \frac{\sqrt{8}}{3}{}^AF f^{aa'c}f^{bb'c} + \frac{3\sqrt{8}}{5}{}^SF d^{aa'c}d^{bb'c}\\ &+\frac{2}{\sqrt{10}}{}^{10}F t_{10}^{aa',bb'} + \frac{2}{\sqrt{10}}{}^{\overline{10}}F\left(t_{10}^{aa',bb'}\right)^* + \frac{4}{\sqrt{27}}{}^{27}F t_{27}^{aa',bb'}\Bigg]\,.\end{aligned} \tag{4.34}$$

The projectors for the higher representations can be found e.g. in [25] and read

$$\begin{aligned}t_{10}^{aa',bb'} &= \delta^{ab}\delta^{a'b'} - \delta^{ab'}\delta^{a'b} - \tfrac{2}{3}f^{aa'c}f^{bb'c} - i(d^{abc}f^{a'b'c} + f^{abc}d^{a'b'c})\,,\\ t_{27}^{aa',bb'} &= \delta^{ab}\delta^{a'b'} + \delta^{ab'}\delta^{a'b} - \tfrac{1}{4}\delta^{aa'}\delta^{bb'} - \frac{6}{5}d^{aa'c}d^{bb'c}\,.\end{aligned} \tag{4.35}$$

The structure functions are given by

$$\begin{aligned}(x_1p^+)(x_2p^+)^1F &= \langle\langle\left(\Pi_{a_2}G_3^bG_2^b\right)\left(\Pi_{a_1}G_4^aG_1^a\right)\rangle\rangle\,,\\ (x_1p^+)(x_2p^+)^AF &= -\frac{\sqrt{N^2-1}}{N}\langle\langle\left(f^{bb'c}\Pi_{a_2}G_3^{b'}G_2^b\right)\left(f^{aa'c}\Pi_{a_1}G_4^{a'}G_1^a\right)\rangle\rangle\,,\\ (x_1p^+)(x_2p^+)^SF &= \frac{N\sqrt{N^2-1}}{N^2-4}\langle\langle\left(d^{bb'c}\Pi_{a_2}G_3^{b'}G_2^b\right)\left(d^{aa'c}\Pi_{a_1}G_4^{a'}G_1^a\right)\rangle\rangle\,,\end{aligned} \tag{4.36}$$

for arbitrary N while for the higher representations we have in the case of $N=3$

$$\begin{aligned}(x_1p^+)(x_2p^+)^{10}F &= \frac{2}{\sqrt{10}}\left(t_{10}^{aa',bb'}\right)^*\langle\langle\left(\Pi_{a_2}G_3^{b'}G_2^b\right)\left(\Pi_{a_1}G_4^{a'}G_1^a\right)\rangle\rangle\,,\\ (x_1p^+)(x_2p^+)^{\overline{10}}F &= \frac{2}{\sqrt{10}}t_{10}^{aa',bb'}\langle\langle\left(\Pi_{a_2}G_3^{b'}G_2^b\right)\left(\Pi_{a_1}G_4^{a'}G_1^a\right)\rangle\rangle\,,\\ (x_1p^+)(x_2p^+)^{27}F &= \frac{4}{\sqrt{27}}t_{27}^{aa',bb'}\langle\langle\left(\Pi_{a_2}G_3^{b'}G_2^b\right)\left(\Pi_{a_1}G_4^{a'}G_1^a\right)\rangle\rangle\,.\end{aligned} \tag{4.37}$$

Once again, the prefactors in (4.34) have been chosen such that all distributions enter the cross section with equal weight:

$$\frac{d\sigma}{\prod_{i=1}^2 dx_i d\bar{x}_i d^2\boldsymbol{q}_i} \sim \frac{1}{64}\left[{}^1F{}^1F + {}^AF{}^AF + {}^SF{}^SF + {}^{\overline{10}}F{}^{10}F + {}^{10}F{}^{\overline{10}}F + {}^{27}F{}^{27}F\right]\,. \tag{4.38}$$

4.2.3. Mixed distributions

What remains to be done is the color decomposition of the quark-gluon distributions, cf. figure 4.2, which is given by

$$\begin{aligned} F_{ii'}^{bb'} &= (x_2 p^+)^{-1} \langle\langle \left(\bar{q}_{4,i'} \Gamma_{a_1} q_{1,i}\right) \left(\Pi_{a_2} G_3^{b'} G_2^b\right) \rangle\rangle \\ &= \frac{1}{N(N^2-1)} \left[{}^1F \delta^{bb'} \delta_{ii'} - {}^AF \sqrt{2} f^{bb'c} t^c_{ii'} + \sqrt{\frac{2N^2}{N^2-4}} {}^SF d^{bb'c} t^c_{ii'} \right] \end{aligned} \tag{4.39}$$

with structure functions

$$\begin{aligned} (x_2 p^+)^1 F &= \langle\langle (\bar{q}_{4,i} \Gamma_{a_1} q_{1,i}) \left(\Pi_{a_2} G_3^b G_2^b\right) \rangle\rangle \\ (x_2 p^+)^A F &= \sqrt{2} \langle\langle \left(\bar{q}_{4,i'} \Gamma_{a_1} t^c_{i'i} q_{1,i}\right) \left(i f^{bb'c} \Pi_{a_2} G_3^{b'} G_2^b\right) \rangle\rangle \\ (x_2 p^+)^S F &= \sqrt{\frac{2N^2}{N^2-4}} \langle\langle \left(\bar{q}_{4,i'} \Gamma_{a_1} t^c_{i'i} q_{1,i}\right) \left(d^{bb'c} \Pi_{a_2} G_3^{b'} G_2^b\right) \rangle\rangle \ . \end{aligned} \tag{4.40}$$

4.3. Cross section for two hard scatters

In the following, we will derive the cross section for double Drell-Yan at the parton level and we will show how the dTMDs defined in the sections above enter the cross section. We will do the derivation for scalar partons in order to avoid having to write down all the indices associated with parton spin and we will also omit the color structure for the moment.

4.3.1. Derivation for scalar partons

We will now derive the cross section for the tree level double Drell-Yan process depicted in figure 4.1 for scalar partons. We work in a frame where $\boldsymbol{p} = \bar{\boldsymbol{p}} = 0$ and we take the virtualities $q_i^2 = 2q_i^+ q_i^- - \boldsymbol{q}_i^2$ of the produced gauge bosons to be large with $|\boldsymbol{q}_i| \ll q_i^+, q_i^-$. We will only consider the case where both virtualities, q_1^2 and q_2^2, are of comparable size. Now we define

$$x_i = q_i^+ / p^+ \,, \qquad\qquad \bar{x}_i = q_i^- / \bar{p}^- \,, \tag{4.41}$$

and approximate

$$q_i^2 \approx 2 q_i^+ q_i^- \approx x_i \bar{x}_i s \,, \tag{4.42}$$

with $s = (p + \bar{p})^2$ being the squared center of mass energy. The target mass can be neglected and therefore we have $s \approx 2p\bar{p} \approx 2p^+ \bar{p}^-$. The flux factor in the cross section is $1/(4p\bar{p})$. The

cross section for double Drell-Yan is then given by[1]

$$
\begin{aligned}
d\sigma = \frac{1}{C}\,\frac{1}{4p\bar{p}}\left[\prod_{i=1}^{2}\frac{d^4q_i}{(2\pi)^4}\right]\sum_{X,\bar{X}}\left[\prod_{j=1}^{m}\int\frac{d^3p_{X,j}}{(2\pi)^3 2p^0_{X,j}}\right]\left[\prod_{j=1}^{\bar{m}}\int\frac{d^3p_{\bar{X},j}}{(2\pi)^3 2p^0_{\bar{X},j}}\right] \\
\times\int\frac{d^4l_1}{(2\pi)^4}\,\frac{d^4\bar{l}_1}{(2\pi)^4}\,(2\pi)^4\delta^{(4)}(q_1-l_1-\bar{l}_1)\int\frac{d^4l_1'}{(2\pi)^4}\,\frac{d^4\bar{l}_1'}{(2\pi)^4}\,(2\pi)^4\delta^{(4)}(q_1-l_1'-\bar{l}_1') \\
\times(2\pi)^4\delta^{(4)}\Bigg(\sum_{i=1}^{2}q_i+\sum_{j=1}^{m}p_{X,j}+\sum_{j=1}^{\bar{m}}p_{\bar{X},j}-p-\bar{p}\Bigg)\left[\prod_{i=1}^{2}H_i(q_i,l_i,\bar{l}_i,l_i',\bar{l}_i')\right] \\
\times\left\langle p\middle|\bar{T}\left[\phi(0)\int d^4\xi_1'\,e^{-i\xi_1'l_1'}\,\phi(\xi_1')\right]\middle|X\right\rangle\left\langle X\middle|T\left[\phi(0)\int d^4\xi_1\,e^{i\xi_1 l_1}\,\phi(\xi_1)\right]\middle|p\right\rangle \\
\times\left\langle \bar{p}\middle|\bar{T}\left[\phi(0)\int d^4\bar{\xi}_1'\,e^{-i\bar{\xi}_1'\bar{l}_1'}\,\phi(\bar{\xi}_1')\right]\middle|\bar{X}\right\rangle\left\langle \bar{X}\middle|T\left[\phi(0)\int d^4\bar{\xi}_1\,e^{i\bar{\xi}_1\bar{l}_1}\,\phi(\bar{\xi}_1)\right]\middle|\bar{p}\right\rangle. \qquad (4.43)
\end{aligned}
$$

C is a combinatorial factor which is 2 if the hard scattering final states are identical and is 1 otherwise. The remnant X ($\bar{X}$) of proton p ($\bar{p}$) consists of m ($\bar{m}$) spectators with momenta $p_{X,j}$ ($p_{\bar{X},j}$) and H_i is the squared matrix element of the ith hard scatter, where the propagators of incoming parton lines are amputated.

As a next step, we rewrite the cross section in terms of the correlation functions defined in eq. (4.1). We first look at the sum over remnants X:

$$
\begin{aligned}
&\sum_X\left[\prod_{j=1}^{m}\int\frac{d^3p_{X,j}}{(2\pi)^3 2p^0_{X,j}}\right](2\pi)^4\delta^{(4)}\Bigg(\sum_{i=1}^{2}l_i+\sum_{j=1}^{m}p_{X,j}-p\Bigg) \\
&\quad\times\left\langle p\middle|\bar{T}\left[\phi(0)\int d^4\xi_1'\,e^{-i\xi_1'l_1'}\,\phi(\xi_1')\right]\middle|X\right\rangle\left\langle X\middle|T\left[\phi(0)\int d^4\xi_1\,e^{i\xi_1 l_1}\,\phi(\xi_1)\right]\middle|p\right\rangle \\
&=\sum_X\left[\prod_{j=1}^{m}\int\frac{d^3p_{X,j}}{(2\pi)^3 2p^0_{X,j}}\right]\int d^4\xi_2\,e^{-i\xi_2\left(p-\sum_{i=1}^{2}l_i-\sum_{j=1}^{m}p_{X,j}\right)}\,e^{i\xi_2\left(p-\sum_{j=1}^{m}p_{X,j}\right)} \\
&\quad\times\left\langle p\middle|\bar{T}\left[\phi(0)\int d^4\xi_1'\,e^{-i\xi_1'l_1'}\,\phi(\xi_1')\right]\middle|X\right\rangle\left\langle X\middle|T\left[\phi(\xi_2)\int d^4\xi_1\,e^{i\xi_1 l_1}\phi(\xi_1+\xi_2)\right]\middle|p\right\rangle \\
&=\sum_X\left[\prod_{j=1}^{m}\int\frac{d^3p_{X,j}}{(2\pi)^3 2p^0_{X,j}}\right] \\
&\quad\times\left\langle p\middle|\bar{T}\left[\phi(0)\int d^4\xi_1'\,e^{-i\xi_1'l_1'}\,\phi(\xi_1')\right]\middle|X\right\rangle\left\langle X\middle|T\left[\prod_{i=1}^{2}\int d^4\xi_i\,e^{i\xi_i l_i}\,\phi(\xi_i)\right]\middle|p\right\rangle \\
&=\int d^4\xi_1'\,e^{-i\xi_1'l_1'}\left[\prod_{i=1}^{2}\int d^4\xi_i\,e^{i\xi_i l_i}\right]\left\langle p\middle|\bar{T}\left[\phi(0)\phi(\xi_1')\right]T\left[\prod_{i=1}^{2}\phi(\xi_i)\right]\middle|p\right\rangle \\
&=(2\pi)^{12}\,\Phi(l_i,l_i'). \qquad (4.44)
\end{aligned}
$$

[1] This actually also describes all other double parton scattering processes, given that the difference essentially lies in the hard scattering matrix elements H_i.

An analogous relation can be used for the sum over remnants $\bar{X}$, and by rewriting

$$\begin{aligned}
&(2\pi)^4\delta^{(4)}\Big(\sum_{i=1}^{2} q_i + \sum_{j=1}^{m} p_{X,j} + \sum_{j=1}^{\bar{m}} p_{\bar{X},j} - p - \bar{p}\Big) \\
&\quad = \int \frac{d^4l_2}{(2\pi)^4}\,\frac{d^4\bar{l}_2}{(2\pi)^4}\,(2\pi)^4\delta^{(4)}\Big(\sum_{i=1}^{2} q_i - \sum_{i=1}^{2} l_i - \sum_{i=1}^{2} \bar{l}_i\Big) \\
&\qquad \times (2\pi)^4\delta^{(4)}\Big(\sum_{i=1}^{2} l_i + \sum_{j=1}^{m} p_{X,j} - p\Big)\,(2\pi)^4\delta^{(4)}\Big(\sum_{i=1}^{2} \bar{l}_i + \sum_{j=1}^{\bar{m}} p_{\bar{X},j} - \bar{p}\Big)\,, \qquad (4.45)
\end{aligned}$$

we can write down the cross section in terms of the parton correlation functions $\Phi(l_i, l_i')$ and $\bar{\Phi}(\bar{l}_i, \bar{l}_i')$, which then reads

$$\begin{aligned}
d\sigma &= \frac{1}{C}\,\frac{1}{4p\bar{p}}\left[\prod_{i=1}^{2}\frac{d^4q_i}{(2\pi)^4}\right]\left[\prod_{i=1}^{2}\int d^4l_i\,d^4\bar{l}_i\;(2\pi)^4\delta^{(4)}(q_i - l_i - \bar{l}_i)\right] \\
&\quad \times \int d^4l_1'\,d^4\bar{l}_1'\;(2\pi)^4\delta^{(4)}(q_1 - l_1' - \bar{l}_1') \\
&\quad \times \left[\prod_{i=1}^{2} H_i(q_i, l_i, \bar{l}_i, l_i', \bar{l}_i')\right]\Phi(l_i, l_i')\,\bar{\Phi}(\bar{l}_i, \bar{l}_i') \\
&= \frac{1}{C}\,\frac{1}{4p\bar{p}}\left[\prod_{i=1}^{2}\frac{d^4q_i}{(2\pi)^4}\right]\left[\prod_{i=1}^{2}\int d^4k_i\,d^4\bar{k}_i\;(2\pi)^4\delta^{(4)}(q_i - k_i - \bar{k}_i)\right] \\
&\quad \times \int d^4r\,d^4\bar{r}\;(2\pi)^4\delta^{(4)}(r + \bar{r}) \\
&\quad \times \left[\prod_{i=1}^{2} H_i(q_i, k_i, \bar{k}_i, r, \bar{r})\right]\Phi(k_i, r)\,\bar{\Phi}(\bar{k}_i, \bar{r})\,. \qquad (4.46)
\end{aligned}$$

In the last step of (4.46) we have switched to symmetric variables. Note that the momentum constraints for the final state momenta q_i do not involve r and $\bar{r}$, which will lead to considerable simplifications.

So far we have not made any approximations for the parton momenta in the derivation of the cross section. Making some specific approximations, we will see that we can express the cross section in terms of the dTMDs defined in section 4.1. As already mentioned, we only consider the case where both final state virtualities are of comparable size and we will denote them by $q_i^2 \sim Q^2$ in the following.

The partons emerging from both protons have small virtualities of order Λ^2. Given that the two protons have large momentum in the $+z$ and $-z$ direction, respectively, one obtains the following scaling of the parton momenta:

$$\begin{aligned}
k_i^+ \sim r^+ \sim p^+ \sim q_i^+ \sim Q\,, \qquad & \bar{k}_i^- \sim \bar{r}^- \sim \bar{p}^- \sim q_i^- \sim Q\,, \\
k_i^- \sim r^- \sim p^- \sim \Lambda^2/Q\,, \qquad & \bar{k}_i^+ \sim \bar{r}^+ \sim \bar{p}^+ \sim \Lambda^2/Q\,, \qquad (4.47)
\end{aligned}$$

and

$$|\boldsymbol{k}_i| \sim |\boldsymbol{r}| \sim |\bar{\boldsymbol{k}}_i| \sim |\bar{\boldsymbol{r}}| \sim |\boldsymbol{q}_i| \sim \Lambda\,. \tag{4.48}$$

Λ is the largest scale of the process that can still be considered small compared to Q. The scaling given above is, however, not true for r^+ and $\bar{r}^-$. The momentum conservation constraint for r and $\bar{r}$ in (4.46) enforces $r = -\bar{r}$ and therefore $r^+ \sim \bar{r}^- \sim \Lambda^2/Q$.
Given that $k_i^+ \gg \bar{k}_i^+$ and $k_i^- \ll \bar{k}_i^-$, we can neglect these small components in the remaining momentum conservation constraints in (4.46) and get

$$k_i^+ \approx q_i^+ \qquad\qquad \bar{k}_i^- \approx q_i^-\,. \tag{4.49}$$

After these approximations, the large longitudinal momenta of the partons are fixed by the final state kinematics. In the squared hard scattering matrix elements H_i we can neglect both the small longitudinal parton momenta and the transverse parton momenta, only leaving a dependence on the large longitudinal parton momenta which are fixed by the final state. Given that the H_i are boost invariant, they can only depend on $q_i^2 \approx 2q_i^+q_i^-$. All of the above leads to

$$\begin{aligned}
&\left[\prod_{i=1}^{2}\int dk_i^+ d\bar{k}_i^+\,\delta(q_i^+ - k_i^+ - \bar{k}_i^+)\int dk_i^- d\bar{k}_i^-\,\delta(q_i^- - k_i^- - \bar{k}_i^-)\right]\\
&\quad\times\int dr^+ d\bar{r}^+\,\delta(r^+ + \bar{r}^+)\int dr^- d\bar{r}^-\,\delta(r^- + \bar{r}^-)\\
&\quad\times\left[\prod_{i=1}^{2} H_i(q_i, k_i, \bar{k}_i, r, \bar{r})\right]\Phi(k_i, r)\,\bar{\Phi}(\bar{k}_i, \bar{r})\\
&= \left[\prod_{i=1}^{2}\int dk_i^+\,dk_i^-\right]\int dr^+\,dr^-\\
&\quad\times\left[\prod_{i=1}^{2} H_i(q_i, k_i, \bar{k}_i, r, \bar{r})\right]\Phi(k_i, r)\,\bar{\Phi}(\bar{k}_i, \bar{r})\Big|_{\substack{k_i^+ = q_i^+ - \bar{k}_i^+,\,\bar{r}^- = -r^-\\ \bar{k}_i^- = q_i^- - k_i^-,\,\bar{r}^+ = -r^+}}\\
&\approx \left[\prod_{i=1}^{2} H_i(q_i^2)\right]\left[\prod_{i=1}^{2}\int dk_i^-\right]\int dr^-\Phi(k_i, r)\Big|_{k_i^+ = q_i^+, r^+ = 0}\\
&\qquad\qquad\times\left[\prod_{i=1}^{2}\int d\bar{k}_i^+\right]\int d\bar{r}^+\bar{\Phi}(\bar{k}_i, \bar{r})\Big|_{\bar{k}_i^- = q_i^-, \bar{r}^- = 0}\,.
\end{aligned} \tag{4.50}$$

We now use this relation, rewrite $d^4q_i = p^+\bar{p}^- dx_i d\bar{x}_i d^2\boldsymbol{q}_i$, and use the definition of the scalar dTMD defined in (4.5) to obtain the final result for the cross section

$$\begin{aligned}
\frac{d\sigma}{\prod_{i=1}^{2} dx_i\,d\bar{x}_i\,d^2\boldsymbol{q}_i} &= \frac{1}{C}\left[\prod_{i=1}^{2}\hat{\sigma}_i(x_i\bar{x}_i s)\right]\left[\prod_{i=1}^{2}\int d^2\boldsymbol{k}_i\,d^2\bar{\boldsymbol{k}}_i\,\delta^{(2)}(\boldsymbol{q}_i - \boldsymbol{k}_i - \bar{\boldsymbol{k}}_i)\right]\\
&\quad\times\left[\int\frac{d^2\boldsymbol{r}}{(2\pi)^2}\right]F(x_i, \boldsymbol{k}_i, \boldsymbol{r})\,F(\bar{x}_i, \bar{\boldsymbol{k}}_i, -\boldsymbol{r})\,,
\end{aligned} \tag{4.51}$$

where we have introduced the cross section

$$\hat{\sigma}_i(q_i^2) = \frac{1}{2q_i^2}\, H_i(q_i^2) \tag{4.52}$$

for the ith parton-level subprocess and used the approximation (4.42). The integration over $\bar{\boldsymbol{r}}$ has been done using the momentum constraint $\boldsymbol{r} = -\bar{\boldsymbol{r}}$. For interpreting the result physically, it is instructive to partially or completely Fourier transform it to postion space. Fourier transforming the $\boldsymbol{r}$ dependence gives

$$\begin{aligned}\frac{d\sigma}{\prod_{i=1}^2 dx_i\, d\bar{x}_i\, d^2\boldsymbol{q}_i} = \frac{1}{C}\left[\prod_{i=1}^2 \hat{\sigma}_i(x_i\bar{x}_i s)\right]\left[\prod_{i=1}^2 \int d^2\boldsymbol{k}_i\, d^2\bar{\boldsymbol{k}}_i\; \delta^{(2)}(\boldsymbol{q}_i - \boldsymbol{k}_i - \bar{\boldsymbol{k}}_i)\right] \\ \times \int d^2\boldsymbol{y} F(x_i, \boldsymbol{k}_i, \boldsymbol{y})\, F(\bar{x}_i, \bar{\boldsymbol{k}}_i, \boldsymbol{y})\end{aligned} \tag{4.53}$$

Note that while in (4.51) the dTMDs are evaluated at opposite values of $\boldsymbol{r}$, they are now evaluated at the same value of $\boldsymbol{y}$. Completely transforming to position space yields

$$\begin{aligned}\frac{d\sigma}{\prod_{i=1}^2 dx_i\, d\bar{x}_i\, d^2\boldsymbol{q}_i} = \frac{1}{C}\left[\prod_{i=1}^2 \hat{\sigma}_i(x_i\bar{x}_i s)\right]\left[\prod_{i=1}^2 \int \frac{d^2\boldsymbol{z}_i}{(2\pi)^2}\, e^{-i\boldsymbol{z}_i\boldsymbol{q}_i}\right] \\ \times \int d^2\boldsymbol{y} F(x_i, \boldsymbol{z}_i, \boldsymbol{y})\, F(\bar{x}_i, \boldsymbol{z}_i, \boldsymbol{y})\,,\end{aligned} \tag{4.54}$$

and now the two dTMDs are evaluated at equal position arguments, as one would expect: For the hard scatters (which are approximately local in position space) to occur the parton positions of the right-and left-moving proton have to match.

4.3.2. Cross section for quarks and antiquarks

We will not repeat every step of the previous derivation for the case of quarks and antiquarks, but will instead only state the main differences and give the result for the cross section. We define the partonic cross section for the production of an electroweak gauge boson by the annihilation of a right-moving quark and a left-moving antiquark as [9]

$$\hat{\sigma}_{i,a\bar{a}} = \frac{1}{2q_i^2}\left[P_a(k_i)\right]_{\alpha\beta}\left[P_{\bar{a}}(\bar{k}_i)\right]_{\bar{\beta}\bar{\alpha}} H_{i,\beta\alpha\bar{\alpha}\bar{\beta}}\,, \tag{4.55}$$

where P_a and $P_{\bar{a}}$ are spin projectors defined as

$$P_q(k) = P_{\bar{q}}(k) = \tfrac{1}{2}\not{k}_c\,, \quad P_{\Delta q}(k) = -P_{\Delta\bar{q}}(k) = \tfrac{1}{2}\gamma_5\not{k}_c\,, \quad P^j_{\delta q}(k) = P^j_{\delta\bar{q}}(k) = \tfrac{1}{2}\gamma_5\not{k}_c\gamma^j\,. \tag{4.56}$$

Here, k_c is the collinear approximation of k, i.e. we have $k_c = (k^+, 0, \mathbf{0})$ for right-moving partons and $k_c = (0, k^-, \mathbf{0})$ for left-moving ones.
Assembling all pieces we can now write down the cross section for the double Drell-Yan production of two electroweak gauge bosons, taking graphs (a) and (b) of figure 4.4 as an

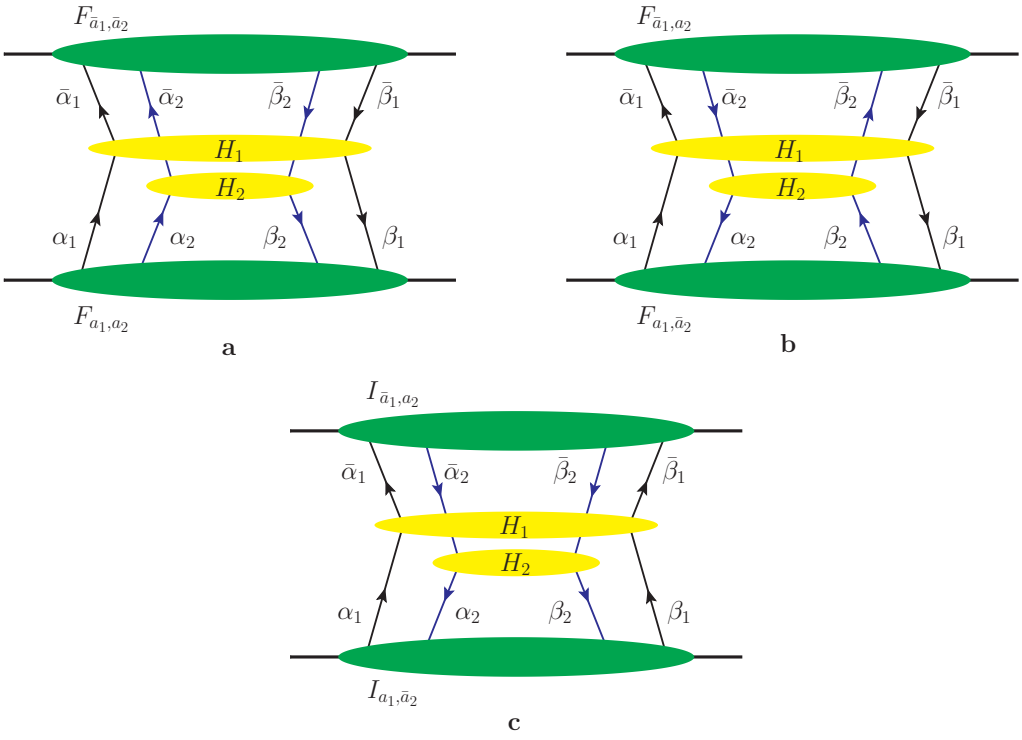

Figure 4.4.: Examples for possible parton combinations in double parton scattering

example,

$$\frac{d\sigma}{\prod_{i=1}^{2} dx_i d\bar{x}_i d^2\boldsymbol{q}_i} = \frac{1}{C} \sum_{\substack{a_1,a_2=q,\Delta q,\delta q \\ \bar{a}_1,\bar{a}_2=\bar{q},\Delta\bar{q},\delta\bar{q}}} \left[\prod_{i=1}^{2} \int d^2\boldsymbol{k}_i d^2\bar{\boldsymbol{k}}_i \delta^{(2)}(\boldsymbol{q}_i - \boldsymbol{k}_i - \bar{\boldsymbol{k}}_i)\right]$$
$$\times \int d^2\boldsymbol{y} \left[\hat{\sigma}_{1,a_1\bar{a}_1}(x_1\bar{x}_1 s)\hat{\sigma}_{2,a_2\bar{a}_2}(x_2\bar{x}_2 s) F_{a_1a_2}(x_i,\boldsymbol{k}_i,\boldsymbol{y}) F_{\bar{a}_1\bar{a}_2}(\bar{x}_i,\bar{\boldsymbol{k}}_i,\boldsymbol{y})\right.$$
$$\left. + \hat{\sigma}_{1,a_1\bar{a}_1}(x_1\bar{x}_1 s)\hat{\sigma}_{2,\bar{a}_2a_2}(x_2\bar{x}_2 s) F_{a_1\bar{a}_2}(x_i,\boldsymbol{k}_i,\boldsymbol{y}) F_{\bar{a}_1a_2}(\bar{x}_i,\bar{\boldsymbol{k}}_i,\boldsymbol{y})\right] , \tag{4.57}$$

where C again is a statistical factor that is 2 if the final states of the two hard scatters are identical and 1 otherwise. In contrast to the cross section for scalar partons, the cross section now depends on the polarization of the partons, even if we average over polarizations of the parent hadron. There are additional diagrams that contribute to the cross section we have not discussed so far. One such example is given in graph (c) of figure 4.4. In that graph, we see that quarks entering the hard scattering in the amplitude are antiquarks in the conjugate and vice versa. The emergence of such graphs is a completely new feature compared with single parton scattering, where these graphs are forbidden by fermion number conservation. The contribution of these graphs to the cross section involves the so-called interference distributions we have defined in section 4.1, which do not admit a probability interpretation but rather represent interference terms in fermion number.

Given that a quark in the amplitude becomes an antiquark in the conjugate, the quark and antiquark labels in the Dirac matrices do not have a physical meaning but are pure convention, and we will choose the labels such that they represent the parton in the amplitude. The graph in figure 4.4(c) contributes to the cross section as

$$\begin{aligned}\left.\frac{d\sigma}{\prod_{i=1}^{2} dx_i\, d\bar{x}_i\, d^2\boldsymbol{q}_i}\right|_{\text{fig. 4.4(c)}} &= \frac{1}{C} \sum_{\substack{a_1,a_2=q,\Delta q,\delta q\\ \bar{a}_1,\bar{a}_2=\bar{q},\Delta\bar{q},\delta\bar{q}}} H_{1,\,\alpha_1\beta_1\bar{\alpha}_1\bar{\beta}_1}(k_1,\bar{k}_1)\left[P_{a_1}(k_1)\right]_{\alpha_1\beta_2}\left[P_{\bar{a}_2}(k_2)\right]_{\beta_1\alpha_2} \\ &\times H_{2,\,\alpha_2\beta_2\bar{\alpha}_2\bar{\beta}_2}(k_2,\bar{k}_2)\left[P_{\bar{a}_1}(\bar{k}_1)\right]_{\bar{\beta}_2\bar{\alpha}_1}\left[P_{a_2}(\bar{k}_2)\right]_{\bar{\alpha}_2\bar{\beta}_1} \\ &\times \left[\prod_{i=1}^{2}\int d^2\boldsymbol{k}_i\, d^2\bar{\boldsymbol{k}}_i\, \delta^{(2)}(\boldsymbol{q}_i-\boldsymbol{k}_i-\bar{\boldsymbol{k}}_i)\right]\int d^2\boldsymbol{y}\, I_{a_1,\bar{a}_2}(x_i,\boldsymbol{k}_i,\boldsymbol{y})\, I_{\bar{a}_1,a_2}(\bar{x}_i,\bar{\boldsymbol{k}}_i,\boldsymbol{y})\,. \end{aligned} \tag{4.58}$$

In contrast to the previous cases we cannot define seperate partonic cross sections here because the two hard scattering kernels H_i are tied together via the spin projectors P.
Interference in fermion number is, however, not the only possibility for interference terms. Taking different quark flavors into account, there may also be interference in quark flavor. Some of the graphs that involve such intereference terms are given in figure 4.5. For example looking at graph (a), we see that an up quark in the amplitude is a down quark in the conjugate and vice versa.
For calculating QCD background signals, it is important to study whether these interference terms are of relevant size or not. At least for small values of x_i, both types of interference distributions should be relatively small, cf. section 2.5 of [9].

4.3.3. Comparison of single and double parton scattering

The approximations used in the last sections give a factorized form of the cross section, which is correct up to power corrections in Λ/Q, where Λ is a hadronic mass scale and Q is the large scale of the process. For double Drell-Yan, Q is given by the invariant mass of the gauge bosons produced.[2] We will now compare how the leading single and double parton scattering cross sections scale with Λ and Q and compare their behaviors to one another.
The mass dimension of the distribution functions is -2. Given that the dTMDs are invariant under a boost along the z axis, we can boost into the rest frame of the proton and obtain a power behavior $F(x_i,\boldsymbol{k}_i,\boldsymbol{y})\sim\Lambda^{-2}$. The single-particle cross sections $\hat{\sigma}_i$ behave like $\hat{\sigma}_i\sim Q^{-2}$ and we have $d^2\boldsymbol{k}_i d^2\bar{\boldsymbol{k}}_i\delta^{(2)}(\boldsymbol{q}_i-\boldsymbol{k}_i-\bar{\boldsymbol{k}}_i)\sim\Lambda^2$. The transverse distance $\boldsymbol{y}$ is, generically, of hadronic size and therefore we can assume $d^2\boldsymbol{y}\sim\Lambda^{-2}$. With this behavior of the individual parts, one obtains the following power behavior for the cross section:

$$\left.\frac{d\sigma}{\prod_{i=1}^{2} dx_i d\bar{x}_i d^2\boldsymbol{q}_i}\right|_{\text{double}} \sim \frac{1}{\Lambda^2 Q^4}\ . \tag{4.59}$$

Now, we introduce the abbreviations

$$x = x_1 + x_2\ ,\quad \bar{x} = \bar{x}_1 + \bar{x}_2\ ,\quad q = q_1 + q_2\ , \tag{4.60}$$

[2] We here only consider the case where the invariant masses of both gauge bosons are of comparable size

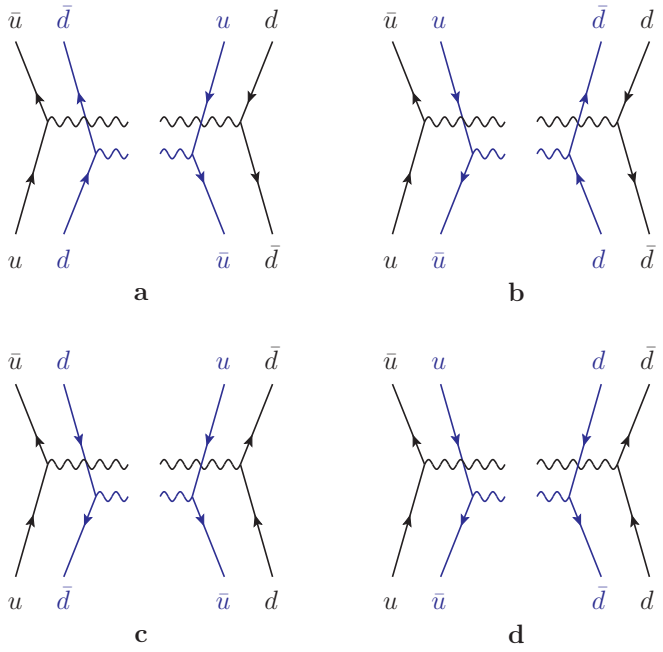

Figure 4.5.: Examples for interference in quark flavor. The blobs depicting the hadron matrix elements are not shown.

in order to compare the cross section of double parton scattering with the one for single parton scattering. The cross section for the latter is

$$\left.\frac{d\sigma}{dx\,d\bar{x}\,d^2\boldsymbol{q}}\right|_{\text{single}} = \hat{\sigma}(x\bar{x}s)\int d^2\boldsymbol{k}\,d^2\bar{\boldsymbol{k}}\,\delta^{(2)}(\boldsymbol{q}-\boldsymbol{k}-\bar{\boldsymbol{k}})\,f(x,\boldsymbol{k})\,\bar{f}(\bar{x},\bar{\boldsymbol{k}})\;, \tag{4.61}$$

with transverse momentum dependent single parton distributions $f(x,\boldsymbol{k})$ and $\bar{f}(\bar{x},\bar{\boldsymbol{k}})$ and the parton-parton scattering cross section $\hat{\sigma}$. We now make the single parton scattering cross section differential in the internal momentum variables of the final state,

$$u_1 = \frac{x_1}{x} = \frac{q_1^+}{q^+}\,, \qquad \bar{u}_1 = \frac{\bar{x}_1}{\bar{x}} = \frac{q_1^-}{q^-}\,, \tag{4.62}$$

and get

$$\left.\frac{d\sigma}{\prod_{i=1}^2 dx_i\,d\bar{x}_i\,d^2\boldsymbol{q}_i}\right|_{\text{single}} = \frac{d\hat{\sigma}}{x\bar{x}\,du_1\,d\bar{u}_1\,d^2\boldsymbol{q}_1}\int d^2\boldsymbol{k}\,d^2\bar{\boldsymbol{k}}\,\delta^{(2)}(\boldsymbol{q}-\boldsymbol{k}-\bar{\boldsymbol{k}})\,f(x,\boldsymbol{k})\,\bar{f}(\bar{x},\bar{\boldsymbol{k}})\,. \tag{4.63}$$

For the TMDs we have $f(x,\boldsymbol{k})$, $\bar{f}(\bar{x},\bar{\boldsymbol{k}}) \sim \Lambda^{-2}$ and the differential hard scattering cross section on the r.h.s. behaves as Q^{-4}. This leads to the power behavior

$$\left.\frac{d\sigma}{\prod_{i=1}^2 dx_i\,d\bar{x}_i\,d^2\boldsymbol{q}_i}\right|_{\text{single}} \sim \frac{1}{\Lambda^2 Q^4}\;. \tag{4.64}$$

This shows that cross sections for single and double parton scattering that are differential in the transverse momenta show the same power behavior in Q, i.e. the double parton scattering processes are not power suppressed.

We will now turn to cross sections integrated over transverse momenta. In this case, the difference between single and double parton scattering lies in the constraints on transverse momenta. While each transverse momentum $\boldsymbol{q}_i$ is subject to the constraint $\boldsymbol{q}_i = \boldsymbol{k}_i + \bar{\boldsymbol{k}}_i$ in the case of double parton scattering and therefore limited to be of size Λ, each of the transverse momenta $\boldsymbol{q}_i$ may be of size Q and only their sum $\boldsymbol{q}$ has to fullfill $\boldsymbol{q} = \boldsymbol{k} + \bar{\boldsymbol{k}}$ in the case of single parton scattering. Consequently, the phase space volumes are

$$\prod_{i=1}^{2} d^2\boldsymbol{q}_i \sim \Lambda^4 \tag{4.65}$$

for double parton scattering and

$$\prod_{i=1}^{2} d^2\boldsymbol{q}_i \sim \Lambda^2 Q^2 \tag{4.66}$$

for single parton scattering, respectively. The cross sections integrated over transverse momenta therefore behave like

$$\left.\frac{d\sigma}{\prod_{i=1}^{2} dx_i d\bar{x}_i}\right|_{\text{double}} \sim \frac{\Lambda^2}{Q^4} \,, \qquad \left.\frac{d\sigma}{\prod_{i=1}^{2} dx_i d\bar{x}_i}\right|_{\text{single}} \sim \frac{1}{Q^2} \,. \tag{4.67}$$

That means, that double scattering is now power suppressed compared with single parton scattering, and only gives power corrections in Λ^2/Q^2 to the latter.

The important result is that while double parton scattering is power suppressed in transverse momentum integrated cross sections, this is not the case for cross sections differential in transverse momenta. Note that dTMDs rise faster at small values of momentum fraction x than single parton distributions (cf. chapter 2.5 of [9]). With the high center of mass energies the LHC provides, typical values of x_i and $\bar{x}_i$ become quite small at a given process scale Q^2. Together with the fact that double parton scattering is not power suppressed compared with single parton scattering, this leads to the conclusion that multiparton scattering may give sizeable contributions to various processes.

Under some quite strong assumptions concerning the nature of double parton scattering which we will discuss in the next section, estimates about the size of the contribution of double parton scattering to the cross section have been made quite some time ago, see e.g. [28]. For the double $\mu^+\mu^-$ production via the double Drell-Yan process or double J/Ψ production, these estimates predict:

double Drell-Yan	DPS	SPS
7 TeV	0.08 fb	0.43 fb
14 TeV	0.16 fb	0.68 fb

double J/Ψ production	DPS	SPS
7 TeV	3.16 fb	1.70 fb
14 TeV	7.69 fb	2.62 fb

These estimates show that double parton scattering will indeed give sizeable contributions to the cross section of certain processes. At the same time it becomes clear that the double Drell-Yan process might not have the biggest rate. Given that there are serious complications with QCD factorization when there are hadrons in the final state even for single parton scattering [12], the treatment of processes like the double J/Ψ production will have to wait until these issues are settled. The double Drell-Yan process, though predicted to have a much smaller cross section, serves as an ideal testing ground for the development of the theory of multiparton scattering as its single parton scattering counterpart is completely understood, see e.g. [5].

4.4. Phenomenology: State of the art

In the previous sections we have seen that double parton scattering gives rise to a rich spin and color structure and even to effects that have not been present in single parton scattering, such as the interference in fermion and flavor number described above. We will conclude this chapter by stating the current state of the art of implementing double parton scattering into the analysis of experimental data.
For the analysis of experimental data, it is usually assumed that the double parton scattering cross section can be factorized in the following way

$$\sigma_{\mathrm{DPS}} = \frac{\sigma_1 \sigma_2}{C \sigma_{\mathrm{eff}}} \,, \tag{4.68}$$

where C is a combinatorial factor, σ_1 and σ_2 are single hard scattering cross sections and σ_{eff} is called the "effective cross section" that characterizes the strength of double parton interactions and is assumed to be an universal constant for all processes. As stated in chapter 2.6 of [9], there are some quite strong assumptions that have to be made in order to arrive at this form of the cross section from the results we have given above. In particular:

- Looking at a typical matrix element $\langle p|\mathcal{O}(0,z_2)\mathcal{O}(y,z_1)|p\rangle$ in a dTMD, we can insert a full set of states and get $\sum_X \langle p|\mathcal{O}(0,z_2)|X\rangle\langle X|\mathcal{O}(y,z_1)|p\rangle$. If one now assumes that the proton state is the dominant one, one can drop all other states in the sum over X and arrives at the product of two single parton distributions.[3]

- There are no correlations between different partons inside the hadron.

- One has to assume that the dependence of single parton distributions in the impact-parameter representation on longitudinal momentum fraction and impact parameter factorizes as $f_c(x,\boldsymbol{b}) \approx F(\boldsymbol{b}) f_c(x)$ with an impact parameter profile $F(\boldsymbol{b})$ that is the same for all parton species c.

- For cross sections differential in transverse momenta one further has to restrict the analysis to the region of measured transverse momenta $\boldsymbol{q}_i$, where the $\boldsymbol{q}_i$ are large compared to a typical hadronic scale Λ but still are small compared to the large scale Q.

[3] This statement is somehow oversimplified as there are more complications, but catches the main idea. For a more detailed treatment, we refer the reader to section 2.1.5 of [9]

Hence, there are lots of possibilities how the assumption (4.68) could be invalidated. Despite being a reasonable first approximation for estimating the contribution of double parton scattering, this well might be not enough when it comes to precision measurements and calculations needed to subtract the QCD background from a potential signal from physics beyond the Standard Model.

5. Perturbative splitting in double parton distributions

In the previous chapter we have always assumed that the transverse momenta of the produced gauge bosons $\boldsymbol{q}_i$ are small and comparable to a typical hadronic scale Λ. When we allow the transverse momenta of the gauge bosons to be much larger than Λ (i.e. in the perturbative regime), but still require them to be much smaller than the large scale Q of the process, we have the following three-scale hierarchy:

$$\Lambda \ll |\boldsymbol{q}_1|,\, |\boldsymbol{q}_2| \sim q_T \ll Q\,. \tag{5.1}$$

Large boson transverse momenta require that at least some of the parton transverse momenta have to be large, and we study one particular mechanism that generates large parton transverse momenta in the following.

One possibility to generate large transverse momenta of a parton pair is that they arise out of the splitting of another parton with low transverse momentum. As the $\boldsymbol{q}_i$ are taken to be in the perturbative regime, one can calculate this splitting perturbatively, adding a lot of predictive power. Note that a parton pair arising out of a perturbative splitting is of course strongly correlated, which immediately invalidates one of the assumptions given in section 4.4 needed to arrive at the simple form (4.68) of the double parton scattering cross section. It is therefore of great interest, whether such parton splittings give sizeable contributions to the cross section.

The following calculations have been checked independently by Markus Diehl and the results have been published in [9, chapter 5.2].

5.1. Calculation of the splitting contributions

We will now calculate the contribution of such splittings to several dTMDs, and we will start with the splitting of a gluon into a quark-antiquark pair shown in figure 5.1, which contributes to the quark-antiquark dTMD $F_{a_1,\bar{a}_2}$.
Calculating the color factors for figure 5.1 (see appendix B for the explicit calculation), we find that the color octet distributions are suppressed by a factor

$$\left.\frac{{}^8F_{a_1,\bar{a}_2}}{{}^1F_{a_1,\bar{a}_2}}\right|_{g\to q\bar{q}} = -\frac{1}{\sqrt{N^2-1}}\,. \tag{5.2}$$

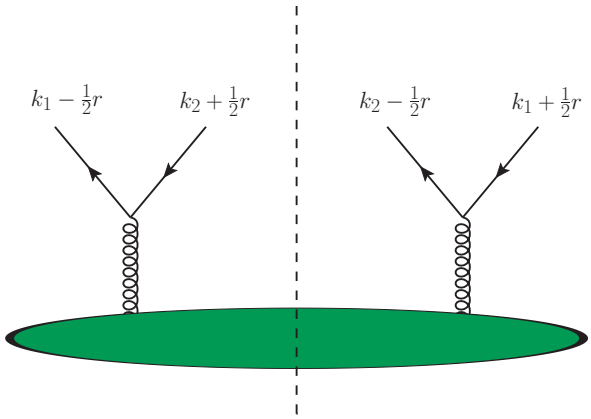

Figure 5.1.: Splitting of a gluon into a quark antiquark pair

We will now calculate the color singlet distributions, which are given by

$$\begin{aligned} {}^1F_{a_1,\bar{a}_2}(x_i,\boldsymbol{k}_i,\boldsymbol{r})\Big|_{g\to q\bar{q}} &= \frac{4\pi\alpha_s}{(2\pi)^5}\,\frac{1}{2}\,2p^+\int dr^-\,dk_1^-\,dk_2^-\;\Phi^g_{\alpha\beta}(k_1+k_2) \\ &\times \mathrm{tr}\Bigg[\Gamma_{a_1}\,\frac{(k_1-\frac{1}{2}r)\gamma}{(k_1-\frac{1}{2}r)^2+i\epsilon}\,\gamma^\alpha\,\frac{(k_2+\frac{1}{2}r)\gamma}{(k_2+\frac{1}{2}r)^2+i\epsilon} \\ &\quad\times\Gamma_{\bar{a}_2}\,\frac{(k_2-\frac{1}{2}r)\gamma}{(k_2-\frac{1}{2}r)^2-i\epsilon}\,\gamma^\beta\,\frac{(k_1+\frac{1}{2}r)\gamma}{(k_1+\frac{1}{2}r)^2-i\epsilon}\Bigg]_{k_2^-=-k_1^-,\,\boldsymbol{k}_2=-\boldsymbol{k}_1}\,, \end{aligned} \tag{5.3}$$

where α and β are the polarization indices of the gluons to the left- and right-hand side of the cut, and Φ^g is the single gluon correlation function, which is the single gluon analogue of the two gluon correlation function discussed in section 4.1.5. We have already summed over color indices and the color trace has given a factor 1/2. As discussed in section 4.1.5, α and β are transverse at leading power. The second and third line in (5.3) represent the perturbative splitting, where we have made the approximation that the minus and transverse momenta of the incoming gluon are much smaller than the minus and transverse momenta of the produced partons due to the splitting being perturbative. The sum of k_1 and k_2 is therefore much smaller than their difference. Now we introduce

$$k = \frac{1}{2}(k_1 - k_2)\,, \qquad\qquad \kappa = k_1 + k_2 \tag{5.4}$$

and change integration variables to k^- and κ^-. As κ^- can be neglected in the hard part, the integration over κ^- then only concerns Φ^g, which then yields [27]

$$xp^+\int d\kappa^-\Phi^{g,jj'}(\kappa)\Big|_{\kappa^+=xp^+} = \frac{1}{2}\,\delta^{jj'}f_1^g(x,\boldsymbol{\kappa}) + \frac{2\boldsymbol{\kappa}^j\boldsymbol{\kappa}^{j'}-\delta^{jj'}\boldsymbol{\kappa}^2}{4M^2}\,h_1^{\perp g}(x,\boldsymbol{\kappa})\,, \tag{5.5}$$

with M being the mass of the proton. This can also be expressed in terms of the operators

we have introduced in section 4.1.5, which read

$$f_1^g(x,\boldsymbol{\kappa}) = \frac{1}{xp^+}\int \frac{dz^- d^2\boldsymbol{z}}{(2\pi)^3}\, e^{ixz^-p^+ - i\boldsymbol{z}\boldsymbol{\kappa}} \left\langle p\right| \mathcal{O}_g(0,z)\left|p\right\rangle ,$$
$$\frac{2\boldsymbol{\kappa}^j\boldsymbol{\kappa}^{j'} - \delta^{jj'}\boldsymbol{\kappa}^2}{4M^2}\, h_1^{\perp g}(x,\boldsymbol{\kappa}) = \frac{1}{xp^+}\int \frac{dz^- d^2\boldsymbol{z}}{(2\pi)^3}\, e^{ixz^-p^+ - i\boldsymbol{z}\boldsymbol{\kappa}} \left\langle p\right| \mathcal{O}^{jj'}_{\delta g}(0,z)\left|p\right\rangle . \tag{5.6}$$

f_1^g is the usual transverse momentum dependent density of gluons, whereas the gluon Boer-Mulders function $h_1^{\perp g}$ describes linearly polarized gluons and is essentially unknown at present. Now we rewrite the propagator denominators in equation (5.3) as

$$\begin{aligned}&\frac{1}{2x_1p^+\big(k-\frac{1}{2}r\big)^- - \big(\boldsymbol{k}-\frac{1}{2}\boldsymbol{r}\big)^2 + i\epsilon}\,\frac{1}{2x_2p^+\big(k-\frac{1}{2}r\big)^- + \big(\boldsymbol{k}-\frac{1}{2}\boldsymbol{r}\big)^2 - i\epsilon}\\ \times\,&\frac{1}{2x_2p^+\big(k+\frac{1}{2}r\big)^- + \big(\boldsymbol{k}+\frac{1}{2}\boldsymbol{r}\big)^2 + i\epsilon}\,\frac{1}{2x_1p^+\big(k+\frac{1}{2}r\big)^- - \big(\boldsymbol{k}+\frac{1}{2}\boldsymbol{r}\big)^2 - i\epsilon}\end{aligned} \tag{5.7}$$

and change variables to $(k-\frac{1}{2}r)^-$ and $(k+\frac{1}{2}r)^-$, after which the integrals over minus momenta can be easily performed using Cauchy's theorem. The fermion trace in equation (5.3) can be calculated e.g. with FORM [29]. The final result for the splitting contribution can be cast into the following form:

$$\begin{aligned}{}^1F_{a_1,\bar a_2}(x_i,\boldsymbol{k}_i,\boldsymbol{r})\Big|_{g\to q\bar q} = \frac{\alpha_s}{4\pi^2}\Bigg[&\frac{f_1^g(x_1+x_2,\boldsymbol{\kappa})}{x_1+x_2}\, T^{ll'}_{a_1,\bar a_2}\bigg(\frac{x_1}{x_1+x_2}\bigg) + \frac{2\boldsymbol{\kappa}^m\boldsymbol{\kappa}^{m'} - \delta^{mm'}\boldsymbol{\kappa}^2}{2M^2}\\ \times\,&\frac{h_1^{\perp g}(x_1+x_2,\boldsymbol{\kappa})}{x_1+x_2}\, U^{ll'mm'}_{a_1,\bar a_2}\bigg(\frac{x_1}{x_1+x_2}\bigg)\Bigg]\frac{\big(\boldsymbol{k}+\frac{1}{2}\boldsymbol{r}\big)^l\big(\boldsymbol{k}-\frac{1}{2}\boldsymbol{r}\big)^{l'}}{\big(\boldsymbol{k}+\frac{1}{2}\boldsymbol{r}\big)^2\big(\boldsymbol{k}-\frac{1}{2}\boldsymbol{r}\big)^2}.\end{aligned} \tag{5.8}$$

With the abbreviations $u = x_1/(x_1+x_2)$ and $\bar u = 1-u$ the kernels T and U read

$$\begin{aligned}T^{ll'}_{q,\bar q}(u) &= -T^{ll'}_{\Delta q,\Delta\bar q}(u) = \delta^{ll'}\,(u^2+\bar u^2),\\ T^{ll'}_{\Delta q,\bar q}(u) &= -T^{ll'}_{q,\Delta\bar q}(u) \;\; = i\epsilon^{ll'}\,(u-\bar u),\\ \big[T^{ll'}_{\delta q,\delta\bar q}(u)\big]^{jj'} &= -2\,\delta^{ll'}\,\delta^{jj'}\,u\bar u\end{aligned} \tag{5.9}$$

and

$$\begin{aligned}U^{ll'mm'}_{q,\bar q}(u) &= -U^{ll'mm'}_{\Delta q,\Delta\bar q}(u) = -2\tau^{ll',mm'}\,u\bar u\,,\\ \big[U^{ll'mm'}_{\delta q,\delta\bar q}(u)\big]^{jj'} &= 2\tau^{ll',j'm'}\,\delta^{jm}\,u + 2\tau^{ll',jm'}\,\delta^{j'm}\,\bar u - 2\tau^{ll',mm'}\,\delta^{jj'}u\bar u\,,\end{aligned} \tag{5.10}$$

where j and j' are the indices of the Dirac matrices $i\sigma^{+j}\gamma_5$ in the definitions of the dTMDs of transversely polarized quarks and antiquarks. All other kernels are zero.

The splitting of a gluon into a quark-antiquark pair also gives a contribution to the interference distribution $I_{a_1,\bar a_2}$ in fermion number, where the color octet distributions are also suppressed by a factor ${}^8I_{a_1,\bar a_2}/\,{}^1I_{a_1,\bar a_2} = -1/\sqrt{N^2-1}$. We once again calculate the contribution to the color singlet distribution. See appendix B for the explicit calculation of the color factors. The expression for ${}^1I_{a_1,\bar a_2}$ can be obtained from the one in (5.3) by interchanging $(k_2-\frac{1}{2}r)\gamma$ and

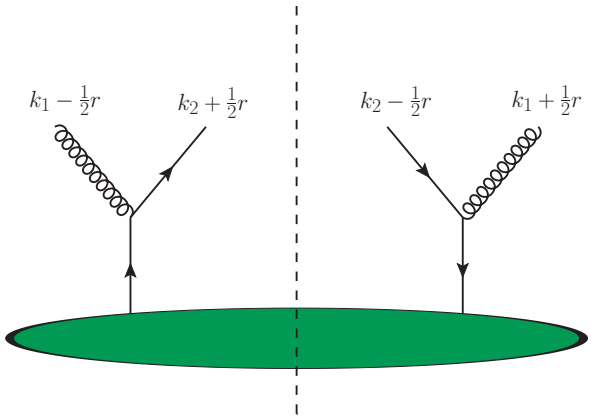

Figure 5.2.: Splitting of a quark into a quark and a gluon

$(k_1 + \frac{1}{2}r)\gamma$ in the fermion trace (which is equivalent to interchanging the quark and antiquark line on the r.h.s. of the cut in figure 5.1). The result has the same structure as in (5.8), with the kernels $T_{a_1,\bar{a}_2}$ replaced by

$$\begin{aligned} V^{ll'}_{q,\bar{q}}(u) &= -V^{ll'}_{\Delta q,\Delta\bar{q}}(u) = -2\delta^{ll'}\, u\bar{u}\,, \\ \big[V^{ll'}_{\delta q,\delta\bar{q}}(u)\big]^{jj'} &= \delta^{ll'}\delta^{jj'}(u^2+\bar{u}^2) + (\delta^{jl}\delta^{j'l'} - \delta^{jl'}\delta^{j'l})(u-\bar{u}) \end{aligned} \tag{5.11}$$

and the kernels $U_{a_1,\bar{a}_2}$ replaced by

$$\begin{aligned} W^{ll'mm'}_{q,\bar{q}}(u) &= -W^{ll'mm'}_{\Delta q,\Delta\bar{q}}(u) = \tau^{ll',mm'}(u^2+\bar{u}^2)\,, \\ W^{ll'mm'}_{\Delta q,\bar{q}}(u) &= -W^{ll'mm'}_{q,\Delta\bar{q}}(u) = \tau^{ll',mn}\, i\epsilon^{m'n}(u-\bar{u})\,, \\ \big[W^{ll'mm'}_{\delta q,\delta\bar{q}}(u)\big]^{jj'} &= -\big(\delta^{jl'}\delta^{j'm}\delta^{lm'} + \delta^{j'l}\delta^{jm}\delta^{l'm'}\big)\,u - \big(\delta^{jl}\delta^{j'm}\delta^{l'm'} + \delta^{j'l'}\delta^{jm}\delta^{lm'}\big)\,\bar{u} \\ &\quad + (\tau^{jj',mm'}\delta^{ll'} + \tau^{ll',mm'}\delta^{jj'})(u^2+\bar{u}^2)\,. \end{aligned} \tag{5.12}$$

All other kernels are zero. From this result it can be seen that the splitting contributions to the distributions $F_{a_1,\bar{a}_2}$ and $I_{a_1,\bar{a}_2}$ are generically of the same size. Thus the contribution from interference terms to the cross section could be relevant if it turns out that the contribution of such splitting graphs is sizeable.

We will now calculate the contribution of a splitting of a quark into a quark and a gluon to the quark-gluon dTMD shown in figure 5.2. This graph involves propagators for the outgoing gluons and requires a choice of gauge. If we work in the light-cone gauge $An = A^+ = 0$ with $n = (1,0,0,-1)/\sqrt{2}$ the gluon propagator has a numerator

$$D^{\alpha\beta}(\ell) = -g^{\alpha\beta} + \frac{n^\alpha \ell^\beta + \ell^\alpha n^\beta}{\ell^+} \tag{5.13}$$

and the splitting contribution to the color singlet quark-gluon distribution is given by

$$
\begin{aligned}
{}^1F_{a_1,a_2}(x_i,\boldsymbol{k}_i,\boldsymbol{r})\Big|_{q\to gq} &= \frac{4\pi\alpha_s}{(2\pi)^5}\,C_F\,(x_1p^+)\,2p^+\int dr^-\,dk_1^-\,dk_2^- \\
&\times \frac{D_{\alpha j}(k_1-\frac{1}{2}r)}{(k_1-\frac{1}{2}r)^2+i\epsilon}\,\Pi_{a_1}^{jj'}\,\frac{D_{j'\beta}(k_1+\frac{1}{2}r)}{(k_1+\frac{1}{2}r)^2-i\epsilon} \\
&\times \mathrm{tr}\bigg[\gamma^\beta\,\frac{(k_2-\frac{1}{2}r)\gamma}{(k_2-\frac{1}{2}r)^2-i\epsilon}\,\Gamma_{\bar a_2}\,\frac{(k_2+\frac{1}{2}r)\gamma}{(k_2+\frac{1}{2}r)^2+i\epsilon}\,\gamma^\alpha\,\Phi^q(k_1+k_2)\bigg]_{k_2^-=-k_1^-,\,\boldsymbol{k}_2=-\boldsymbol{k}_1}\,. \qquad (5.14)
\end{aligned}
$$

The expression (5.14) involves the quark correlation function Φ^q for an unpolarized proton, which fulfills

$$
\int d\kappa^-\,\Phi^q(\kappa)\Big|_{\kappa^+=xp^+} = \frac{1}{2}\gamma^- f_1^q(x,\boldsymbol{\kappa}) + \frac{1}{2}i\sigma^{j-}\gamma_5\,\frac{\epsilon^{jj'}\boldsymbol{\kappa}^{j'}}{M}\,h_1^{\perp q}(x,\boldsymbol{\kappa}) \qquad (5.15)
$$

to leading-twist accuracy, or equivalently

$$
\begin{aligned}
f_1^q(x,\boldsymbol{\kappa}) &= \int\frac{dz^-d^2\boldsymbol{z}}{(2\pi)^3}\,e^{ixz^-p^+-i\boldsymbol{z}\boldsymbol{\kappa}}\,\langle p|\,\mathcal{O}_q(0,z)|p\rangle \\
\frac{\epsilon^{jj'}\boldsymbol{\kappa}^{j'}}{M}\,h_1^{\perp q}(x,\boldsymbol{\kappa}) &= \int\frac{dz^-d^2\boldsymbol{z}}{(2\pi)^3}\,e^{ixz^-p^+-i\boldsymbol{z}\boldsymbol{\kappa}}\,\langle p|\,\mathcal{O}^j_{\delta q}(0,z)|p\rangle\,. \qquad (5.16)
\end{aligned}
$$

We now calculate the color factors for the different color projections (cf. appendix B) in section 4.2.3 and obtain

$$
\frac{{}^SF_{a_1,a_2}}{{}^1F_{a_1,a_2}}\bigg|_{q\to gq} = \sqrt{\frac{N^2-4}{2}}\,, \qquad\qquad \frac{{}^AF_{a_1,a_2}}{{}^1F_{a_1,a_2}}\bigg|_{q\to gq} = -\frac{N}{\sqrt{2}}\,. \qquad (5.17)
$$

Contrary to the case of $g\to q\bar q$ analyzed above, the splitting mechanism now favors color octet distributions over color singlet ones.

The denominator of equation (5.14) can be treated in exactly the same way as we have done for (5.3) while the numerator can be calculated using FORM, and the final result is

$$
\begin{aligned}
{}^1F_{a_1,a_2}(x_i,\boldsymbol{k}_i,\boldsymbol{r})\Big|_{q\to gq} &= \frac{\alpha_s}{2\pi^2}\,C_F\bigg[\frac{f_1^q(x_1+x_2,\boldsymbol{\kappa})}{x_1+x_2}\,T^{ll'}_{a_1,a_2}\bigg(\frac{x_1}{x_1+x_2}\bigg) \\
&+ \frac{\epsilon^{mm'}\boldsymbol{\kappa}^{m'}}{M}\,\frac{h_1^{\perp q}(x_1+x_2,\boldsymbol{\kappa})}{x_1+x_2}\,U^{ll'm}_{a_1,a_2}\bigg(\frac{x_1}{x_1+x_2}\bigg)\bigg]\,\frac{\big(\boldsymbol{k}+\frac{1}{2}\boldsymbol{r}\big)^l\big(\boldsymbol{k}-\frac{1}{2}\boldsymbol{r}\big)^{l'}}{\big(\boldsymbol{k}+\frac{1}{2}\boldsymbol{r}\big)^2\big(\boldsymbol{k}-\frac{1}{2}\boldsymbol{r}\big)^2} \qquad (5.18)
\end{aligned}
$$

with

$$
\begin{aligned}
T^{ll'}_{g,q}(u) &= \delta^{ll'}\,(1+\bar u^2)/u\,, & T^{ll'}_{\Delta g,\Delta q}(u) &= \delta^{ll'}\,(1+\bar u)\,, \\
T^{ll'}_{\Delta g,q}(u) &= -i\epsilon^{ll'}\,(1+\bar u^2)/u\,, & T^{ll'}_{g,\Delta q}(u) &= -i\epsilon^{ll'}\,(1+\bar u)\,, \\
\big[T^{ll'}_{\delta g,q}(u)\big]^{jj'} &= 2\tau^{ll',jj'}\bar u/u & & \qquad (5.19)
\end{aligned}
$$

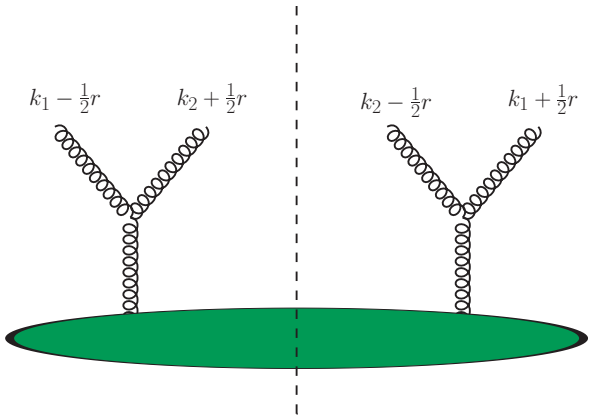

Figure 5.3.: Splitting of a gluon into a gluon pair

and

$$\begin{aligned}
\big[U^{ll'm}_{g,\delta q}(u)\big]^k &= 2\delta^{ll'}\delta^{km}\,\bar{u}/u\,, & \big[U^{ll'm}_{\Delta g,\delta q}(u)\big]^k &= -2i\epsilon^{ll'}\delta^{km}\,\bar{u}/u\,,\\
\big[U^{ll'm}_{\delta g,\delta q}(u)\big]^{jj',k} &= \tau^{jj',ml}\delta^{kl'} + \tau^{jj',ml'}\delta^{kl} - (\tau^{jj',kl}\delta^{ml'} + \tau^{jj',kl'}\delta^{ml})\,\bar{u} - \tau^{jj',km}\delta^{ll'}\,u\\
&\quad + 2\tau^{jj',ll'}\delta^{km}\,\bar{u}/u\,. \qquad (5.20)
\end{aligned}$$

The remaining kernels are zero.

The last splitting contribution we will calculate is the splitting of a gluon into a gluon pair shown in figure 5.3. In light-cone gauge ($A^+ = 0$) the color singlet distribution is given by

$$\begin{aligned}
{}^1F_{a_1,a_2}(x_i,\boldsymbol{k}_i,\boldsymbol{r})\Big|_{g\to gg} &= \frac{4\pi\alpha_s}{(2\pi)^5}\,N\,(x_1p^+)\,(x_2p^+)\,2p^+\int dr^-\,dk_1^-\,dk_2^-\;\Phi^g_{\alpha\beta}(k_1+k_2)\\
&\times\Bigg[\frac{D_{\mu j}(k_1-\frac{1}{2}r)}{(k_1-\frac{1}{2}r)^2+i\epsilon}\,\Pi^{jj'}_{a_1}\,\frac{D_{j'\mu'}(k_1+\frac{1}{2}r)}{(k_1+\frac{1}{2}r)^2-i\epsilon}\,\frac{D_{\nu k}(k_2+\frac{1}{2}r)}{(k_2+\frac{1}{2}r)^2+i\epsilon}\,\Pi^{kk'}_{a_2}\,\frac{D_{k'\nu'}(k_2-\frac{1}{2}r)}{(k_2-\frac{1}{2}r)^2-i\epsilon}\\
&\times\Big(g^{\mu'\nu'}(k_1-k_2+r)^\beta - g^{\beta\mu'}(2k_1+k_2+\frac{1}{2}r)^{\nu'} + g^{\beta\nu'}(k_1+2k_2-\frac{1}{2}r)^{\mu'}\Big)\\
&\times\Big(g^{\mu\nu}(k_1-k_2-r)^\alpha - g^{\alpha\mu}(2k_1+k_2-\frac{1}{2}r)^\nu + g^{\alpha\nu}(k_1+2k_2+\frac{1}{2}r)^\mu\Big)\Bigg]_{\substack{k_2^-=-k_1^-\\ \boldsymbol{k}_2=-\boldsymbol{k}_1}} \qquad (5.21)
\end{aligned}$$

We use the same techniques as in the calculation of the other splitting contributions and arrive at a result that has the same structure as for the splitting $g \to q\bar{q}$ (see eq. (5.8)) and reads,

$$\begin{aligned}
{}^1F_{a_1,a_2}(x_i,\boldsymbol{k}_i,\boldsymbol{r})\Big|_{g\to gg} &= \frac{\alpha_s}{2\pi^2}\,N\Bigg[\frac{f_1^g(x_1+x_2,\boldsymbol{\kappa})}{x_1+x_2}\,T^{ll'}_{a_1,a_2}\Big(\frac{x_1}{x_1+x_2}\Big) + \frac{2\boldsymbol{\kappa}^m\boldsymbol{\kappa}^{m'} - \delta^{mm'}\boldsymbol{\kappa}^2}{2M^2}\\
&\times\frac{h_1^{\perp g}(x_1+x_2,\boldsymbol{\kappa})}{x_1+x_2}\,U^{ll'mm'}_{a_1,a_2}\Big(\frac{x_1}{x_1+x_2}\Big)\Bigg]\,\frac{\big(\boldsymbol{k}+\frac{1}{2}\boldsymbol{r}\big)^l\big(\boldsymbol{k}-\frac{1}{2}\boldsymbol{r}\big)^{l'}}{\big(\boldsymbol{k}+\frac{1}{2}\boldsymbol{r}\big)^2\big(\boldsymbol{k}-\frac{1}{2}\boldsymbol{r}\big)^2}\,, \qquad (5.22)
\end{aligned}$$

with

$$
\begin{aligned}
T^{ll'}_{g,g}(u) &= 2\delta^{ll'}\left(u/\bar{u}+\bar{u}/u+u\bar{u}\right), & T^{ll'}_{\Delta g,\Delta g}(u) &= 2\delta^{ll'}\left(2-u\bar{u}\right),\\
T^{ll'}_{g,\Delta g}(u) &= -2i\epsilon^{ll'}\left(2\bar{u}+u/\bar{u}\right), & \left[T^{ll'}_{g,\delta g}(u)\right]^{kk'} &= 2\tau^{ll',kk'}\,u/\bar{u}\,,\\
\left[T^{ll'}_{\delta g,\delta g}(u)\right]^{jj',kk'} &= \delta^{ll'}\,\tau^{jj',kk'}\,u\bar{u}
\end{aligned}
\tag{5.23}
$$

and

$$
\begin{aligned}
U^{ll'mm'}_{g,g}(u) &= -U^{ll'mm'}_{\Delta g,\Delta g}(u) = 2\tau^{ll',mm'}\,u\bar{u}\,,\\
\left[U^{ll'mm'}_{g,\delta g}(u)\right]^{kk'} &= \delta^{ll'}\,\tau^{kk',mm'}\,\bar{u}/u\,, & \left[U^{ll'mm'}_{\Delta g,\delta g}(u)\right]^{kk'} &= -i\epsilon^{ll'}\tau^{kk',mm'}\,\bar{u}/u\,,\\
\left[U^{ll'mm'}_{\delta g,\delta g}(u)\right]^{jj',kk'} &= \tau^{ll',kk'}\,\tau^{mm',jj'}\,u/\bar{u}+\tau^{ll',jj'}\,\tau^{mm',kk'}\,\bar{u}/u+\tau^{ll',mm'}\,\tau^{jj',kk'}\,u\bar{u}\\
&\quad+\tau^{lm,jj'}\,\tau^{l'm',kk'}+\tau^{l'm,jj'}\,\tau^{lm',kk'}\\
&\quad-\left(\tau^{jj',mn}\,\tau^{nl',kk'}\,\delta^{lm'}+\tau^{jj',mn}\,\tau^{nl,kk'}\,\delta^{l'm'}\right)u\\
&\quad-\left(\tau^{kk',mn}\,\tau^{nl',jj'}\,\delta^{lm'}+\tau^{kk',mn}\,\tau^{nl,jj'}\,\delta^{l'm'}\right)\bar{u}\,.
\end{aligned}
\tag{5.24}
$$

The kernels $T_{\Delta g,g}$, $T_{\delta g,g}$, $U_{\delta g,g}$ and $U_{\delta g,\Delta g}$ are respectively obtained from $T_{g,\Delta g}$, $T_{g,\delta g}$, $U_{g,\delta g}$ and $U_{\Delta g,\delta g}$ by interchanging $u \leftrightarrow \bar{u}$ and the appropriate indices. The remaining kernels are zero.
We now calculate the color factors for the different color projections in section 4.2.2. We obtain (see appendix B for the explicit calculation)

$$
\frac{{}^{S}F_{a_1,a_2}}{{}^{1}F_{a_1,a_2}}\bigg|_{g\to gg} = -\frac{{}^{A}F_{a_1,a_2}}{{}^{1}F_{a_1,a_2}}\bigg|_{g\to gg} = \frac{\sqrt{N^2-1}}{2} \underset{N=3}{=} \sqrt{2}\,, \tag{5.25}
$$

where as in the case $q \to gq$ color octet distributions are enhanced over color singlet ones. The factors for the higher color representations in the case $N = 3$ are

$$
{}^{10}F_{a_1,a_2}\big|_{g\to gg} = \overline{{}^{10}}F_{a_1,a_2}\big|_{g\to gg} = 0\,, \qquad \frac{{}^{27}F_{a_1,a_2}}{{}^{1}F_{a_1,a_2}}\bigg|_{g\to gg} = -\sqrt{3}\,. \tag{5.26}
$$

The 27 representation is hence even more strongly enhanced than the two color octet combinations. Decuplet and antidecuplet distributions are not generated by perturbative splitting at lowest order.

We conclude these calculations with an overview of the dTMDs generated by the perturbative splitting mechanism, which is given in table 5.1.

5.2. Double counting

It would now be of great interest to know how big the contribution of such splittings to the dTMDs and thereby to the cross section is. There is, however, an additional problem that arises when looking at graphs like the one shown in figure 5.4. On one hand, this graph looks like a one loop correction to usual single parton gluon-gluon scattering, and it is indeed UV divergent. On the other hand, this graph could also be obtained by having a splitting contribution to the quark-antiquark distribution for both the left- and the right-moving proton.

	$F_{q,\bar{q}}$	$F_{\Delta q,\Delta\bar{q}}$	$F_{\Delta q,\bar{q}}$	$F_{q,\Delta\bar{q}}$	$F_{\delta q,\delta\bar{q}}$	$F_{\delta q,\bar{q}}$	$F_{\delta q,\Delta\bar{q}}$	$F_{q,\delta\bar{q}}$	$F_{\Delta q,\delta\bar{q}}$
f_1^g	×	×	×	×	×				
$h_1^{\perp g}$	×	×			×				

	$I_{q,\bar{q}}$	$I_{\Delta q,\Delta\bar{q}}$	$I_{\Delta q,\bar{q}}$	$I_{q,\Delta\bar{q}}$	$I_{\delta q,\delta\bar{q}}$	$I_{\delta q,\bar{q}}$	$I_{\delta q,\Delta\bar{q}}$	$I_{q,\delta\bar{q}}$	$I_{\Delta q,\delta\bar{q}}$
f_1^g	×	×			×				
$h_1^{\perp g}$	×	×	×	×	×				

	$F_{g,q}$	$F_{\Delta g,\Delta q}$	$F_{\Delta g,q}$	$F_{g,\Delta q}$	$F_{\delta g,\delta q}$	$F_{\delta g,q}$	$F_{\delta g,\Delta q}$	$F_{g,\delta q}$	$F_{\Delta g,\delta q}$
f_1^q	×	×	×	×		×			
$h_1^{\perp q}$					×			×	×

	$F_{g,g}$	$F_{\Delta g,\Delta g}$	$F_{\Delta g,g}$	$F_{g,\Delta g}$	$F_{\delta g,\delta g}$	$F_{\delta g,g}$	$F_{\delta g,\Delta g}$	$F_{g,\delta g}$	$F_{\Delta g,\delta g}$
f_1^g	×	×	×	×	×	×		×	
$h_1^{\perp g}$	×	×			×	×	×	×	×

Table 5.1.: Overview of the two-parton distributions that receive nonzero contributions from perturbative splitting of a single quark or gluon. A cross indicates a nonzero contribution at order α_s. Not shown are entries for $F_{q,g}$ and its analogs with polarization, which are like those for $F_{g,q}$ and its polarized counterparts.

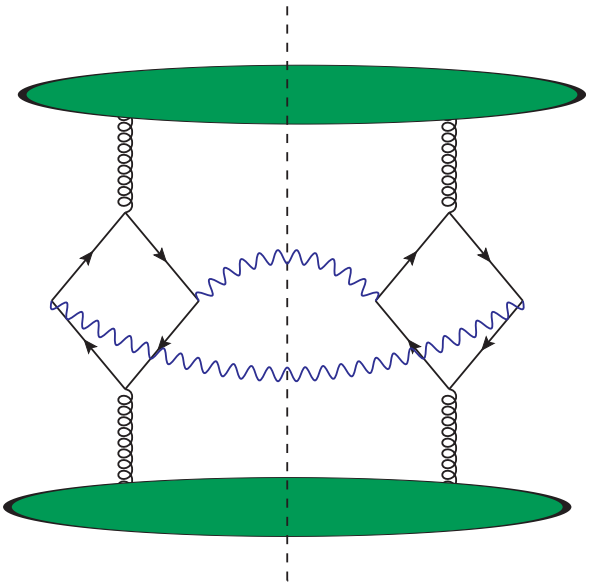

Figure 5.4.: Example graph which could be considered both single and double parton scattering

Studying this box diagram, we find that the graph has indeed two leading momentum regions. The first leading region is the region of small transverse momenta $\ll Q$, which would naturally be associated with double parton scattering. The second leading region is the region of high transverse momenta $\sim Q$, which is associated with a one loop correction to single parton scattering.

Both single and double parton scattering contribute to the total cross section and it is important to find a consistent way of separating the two in order to prevent double counting of contributions. This issue has been a matter of discussion for some years, see e.g. [9, 30, 31, 32, 33]. A way to solve this problem has now been found, but is not published yet [34].

6. Double Drell-Yan beyond leading order

A complete treatment of hard scattering factorization has, of course, to take additional gluon exchange into account. When going beyond leading order, one first has to identify the leading graphs and integration regions in the kinematic limit under consideration. We will briefly explain the method to achieve this in section 6.2. Then one has to apply suitable approximations for each of the relevant integration regions, such that when subtracting the approximated graph from the the exact graph the remainder is power suppressed by at least one power of Λ^2/Q^2. We give the corresponding analysis at the one gluon exchange level in section 6.3. In section 6.4 we give a method to correct for double counting of the soft region and give two possibilities of consistently defining dTMDs beyond leading order.

6.1. Definition of momentum regions

We will often refer to lines being either hard, collinear to an external momentum or soft in the following. The corresponding typical momentum scalings for a line with momentum $l \sim (l^+, l^-, |\boldsymbol{l}|)$ are

$$\begin{aligned} &l \sim (Q, Q, Q) && \text{for hard lines,} \\ &l \sim (Q, \Lambda^2/Q, \Lambda) && \text{for right-moving collinear lines,} \\ &l \sim (\Lambda^2/Q, Q, \Lambda) && \text{for left-moving collinear lines.} \end{aligned} \tag{6.1}$$

We will speak of soft lines whenever all momentum components are of size Λ or smaller. There are, however, several subregions which have different scalings, namely

$$\begin{aligned} &l \sim (\Lambda, \Lambda, \Lambda) && \text{is called the soft region,} \\ &l \sim (\Lambda^2/Q, \Lambda^2/Q, \Lambda^2/Q) && \text{is called the ultrasoft region,} \\ &l \sim (\Lambda^2/Q, \Lambda^2/Q, \Lambda) && \text{is called the Glauber region.} \end{aligned} \tag{6.2}$$

There are more possible scalings of the momenta in the soft region. These are, however, not needed as the methods stated below also correctly treat these subregions of the soft region [5, 13]. Special attention has to be paid to gluons in the Glauber region because some of the approximations that have to be made in order to obtain the factorized form of the cross section are not valid in this case. Proving that either there is no contribution from the Glauber region or that contributions cancel in the sum over diagrams is therefore an important part of every factorization proof. We will explicitly show that there are no such contributions for double Drell-Yan at one loop order in chapter 7, and we will review the main ideas of the proof that these contributions cancel to all orders in chapter 9.

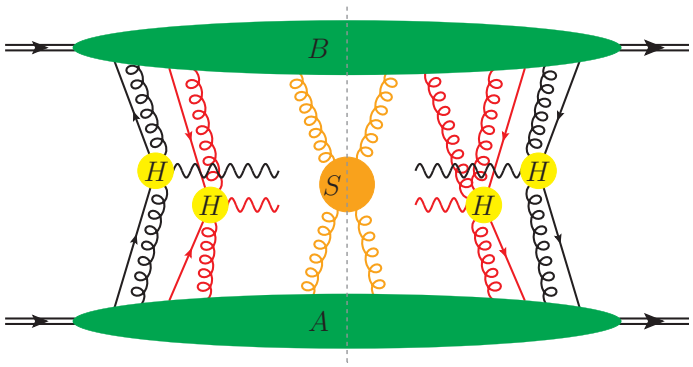

Figure 6.1.: Dominant graphs for double Drell-Yan when the transverse momenta $|\boldsymbol{q}_i|$ of the final state photons are much smaller than Q. The upper and lower blobs denote collinear subgraphs, the blob crossing the final-state cut (dashed line) denotes a soft subgraph, and the blobs with a final-state photon denote hard subgraphs.

6.2. Leading regions

The method to identify the dominant graphs and integration regions has been developed by Libby and Sterman [35, 36]. First, one trades the limit of large kinematic invariants for the limit of vanishing masses and also sends all external transverse momenta to zero. Then one has to identify integration regions, where the integration contour is pinched between coalescing poles. Note that when the integration contour is not pinched near a pole, one can always deform the integration contour away from it.
The result of the analysis is, that there are two types of regions giving rise to pinches of the integration contour (and therefore regions that give leading contributions). On one hand one finds pinch singularities in the collinear regions, i.e. regions where the gluon momentum is collinear to one of the incoming particles. On the other hand, one also finds pinch singularities in the soft region, i.e. in the region where all components of the gluon momentum are small. The integration contour of all other lines can be deformed such that these lines are far off-shell and can be organized into hard subgraphs which can be calculated perturbatively. The leading graphs for double Drell-Yan are shown in figure 6.1.
Having identified the dominant graphs, one now has to find suitable approximations for each of the leading integration regions. These individual contributions can then be factorized using Ward identities, leading to the factorized form of the cross section depicted in figure 6.2, which is a momentum convolution of a hard factor H, two collinear factors F and $\bar{F}$ and a soft factor S. Schematically, this factorized form reads

$$\frac{d\sigma}{\prod_{i=1}^{2} dx_i d\bar{x}_i d^2\boldsymbol{q}_i} = H \otimes F \otimes \bar{F} \otimes S \otimes \text{subtractions} + \text{power suppressed} \,, \tag{6.3}$$

where $\otimes$ denotes a (possibly complicated) momentum convolution. In the following we will focus on the main ingredients needed to obtain this factorized form for one additional gluon.

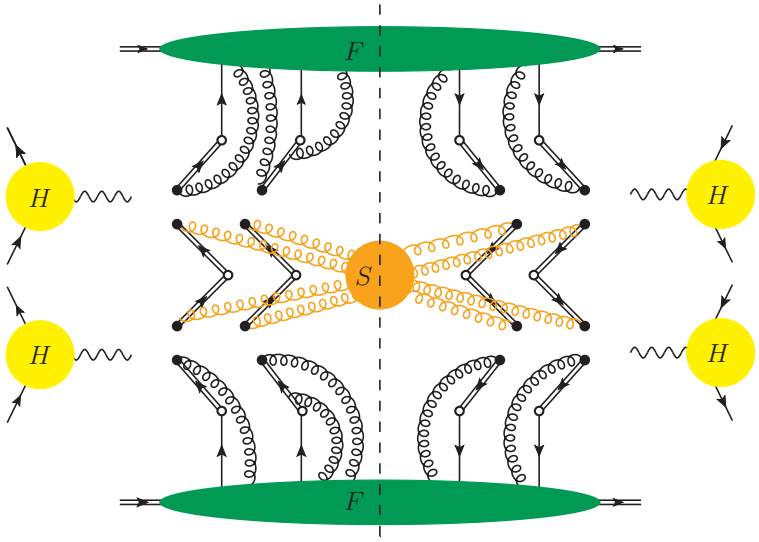

Figure 6.2.: Factorized form of double Drell-Yan at measured $q_T \ll Q$.The upper and lower blobs denote the collinear factors, the blob crossing the final-state cut (dashed line) denotes the soft factor, and the blobs with a final-state gauge boson denote the hard parts. The double lines denote Wilson lines.

6.3. Collinear and soft gluons

The analysis given in the following has been published in [9], which we will closely follow throughout this section. Also see [5] for a comprehensive account of the whole factorization procedure.

6.3.1. Collinear gluons

We first look at the case where a left-moving quark or antiquark is struck by a gluon collinear to the right-moving hadron, i.e. the gluon momentum fulfills $\ell^+ \gg |\ell^-|, |\boldsymbol{\ell}|$. The relevant subgraphs are depicted in figure 6.3. In the case of figure 6.3(a), the left-moving quark is taken far off-shell and thus its coupling to the gluon and its propagator are part of the hard subgraph. The relevant part of the graph can be written as

$$T_a = \langle \dots \bar{q}_j \, A^{\alpha,a} \dots \rangle \, \frac{i}{\gamma(\ell + \bar{l}_c)} \, (-ig) \, t^a_{jj'} \gamma_\alpha \, u(\bar{l}_c) \, \langle \dots q_{j'} \dots \rangle \,, \tag{6.4}$$

where in a shorthand notation we write $\langle \dots \bar{q}_j \, A^{\alpha,a} \dots \rangle$ and $\langle \dots q_{j'} \dots \rangle$ for the hadronic matrix elements of the right- and left-moving proton, respectively. The subscript c on $\bar{l}$ indicates the collinear approximation, i.e. $\bar{l}^-_c = \bar{l}^-$, $\bar{l}^+_c = 0$ and $\bar{\boldsymbol{l}}_c = \boldsymbol{0}$.

The r.h.s. of eq. (6.4) has the structure $A^\mu H_\mu$, where A describes the collinear factor of the right-moving hadron and H describes the hard subgraph (cf. figure 6.1). Making use of the fact that $|A^+| \gg |A^-|, |\boldsymbol{A}|$ and that all components of H are of comparable size, one can

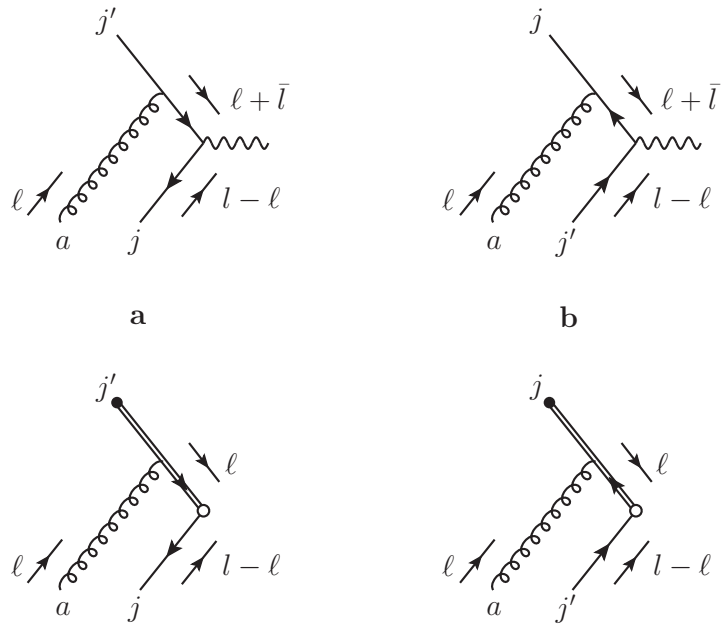

Figure 6.3.: Coupling of one collinear gluon in the Drell-Yan process. Top row: subgraphs with a right-moving gluon coupling to a left-moving quark or antiquark before it annihilates. Bottom row: corresponding graphs after the off-shell propagators have been replaced by eikonal lines.

rewrite this as

$$A^\mu H_\mu \approx A^+ H^- = A^+ v_A^- \frac{1}{\ell^+ v_A^- + i\eta}\ \ell^+ H^- \approx A_\mu \frac{v_A^\mu \ell_\nu}{\ell v_A + i\eta}\ H^\nu\ . \tag{6.5}$$

The case of a right-moving quark struck by a gluon collinear to the left-moving hadron can be treated exactly in the same way and we get

$$B^\mu H_\mu \approx B^- H^+ = B^- v_B^+ \frac{1}{\ell^- v_B^+ - i\eta'}\ \ell^- H^+ \approx B_\mu \frac{v_B^\mu \ell_\nu}{\ell v_B - i\eta'}\ H^\nu\ . \tag{6.6}$$

Here, we have introduced auxiliary vectors $v_A = (v_A^+, v_A^-, \mathbf{0})$ with $v_A^- \gg |v_A^+|$ or $v_A^- \sim |v_A^+|$ and $v_B = (v_B^+, v_B^-, \mathbf{0})$ with $v_B^+ \gg |v_B^-|$ or $v_B^+ \sim |v_B^-|$.[1] We have also provided $i\eta$ and $i\eta'$ prescriptions suitable for a gluon momentum ℓ that flows out of A and into H or out of H and into B, respectively. The sign of $i\eta$ has been chosen such that the pole of the eikonal propagator, i.e. the pole of $1/(\ell \cdot v_A)$ in ℓ^+, lies on the same side of the real axis as the pole of the original off-shell quark propagator. The same holds for the sign of $i\eta'$, with the only difference being that now the pole in ℓ^- is the relevant one. For the case of figure 6.3(a),

[1] We only have to require that the rapidity $y_i = \frac{1}{2}\log\frac{|v_i^+|}{|v_i^-|}$ of the auxiliary vector v_A (v_B) is significantly different from the rapidity of the right (left) moving gluon. It can therefore be large and negative (positive) or central.

these poles read

$$\ell v_A + i\eta = \ell^+ v_A^- - \ell^- |v_A^+| + i\eta\,, \qquad (\ell + \bar{l}_c)^2 + i\eta = 2\ell^+ \bar{l}^- + i\eta\,, \tag{6.7}$$

from which can be clearly seen that the poles in ℓ^+ are on the same side of the real axis. We will now show how these replacements lead to the appearance of Wilson lines for a single collinear gluon. With the replacements made above, we can rewrite eq. (6.4) as

$$T_a = \langle \dots \bar{q}_j\, A_\alpha^a \dots \rangle (-igt_{jj'}^a v_\alpha^A)\, \frac{i}{\ell v_A + i\eta} \left[\frac{1}{\gamma(\ell + \bar{l}_c)}\, (\gamma\ell)\, u(\bar{l}_c) \right] \langle \dots q_{j'} \dots \rangle\,, \tag{6.8}$$

and using $\gamma\ell = \gamma(\ell + \bar{l}_c) - \gamma\bar{l}_c$ and $(\gamma\bar{l}_c)\, u(\bar{l}_c) = 0$ we finally obtain

$$T_a = \langle \dots \bar{q}_j\, A_\alpha^a \dots \rangle (-igt_{jj'}^a v_A^\alpha)\, \frac{i}{\ell v_A + i\eta}\, u(\bar{l}_c)\, \langle \dots q_{j'} \dots \rangle\,. \tag{6.9}$$

In the hard scattering amplitude we have thus traded the coupling $-igt^a\gamma_\alpha$ of the gluon to the quark and the adjacent quark propagator $i/\gamma(\ell+\bar{l}_c)$ for the coupling $-igt^a v^\alpha$ of the gluon to a so-called eikonal line and the eikonal propagator $i/(\ell v_A + i\eta)$. Repeating the same steps for the graph in figure 6.3(b) gives

$$\begin{aligned} T_b &= \langle \dots \bar{q}_j \dots \rangle\, \bar{v}(\bar{l}_c)\, \gamma_\alpha\, \frac{-i}{\gamma(\ell + \bar{l}_c)}\, (-ig)\, t_{jj'}^a\, \langle \dots A^{\alpha,a}\, q_{j'} \dots \rangle \\ &= \langle \dots \bar{q}_j \dots \rangle\, \bar{v}(\bar{l}_c)\, \frac{-i}{\ell v_A + i\eta}\, (-igt_{jj'}^a v_A^\alpha)\, \langle \dots A_\alpha^a\, q_{j'} \dots \rangle\,. \end{aligned} \tag{6.10}$$

The change from an incoming quark to an incoming antiquark in the hard scattering reflects in an overall sign change of the propagator $i/\gamma(\ell+\bar{l}_c)$, which then yields an overall sign change of the eikonal propagator $i/(\ell v_A + i\eta)$. The momentum flow of the large quark momentum with regards to the gluon momentum and therefore the resulting $i\eta$ prescriptions have remained the same. The sign of $i\eta$ depends on (while keeping the routing of the gluon momentum the same) whether the original large quark momentum is incoming or outgoing in the hard scattering subprocess. This means that in Semi Inclusive Deep Inelastic Scattering (SIDIS), where the large momentum of the quark that is struck by the virtual photon is outgoing, one gets the opposite sign of $i\eta$ in the eikonal propagators.

With these results, one sees that a graphical notation in the context of Feynman diagrams for eikonal lines always needs to specify the flow of the gluon momentum ℓ relative to

- the color flow of the hard subprocess, which means also to the fermion number flow in the quark line which is represented by the eikonal line. This determines the overall sign of the eikonal propagator. We denote the color flow by an arrow on the eikonal line, which points in the same direction as the arrow on the original fermion line.
- the flow of the large momentum $\bar{l}_c$ in the original fermion line, which is either an incoming or an outgoing line in the hard scattering subprocess. This determines the sign of $i\eta$ in the eikonal propagator. We indicate this graphically by a full or an empty circle at the end of the eikonal line, such that the large momentum flows from the full to the empty circle.

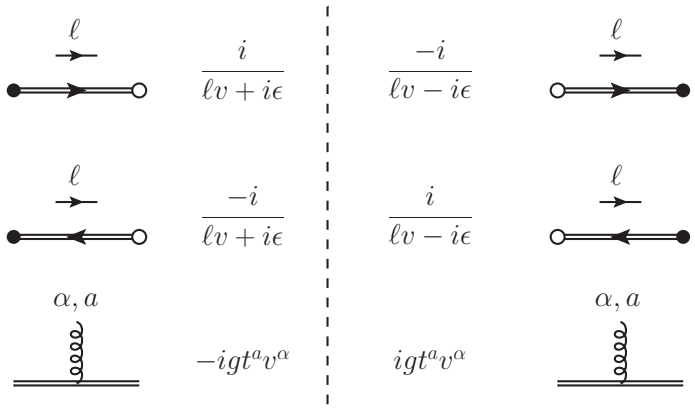

Figure 6.4.: Feynman rules for eikonal lines representing quarks or antiquarks.

The resulting Feynman rules for the eikonal propagators and vertices are given in figure 6.4. We will now briefly review how eikonal lines are generated by Wilson line operators in the hadronic matrix elements that appear in a factorization formula. The relevant part of the expression (6.9), together with the relevant integrations over momentum and position variables reads

$$X_{j'} = \int d^4\ell\, e^{i\xi(l-\ell)}\, \bar{q}_j(\xi) \int \frac{d^4\zeta}{(2\pi)^4}\, e^{i\zeta\ell}\, v_A A^a(\zeta)\, (-igt^a_{jj'})\, \frac{i}{\ell v_A + i\epsilon}\,. \tag{6.11}$$

Using the representation

$$\frac{i}{\ell v_A + i\epsilon} = \int_0^\infty d\lambda\, e^{i\lambda(\ell v_A + i\epsilon)} \tag{6.12}$$

we can rewrite this as

$$\begin{aligned} X_{j'} &= e^{i\xi l}\, \bar{q}_j(\xi) \int d^4\ell \int \frac{d^4\zeta}{(2\pi)^4} \int_0^\infty d\lambda\, e^{i(\lambda v_A + \zeta - \xi)\ell}\, v_A A^a(\zeta)\, (-igt^a_{jj'}) \\ &= e^{i\xi l}\, \bar{q}_j(\xi) \left[-ig \int_0^\infty d\lambda\, v_A A^a(\xi - \lambda v_A)\, t^a_{jj'} \right]. \end{aligned} \tag{6.13}$$

We now introduce the Wilson line, which is essentially a path ordered exponential of gluon fields:

$$W(\xi; v_A) = \mathrm{P} \exp\left[ig \int_0^\infty d\lambda\, v_A A^a(\xi - \lambda v_A)\, t^a \right]. \tag{6.14}$$

We now see, that the term in square brackets in (6.13) is the term of order g in the expansion of $W^\dagger(\xi; v_A)$. In a full factorization proof, one has to show that the coupling of two or more collinear gluons to the incoming quark line in figure 6.3(a) exponentiates, so that their combined effect is the replacement

$$\bar{q}_{j'}(\xi) \to \bar{q}_j(\xi)\, \left[W^\dagger(\xi; v_A) \right]_{jj'} \tag{6.15}$$

in the operator defining the parton distribution. The same holds for the case of (6.10), where the collinear gluon couples to an antiquark. The resulting replacement is

$$q_j(\xi) \to \big[W(\xi; v_A)\big]_{jj'}\, q_{j'}(\xi)\,. \tag{6.16}$$

The manipulations on which the preceding arguments are based are all concerned with a single hard scattering subprocess at a time, so that they also apply to double Drell-Yan graphs with only one extra gluon. The result is, that for instance the operator

$$\Big(\bar q_{k'}(-\frac{1}{2}z_2)\Gamma_{a_2} q_k(\frac{1}{2}z_2)\Big)\,\Big(\bar q_{j'}(y-\frac{1}{2}z_1)\Gamma_{a_1} q_j(y+\frac{1}{2}z_1)\Big) \tag{6.17}$$

which appears in two quark distributions is replaced with the following:

$$\begin{aligned}&\big[\bar q(-\frac{1}{2}z_2)\,W^\dagger(-\frac{1}{2}z_2; v_A)\big]_{k'}\,\Gamma_{a_2}\,\big[W(\frac{1}{2}z_2; v_A)\,q(\frac{1}{2}z_2)\big]_k \\ &\quad\times\big[\bar q(y-\frac{1}{2}z_1)\,W^\dagger(y-\frac{1}{2}z_1; v_A)\big]_{j'}\,\Gamma_{a_1}\,\big[W(y+\frac{1}{2}z_1; v_A)\,q(y+\frac{1}{2}z_1)\big]_j\,\Big|_{z_2^+=z_1^+=y^+=0}\,.\end{aligned} \tag{6.18}$$

The open color indices j, j', k, k', which were carried by quark fields in the lowest order formula, are now carried by the "ends" of the four past-pointing Wilson lines. The projection on color singlet and octet distributions can be done in the same way as explained in section 4.2.

Let us now mention how the previous arguments need to be generalized to obtain a complete factorization proof for double Drell-Yan production.

- In the step from (6.8) to (6.9), we have eliminated an internal fermion propagator in the hard scattering graph. When going to more complicated graphs, possibly with loops or further external gluons, this simplification is not as easy to obtain and involves the use of Ward identities. In a model theory with Abelian gluons, this is quite simple to establish, see e.g. [5, chapter 10.8]. The formulation for QCD is more complicated and involves external ghost lines in addition to external gluons in the hard scattering (see [5, chapters 11.3 and 11.9]).

- In the analysis given above, we have considered the case where only one gluon couples to each hard subgraph. For a full proof of factorization to all orders, it has of course to be shown that the coupling of an arbitrary number of gluons exponentiates into a full Wilson line. Again, this is not too complicated to show for Abelian gluons (see [5, chapter 10.8]), but to the best of our knowledge, an explicit proof for transverse-momentum dependent distributions in QCD has not yet been given.

- The two Wilson lines $W(\frac{1}{2}z_2; v_A)$ and $W(y+\frac{1}{2}z_1; v_A)$ in (6.18) correspond to gluons in the scattering amplitude, where all gluon fields should be time ordered. With the choice $v_A^2 < 0$ the gluon operators in one Wilson line have a spacelike separation. They therefore commute because of causality and can be brought into the order required by path ordering. This is, however, not necessarily true for gluon operators from two different Wilson lines, and the possibility of reordering them in this case requires some more investigation.

- The operator in (6.18) is not explicitly gauge invariant, because the Wilson lines "end" at different positions, namely at $a_i - \infty v_A$ with finite spacelike a_i for $i = 1, 2, 3, 4$. This issue has already been studied for single parton distributions using lightlike Wilson lines, i.e. $v_A^2 = 0$ [37, 38]. In a gauge where the gluon potential has zero expectation value at $a_i - \infty v_A$, one can complement the operator (6.18) with Wilson lines that point into the transverse direction and connect the lightlike Wilson lines to a common reference point, e.g. to $-\infty v_A$. After projecting the open color indices at this reference point onto color-singlet or color-octet combinations, the resulting operator is explicitly invariant under local gauge transformations. The extra Wilson lines in the transverse direction are essential in the gauge $v_A A = 0$, where the Wilson lines in (6.18) reduce to unity, see the discussion in [37].

6.3.2. Soft gluons and soft factor

Next we consider the exchange of a soft gluon between the soft subgraph S and the collinear subgraph A in figure 6.1. The soft gluon momentum components are all small and fulfill $|\ell^+| \sim |\ell^-| \sim |\boldsymbol{\ell}|$. Then we can rewrite

$$S^\mu A_\mu \approx S^- A^+ = S^- v_R^+ \frac{1}{\ell^- v_R^+ + i\eta'} \; \ell^- A^+ \approx S_\mu \frac{v_R^\mu \ell_\nu}{\ell v_R + i\eta'} \; A^\nu \; . \tag{6.19}$$

Similarly, for the coupling of a soft gluon between the soft subgraph S and the collinear subgraph B we rewrite

$$S^\mu B_\mu \approx S^+ B^- = S^+ v_L^- \frac{1}{\ell^+ v_L^- - i\eta} \; \ell^+ B^- \approx S_\mu \frac{v_L^\mu \ell_\nu}{\ell \cdot v_L - i\eta} \; B^\nu \; . \tag{6.20}$$

Here we require the rapidities of v_L (v_R) to be large and negative (positive). Note that for these approximations to hold we have to require that all gluon momentum components are small and of the same size. In particular, these approximations break down in the so called Glauber region, where we have $|\boldsymbol{\ell}| \gg |\ell^+|, |\ell^-|$. Proving that there is no leading contribution from the Glauber region must therefore be part of any comprehensive proof of factorization for the process under consideration. Like for the collinear gluons, the $i\eta$ and $i\eta'$ prescriptions are suitable for a gluon momentum ℓ flowing out of S and into A or out of B and into S, respectively. A soft gluon can either couple to an active quark or to a spectator, as shown in figure 6.5. With the $i\eta'$ prescription we have given above, the pole of the propagator of the Wilson line $1/(\ell v_R + i\eta')$ lies on the same side of the real axis as the pole of the off-shell quark in the case of figure 6.5(a), where the soft gluon couples to an active quark. In this case, one can deform the ℓ^- integration contour out of the Glauber region and the Grammer-Yennie approximations given above hold. The same is, however, not true for the coupling of a soft gluon to a spectator quark as shown in figure 6.5(b), and we will discuss this issue in some more detail in chapter 7.
The next step is to use a Ward identity argument that relates the collinear subgraph with an additional gluon attachment to the same subgraph without an extra gluon. For the correlation function describing quark-antiquark emission and an additional gluon in the amplitude, this

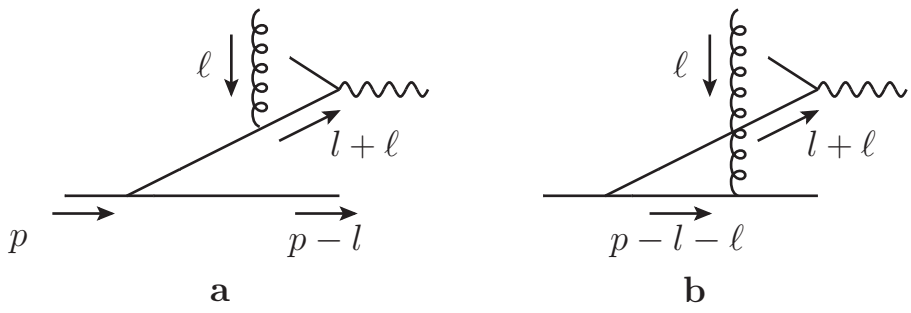

Figure 6.5.: Coupling of a soft gluon to a collinear parton that (a) enters the hard scattering or (b) is a spectator.

identity reads

$$\frac{Sv_R}{\ell v_R + i\eta'}\,\ell_\alpha\,\Phi^{\alpha,a}_{jj',kk'}(\ell;l_1,l_2,l_1',l_2') = Sv_R\,(-igt^a_{jm})\,\frac{i}{\ell v_R + i\eta'}\,\Phi_{mj',kk'}(l_1-\ell,l_2,l_1',l_2') + Sv_R\,(-igt^a_{mk})\,\frac{-i}{\ell v_R + i\eta'}\,\Phi_{jj',mk'}(l_1,l_2-\ell,l_1',l_2')\,. \tag{6.21}$$

On the r.h.s. of eq. (6.21) one can see that the soft gluon has decoupled from the collinear part. Compared with the tree level expression, this will result in an additional soft factor in the factorized form of the cross section. Analogous identities can be written down for the emission of two quarks or two antiquarks, with a factor $i/(\ell v_R + i\eta')$ for each quark line and $-i/(\ell v_R + i\eta')$ for each antiquark line in the amplitude. A general proof of these identities is not too difficult in Abelian gauge theories like QED, but to the best of our knowledge has not been given yet for non Abelian gauge theories. In chapter 3.2.2 of [9] these identities have been verified for two simple examples.

We will now show how the soft factor emerges in the factorization formula when there is exactly one soft gluon connecting the collinear subgraphs A and B in figure 6.1. More precisely, we will study the case where this gluon is exchanged in the amplitude, given that derivation for a gluon in the conjugate amplitude can be done completely analogously. The contribution to the cross section is proportional to

$$\int \frac{d^4\ell}{(2\pi)^4}\,\frac{d^4\bar\ell}{(2\pi)^4}\,(2\pi)^4\delta^{(4)}(\ell+\bar\ell)\,S^{ab}_{\alpha\beta}(\ell,\bar\ell) \times\left[\prod_{i=1}^{2}\int d^4l_i\,d^4\bar l_i\,(2\pi)^4\delta^{(4)}(q_i-l_i-\bar l_i)\right]\int d^4l_1'\,d^4\bar l_1'\,(2\pi)^4\delta^{(4)}(q_1-l_1'-\bar l_1') \times\left[\Phi_{a_1,\bar a_2}\right]^{\alpha,a}_{jj',kk'}(\ell;l_1,l_2,l_1',l_2')\left[\Phi_{\bar a_1,a_2}\right]^{\beta,b}_{jj',kk'}(\bar\ell;\bar l_1,\bar l_2,\bar l_1',\bar l_2')$$

$$
\begin{aligned}
&\approx \int \frac{d^4\ell}{(2\pi)^4}\,\frac{d^4\bar\ell}{(2\pi)^4}\,(2\pi)^4\delta^{(4)}(\ell+\bar\ell)\,\frac{iv_R^\alpha}{\ell v_R+i\eta'}\,S^{ab}_{\alpha\beta}(\ell,\bar\ell)\,\frac{iv_L^\beta}{\bar\ell v_L+i\eta}\\
&\quad\times\left[\prod_{i=1}^{2}\int d^4l_i\,d^4\bar l_i\,(2\pi)^4\delta^{(4)}(q_i-l_i-\bar l_i)\right]\int d^4l_1'\,d^4\bar l_1'\,(2\pi)^4\delta^{(4)}(q_1-l_1'-\bar l_1')\\
&\quad\times\left[(-igt^a_{jm})\left[\Phi_{a_1,\bar a_2}\right]_{mj',kk'}(l_1-\ell,l_2,l_1',l_2')-(-igt^a_{mk})\left[\Phi_{a_1,\bar a_2}\right]_{jj',mk'}(l_1,l_2-\ell,l_1',l_2')\right]\\
&\quad\times\left[(-igt^b_{kn})\left[\Phi_{\bar a_1,a_2}\right]_{jj',nk'}(\bar l_1,\bar l_2-\bar\ell,\bar l_1',\bar l_2')-(-igt^b_{nj})\left[\Phi_{\bar a_1,a_2}\right]_{nj',kk'}(\bar l_1-\bar\ell,\bar l_2,\bar l_1',\bar l_2')\right]\\
&=\int \frac{d^4\ell}{(2\pi)^4}\,\frac{d^4\bar\ell}{(2\pi)^4}\,(2\pi)^4\delta^{(4)}(\ell+\bar\ell)\,(-igt^a_{jm})\,\frac{iv_R^\alpha}{\ell v_R+i\eta'}\,S^{ab}_{\alpha\beta}(\ell,\bar\ell)\,(-igt^b_{kn})\,\frac{iv_L^\beta}{\bar\ell v_L+i\eta}\\
&\quad\times\int d^4l_1\,d^4\bar l_1\,(2\pi)^4\delta^{(4)}(q_1-l_1-\bar l_1-\ell)\int d^4l_2\,d^4\bar l_2\,(2\pi)^4\delta^{(4)}(q_2-l_2-\bar l_2-\bar\ell)\\
&\quad\times\int d^4l_1'\,d^4\bar l_1'\,(2\pi)^4\delta^{(4)}(q_1-l_1'-\bar l_1')\\
&\quad\times\left[\Phi_{a_1,\bar a_2}\right]_{mj',kk'}(l_1,l_2,l_1',l_2')\left[\Phi_{\bar a_1,a_2}\right]_{jj',nk'}(\bar l_1,\bar l_2,\bar l_1',\bar l_2')+\{\text{three more terms}\}\,,
\end{aligned}
\tag{6.22}
$$

where in the first step we have used the Ward identity given in (6.21) and in the last step we have shifted the integration variables l_1 and $\bar l_2$ such that the soft momenta ℓ and $\bar\ell$ do not appear in the parton correlation functions any more. For simplicity we have omitted a global factor, as well as the hard scattering part for $q\bar q\to\gamma^*$, which only depends on the external momenta q_1 and q_2 and is therefore independent of all the integration variables in (6.22).
The soft subgraph, which for one soft gluon connecting the two collinear subgraphs is just the gluon propagator, can be represented as a matrix element

$$
(2\pi)^4\delta^{(4)}(\ell+\bar\ell)\,S^{ab}_{\alpha\beta}(\ell,\bar\ell)=\int d^4\xi\,d^4\bar\xi\,e^{i\xi\ell+i\bar\xi\bar\ell}\,\langle 0|A^a_\alpha(\xi)\,A^b_\beta(\bar\xi)|0\rangle\,,
\tag{6.23}
$$

which also has meaning beyond perturbation theory. Using (6.23) and (6.12) the first term in (6.22) becomes

$$
\begin{aligned}
&\int\frac{d^4\bar\ell\,d^4\bar\xi}{(2\pi)^4}\int\frac{d^4\ell\,d^4\xi}{(2\pi)^4}\,e^{i\xi\ell+i\bar\xi\bar\ell}\int_0^\infty d\lambda\int_0^\infty d\bar\lambda\,e^{i\lambda\ell v_R+i\bar\lambda\bar\ell v_L}\,(-igt^a_{jm})\,(-igt^b_{kn})\langle 0|v_RA^a(\xi)\,v_LA^b(\bar\xi)|0\rangle\\
&\quad\times\int d^4l_1\,d^4\bar l_1\,(2\pi)^2\,\delta(q_1^+-l_1^+)\,\delta(q_1^--\bar l_1^-)\int d^2\boldsymbol{\xi}_1\,e^{-i\boldsymbol{\xi}_1(\boldsymbol{q}_1-\boldsymbol{l}_1-\bar{\boldsymbol{l}}_1-\boldsymbol{\ell})}\\
&\quad\times\int d^4l_2\,d^4\bar l_2\,(2\pi)^2\,\delta(q_2^+-l_2^+)\,\delta(q_2^--\bar l_2^-)\int d^2\boldsymbol{\xi}_2\,e^{-i\boldsymbol{\xi}_2(\boldsymbol{q}_2-\boldsymbol{l}_2-\bar{\boldsymbol{l}}_2-\bar{\boldsymbol{\ell}})}\\
&\quad\times\int d^4l_1'\,d^4\bar l_1'\,(2\pi)^2\,\delta(q_1^+-l_1'^+)\,\delta(q_1^--\bar l_1'^-)\int d^2\boldsymbol{\xi}_1'\,e^{-i\boldsymbol{\xi}_1'(\boldsymbol{q}_1-\boldsymbol{l}_1'-\bar{\boldsymbol{l}}_1')}\\
&\quad\times\left[\Phi_{a_1,\bar a_2}\right]_{mj',kk'}(l_1,l_2,l_1',l_2')\left[\Phi_{\bar a_1,a_2}\right]_{jj',nk'}(\bar l_1,\bar l_2,\bar l_1',\bar l_2')
\end{aligned}
$$

$$
\begin{aligned}
&= \int d^2\boldsymbol{\xi}_1\, d^2\boldsymbol{\xi}_1\, d^2\boldsymbol{\xi}_1'\; e^{-i\boldsymbol{\xi}_1\boldsymbol{q}_1 - i\boldsymbol{\xi}_2\boldsymbol{q}_2 - i\boldsymbol{\xi}_1'\boldsymbol{q}_1} \\
&\quad \times \int d^4l_1\, d^4l_2\, d^4l_1'\; e^{i\boldsymbol{\xi}_1\boldsymbol{l}_1 + i\boldsymbol{\xi}_2\boldsymbol{l}_2 + i\boldsymbol{\xi}_1'\boldsymbol{l}_1'}\, (2\pi)^3\, \delta(q_1^+ - l_1^+)\, \delta(q_2^+ - l_2^+)\, \delta(q_1^+ - l_1'^+) \\
&\qquad \times \big[\Phi_{a_1,\bar{a}_2}\big]_{mj',kk'}(l_1, l_2, l_1', l_2') \\
&\quad \times \int d^4\bar{l}_1\, d^4\bar{l}_2\, d^4\bar{l}_1'\; e^{i\boldsymbol{\xi}_1\bar{\boldsymbol{l}}_1 + i\boldsymbol{\xi}_2\bar{\boldsymbol{l}}_2 + i\boldsymbol{\xi}_1'\bar{\boldsymbol{l}}_1'}\, (2\pi)^3\, \delta(q_1^- - \bar{l}_1^-)\, \delta(q_2^- - \bar{l}_2^-)\, \delta(q_1^- - \bar{l}_1'^-) \\
&\qquad \times \big[\Phi_{\bar{a}_1,a_2}\big]_{jj',nk'}(\bar{l}_1, \bar{l}_2, \bar{l}_1', \bar{l}_2') \\
&\quad \times \big\langle 0\big|\left[-ig\int_0^\infty d\lambda\, v_R A^a(\xi_{1T} - \lambda v_R)\, t^a_{jm}\right]\left[-ig\int_0^\infty d\bar{\lambda}\, v_L A^b(\xi_{2T} - \bar{\lambda} v_L)\, t^b_{kn}\right]\big|0\big\rangle\,,
\end{aligned}
\tag{6.24}
$$

where ξ_{iT} are transverse four-vectors, i.e. their longitudinal components ξ_{iT}^+ and ξ_{iT}^- are zero and they only have transverse components $\boldsymbol{\xi}_i$. We can now compare the r.h.s. of eq. (6.24) with the tree level expression of the cross section. At tree level the color indices of the partons entering the hard scattering have to match and in this case we have a factor $\delta_{jm}\delta_{kn}$ instead of the last line in (6.24), which is the only difference between the two expressions. The factors in square brackets in the last line of (6.24) are exatly the $\mathcal{O}(g)$ terms in the expansion of the conjugate Wilson lines $W^\dagger(\xi_{1T}; v_R)$ and $W^\dagger(\xi_{2T}; v_L)$. In the transverse plane, the starting points of the paths of these Wilson lines are at the positions that are Fourier conjugate to the transverse quark momenta $\boldsymbol{l}_1$ and $\bar{\boldsymbol{l}}_2$ in (6.24). This means that in the position space representation the transverse positions of the quark fields und the starting points of the Wilson lines have to match. This is, however, not true for the longitudinal position arguments which are zero for the Wilson lines but in general non-zero for the quark fields.
The contribution from the three other terms in (6.22) can be obtained in the same way and give very similar results, but with Wilson lines $W(\xi_{2T}; v_R)$ and $W(\xi_{1T}, v_L)$ at the positions that are Fourier conjugate to the transverse antiquark momenta $\boldsymbol{l}_2$ and $\bar{\boldsymbol{l}}_1$, respectively.
Changing to symmetric momentum and position variables and restoring global kinematic factors omitted in the derivation given above, the second to fifth lines on the r.h.s. of (6.24) turn into the product $F_{a_1,\bar{a}_2}(x_i, \boldsymbol{z}_i, \boldsymbol{y}) F_{\bar{a}_1,a_2}(\bar{x}_i, \boldsymbol{z}_i, \boldsymbol{y})$ of two-parton distributions in transverse position space, and the Wilson lines are to be evaluated at the appropriate transverse positions of the quark or antiquark fields in the definition of these distributions.
When going to higher orders in the strong coupling, one has to show that soft subgraphs with an arbitrary number of external gluons add up to full Wilson lines. This proof is quite involved even for the single Drell-Yan process, and to the best of our knowledge there is no such proof for the transverse momentum dependent double parton scattering case, yet. The structure suggested by our analysis of one-gluon exchange is however clear: the effect of all soft subgraphs is to multiply the Born-level cross section (4.54) in position space representation by a soft factor. This factor is the vacuum expectation value of a product of Wilson lines, with one Wilson line for each external quark or antiquark in the multiparton distributions.

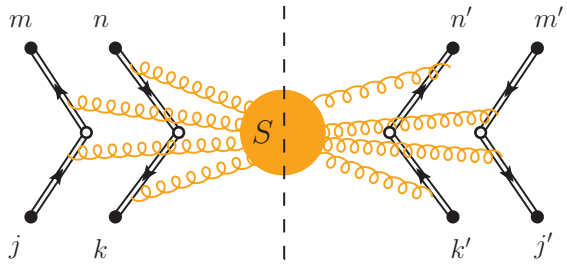

Figure 6.6.: Graphical representation of the soft factor (6.26). The four open color indices at the top and the bottom can be projected on a color singlet-octet basis, respectively.

The resulting expression for the cross section then reads

$$\begin{aligned}\frac{d\sigma}{\prod_{i=1}^{2} dx_i\, d\bar{x}_i\, d^2\boldsymbol{q}_i} &= \frac{1}{C}\left[\prod_{i=1}^{2}\hat{\sigma}_i(x_i\bar{x}_i s)\right]\left[\prod_{i=1}^{2}\int\frac{d^2\boldsymbol{z}_i}{(2\pi)^2}\,e^{-i\boldsymbol{z}_i\boldsymbol{q}_i}\right]\int d^2\boldsymbol{y} \\ &\quad\times\left[F_{\bar{a}_1,a_2}\right]_{mm',nn'}(\bar{x}_i,\boldsymbol{z}_i,\boldsymbol{y})\left[S_{q\bar{q}}\right]_{mm',nn';jj',kk'}(\boldsymbol{z}_i,\boldsymbol{y})\left[F_{a_1,\bar{a}_2}\right]_{jj',kk'}(x_i,\boldsymbol{z}_i,\boldsymbol{y}) \\ &\quad+\{\text{further terms}\}\,, \end{aligned} \tag{6.25}$$

where the "further terms" describe the remaining combinations of quarks or antiquarks in the two-parton distributions, as discussed in section 4.1. The soft factor is a vacuum expectation value of Wilson lines and reads

$$\begin{aligned}&\left[S_{q\bar{q}}\right]_{mm',nn';jj',kk'}(\boldsymbol{z}_i,\boldsymbol{y}) \\ &\quad=\big\langle 0\,\big|\left[W(y_T+\tfrac{1}{2}z_{1T};v_L)\,W^\dagger(y_T+\tfrac{1}{2}z_{1T};v_R)\right]_{mj}\left[W(y_T-\tfrac{1}{2}z_{1T};v_R)\,W^\dagger(y_T-\tfrac{1}{2}z_{1T};v_L)\right]_{j'm'} \\ &\qquad\times\left[W(\tfrac{1}{2}z_{2T};v_R)\,W^\dagger(\tfrac{1}{2}z_{2T};v_L)\right]_{kn}\left[W(-\tfrac{1}{2}z_{2T};v_L)\,W^\dagger(-\tfrac{1}{2}z_{2T};v_R)\right]_{n'k'}\big|\,0\big\rangle\,. \end{aligned} \tag{6.26}$$

The graphical representation of the soft factor in terms of Feynman diagrams is given in figure 6.6. The Wilson lines $W(\xi;v_L)\,W^\dagger(\xi;v_R)$ and $W(\xi;v_R)\,W^\dagger(\xi;v_L)$ in the soft factor are contracted pairwise with respect to their color indices. This is due to the fact that the gauge bosons produced in the annihilation of quarks and antiquarks are colorless and therefore the color indices of quarks and antiquarks are directly contracted. The "further terms" in (6.25) have a soft factor S_{qq} multiplying $F_{\bar{a}_1,\bar{a}_2}F_{a_1,a_2}$ and a soft factor S_I multiplying the product of interference distributions $I_{\bar{a}_1,a_2}I_{a_1,\bar{a}_2}$. These factors are defined in analogy to (6.26) with an appropriate interchange of arguments and indices for W and $W^\dagger$.
The soft factor (6.26) has eight open color indices, cf. figure 6.6. In analogy to two parton distributions, the four color indices at the top and the bottom can be projected on a color singlet-octet basis, respectively. The color decomposition reads

$$\begin{aligned}\left[S_{q\bar{q}}\right]_{mm',nn';jj',kk'} &= \frac{1}{N^2}\Bigg[{}^{11}S_{q\bar{q}}\,\delta_{mm'}\delta_{n'n}\delta_{j'j}\delta_{kk'}+\frac{2N}{\sqrt{N^2-1}}\,{}^{18}S_{q\bar{q}}\,\delta_{mm'}\delta_{n'n}t^a_{j'j}t^a_{kk'} \\ &\quad+\frac{2N}{\sqrt{N^2-1}}\,{}^{81}S_{q\bar{q}}\,t^b_{mm'}t^b_{n'n}\delta_{j'j}\delta_{kk'}+\frac{4N^2}{N^2-1}\,{}^{88}S_{q\bar{q}}\,t^b_{mm'}t^b_{n'n}t^a_{j'j}t^a_{kk'}\Bigg]\,. \end{aligned} \tag{6.27}$$

We now define the matrix

$$\mathbf{S}_{q\bar{q}} = \begin{pmatrix} {}^{11}S_{q\bar{q}} & {}^{18}S_{q\bar{q}} \\ {}^{81}S_{q\bar{q}} & {}^{88}S_{q\bar{q}} \end{pmatrix} \tag{6.28}$$

and the cross section can then be expressed as

$$\begin{aligned} \frac{d\sigma}{\prod_{i=1}^{2} dx_i\, d\bar{x}_i\, d^2\boldsymbol{q}_i} &= \frac{1}{C}\left[\prod_{i=1}^{2} \hat{\sigma}_i(x_i\bar{x}_i s)\right]\left[\prod_{i=1}^{2}\int \frac{d^2\boldsymbol{z}_i}{(2\pi)^2}\, e^{-i\boldsymbol{z}_i\boldsymbol{q}_i}\right]\int d^2\boldsymbol{y} \\ &\times \begin{pmatrix} {}^{1}F_{\bar{a}_1,a_2}(\bar{x}_i,\boldsymbol{z}_i,\boldsymbol{y}) \\ {}^{8}F_{\bar{a}_1,a_2}(\bar{x}_i,\boldsymbol{z}_i,\boldsymbol{y}) \end{pmatrix}^{\mathrm{T}} \mathbf{S}_{q\bar{q}}(\boldsymbol{z}_i,\boldsymbol{y}) \begin{pmatrix} {}^{1}F_{a_1,\bar{a}_2}(x_i,\boldsymbol{z}_i,\boldsymbol{y}) \\ {}^{8}F_{a_1,\bar{a}_2}(x_i,\boldsymbol{z}_i,\boldsymbol{y}) \end{pmatrix} + \{\text{further terms}\}\,. \end{aligned} \tag{6.29}$$

We see that in position space the cross section is a simple product or more precisely a simple matrix multiplication. Perturbative calculations are usually done in momentum representation. Fourier transforming the cross section (6.29) to momentum space one gets a complicated convolution in transverse momenta of the distributions $F(x_i, \boldsymbol{k}_i, \boldsymbol{r})$ and the soft factor.

6.4. Double counting subtractions and rapidity divergences

The collinear regions and the soft region of the gluon momentum are not strictly seperated, but in fact the soft region is contained within the collinear regions. The collinear factors one obtains from the method described above therefore do not only contain the contributions from collinear gluons, but also contributions from the soft region. To avoid double counting of the soft region, one has to subtract the soft region from each of the collinear factors and eq. (6.3) schematically becomes

$$\frac{d\sigma}{\prod_{i=1}^{2} dx_i d\bar{x}_i d^2\boldsymbol{q}_i} = H \otimes \frac{F}{S'} \otimes \frac{\bar{F}}{S''} \otimes S + \text{power suppressed}\,. \tag{6.30}$$

Note that the soft factors S, S' and S'' do not need to be equal to each other. Generally speaking, one makes certain approximations for each leading region of a graph, which may overlap. The resulting terms are still integrated over the full range of loop momenta, as the application of a cutoff would bring serious complications to the analysis. As these approximations were not designed to be accurate outside of their corresponding region, the quality and therefore the accuracy of the approximations may be spoiled. There is, however, a sequential subtraction procedure (cf. chapter 10.1 and 10.7 of [5]) that takes care of both the double counting problem and the problem of integrating approximated graphs over momentum regions where they were not designed to be accurate. This procedure makes sure that the sum of all terms correctly reproduces the original graph up to power corrections and we will briefly recapitulate it in section 6.4.1. Moreover, there are several ways of choosing the auxiliary vectors v_A, v_B, v_L and v_R, and of rearranging the individual factors in eq. (6.30) for practical applications. We will present some of these possibilities in section 6.4.2.

6.4.1. Subtraction procedure

Let R, R' and R'' be different momentum regions of a Feynman graph Γ, i.e. R and R' specify for all lines of Γ whether they are hard, collinear to an external line or soft. We call a region R' smaller than a region R ($R' < R$), when a hard line in R is collinear or soft in R', or if a collinear line in R is soft in R'. Conversely, we call a momentum region R'' bigger than a region R ($R'' > R$) when a soft line in R is collinear in R'', or when a collinear or soft line in R is hard in R''.

We define $T_R\Gamma$ to be the Feynman graph Γ with approximations made as appropriate for the momentum region R, which still may have leading contributions from regions smaller or bigger than R. The contributions from smaller regions are removed by the following subtraction:

$$C_R\Gamma := T_R\Gamma - \sum_{R'<R} T_R C_{R'}\Gamma \tag{6.31}$$

When a region R_0 does not have a smaller leading subregion, we simply have $C_{R_0}\Gamma = T_{R_0}\Gamma$. Eq. (6.31) can therefore be understood as a recursive defintion, starting from the smallest leading region, i.e. the soft region. The sum over all approximators then reproduces the whole graph up to power corrections,

$$\Gamma \approx \sum_R C_R\Gamma\,. \tag{6.32}$$

This subtraction procedure removes both the double counting of contributions from regions smaller than R and the unwanted contributions from the integral over all loop momenta outside of the design region of the approximators $T_{R'}\Gamma$. Note that if $C_R\Gamma$ still has a leading contribution from a region $R'' > R$, this contribution is removed by the subtraction $C_{R''}\Gamma$. The different collinear regions intersect as they have the soft region as a common subregion. It is proven in [5] that the subtraction procedure (6.31) still gives the correct result for the case of intersecting regions.

The schematic factorization formula in eq. (6.30) therefore contains the following terms:

- the hard part H, from which the collinear factors have to be subtracted (a soft factor has to be subtracted from each of the collinear factors) and the soft factor
- the collinear factors F and $\bar{F}$, where a soft factor has to be subtracted from each collinear factor
- the soft factor S, which does not receive any subtractions because the soft momentum region is the smallest

The corresponding subtracted and unsubtracted dTMDs are related by

$$\begin{aligned} F_{\text{unsub}}(v_A) &= S(v_A, v_R) \cdot F_{\text{sub}}\ , \\ \bar{F}_{\text{unsub}}(v_B) &= S(v_L, v_B) \cdot \bar{F}_{\text{sub}}\ . \end{aligned} \tag{6.33}$$

Bearing in mind that the soft factors are matrices in color space, this can be inverted and we get

$$\begin{aligned} F_{\text{sub}}(v_A) &= S^{-1}(v_A, v_R) \cdot F_{\text{unsub}} \ , \\ \bar{F}_{\text{sub}}(v_B) &= S^{-1}(v_L, v_B) \cdot \bar{F}_{\text{unsub}} \ . \end{aligned} \tag{6.34}$$

The product of soft factors and dTMDs in eq. (6.30) therefore reads

$$\begin{aligned} &\bar{F}^T_{\text{sub}} \cdot S(v_L, v_R) \cdot F_{\text{sub}} \\ &\quad = \bar{F}^T_{\text{unsub}}(v_B) \cdot S^{-1}(v_L, v_B) \cdot S(v_L, v_R) \cdot S^{-1}(v_A, v_R) \cdot F_{\text{unsub}}(v_A) \ . \end{aligned} \tag{6.35}$$

Note that we still have not stated anything about the auxiliary vectors v_A and v_B other than that their rapidity has to be widely seperated from the gluon's rapidity. There are multiple possible choices of these vectors, each with its own advantages. We will give some of the possible choices made in the litarature in the following.

6.4.2. Rapidity divergences and choice of auxiliary vectors

In order to simplify practical calculations, it would be desirable to take as many of the auxiliary vectors in (6.35) to be lightlike as possible. However, when one or more of the auxiliary vectors is lightlike one encounters so-called rapidity divergences which are typically of the form

$$\int_0^1 \mathrm{d}\alpha \ \frac{1}{\alpha} \frac{(1-\alpha)}{[\boldsymbol{\ell}^2 - \alpha(1-\alpha)k^2 - i\varepsilon]} \ . \tag{6.36}$$

These divergences can neither be regulated by taking a finite fermion mass and/or gluon mass nor by using dimensional regularization. There are several different ways of dealing with these divergences and we will give the two relevant ones for this work in the following. The first possibility is to take the auxiliary vectors to be off the light-cone, which was e.g. used in [39] for Drell-Yan and in [40] for the proof of factorization of SIDIS. One then still has the freedom to choose them to be spacelike or timelike. The first choice has been adapted in [39] while the latter has been chosen in [40]. Although there are some arguments regarding maximum universality of the TMDs and the factorization proof itself why the spacelike version should be used, see e.g. [41], we did not find problems with the timelike version at least to one loop order in our explicit calculations in chapter 7. Some years ago, Collins proposed a more complicated scheme, where v_A and v_B can be taken to be lightlike. This new scheme involves additional soft factors and leads to an expression for the cross section without an explicit soft factor [5, chapter 13.7]. There are other possible methods to regularize the rapidity divergences, e.g. the η-regulator, where one keeps η and η' that are used to regularize the eikonal propagators in eqs. (6.5) and (6.6) finite [42], but these will not be needed for the work at hand.
Moreover, one still has the freedom to choose whether v_A and v_B have large or central rapidity. One possible choice is to take e.g. $v_A = v_L$ and $v_B = v_R$. We will discuss two possible choices of auxiliary vectors that are relevant for this work in the following.

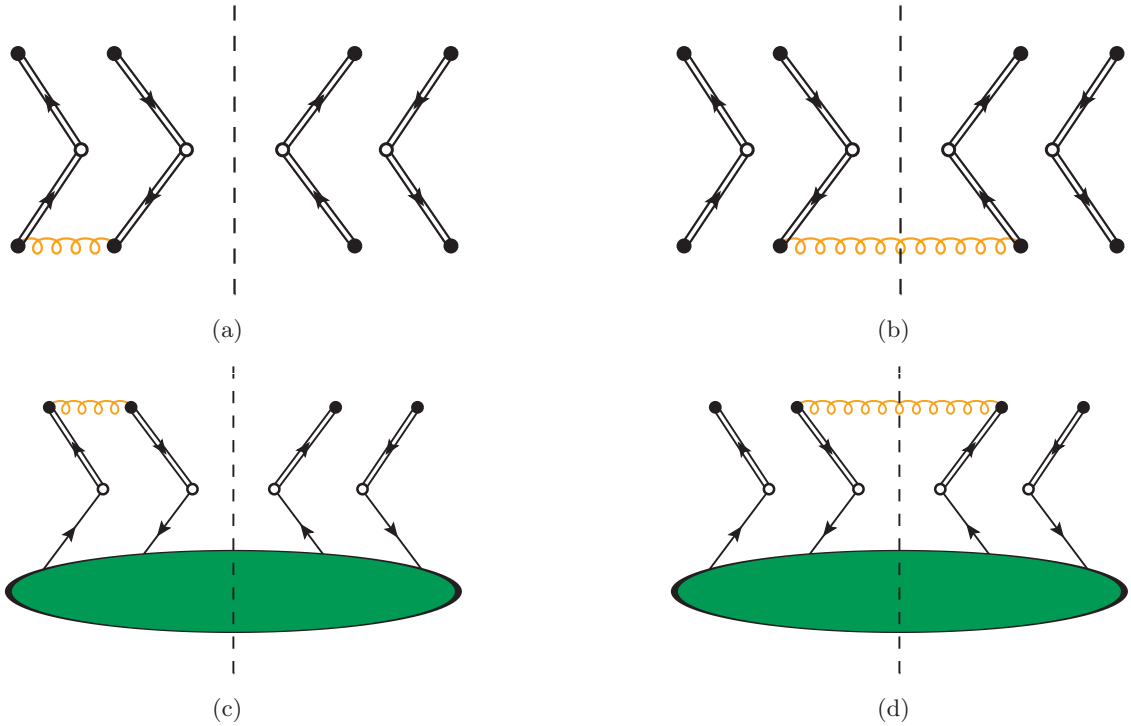

Figure 6.7.: Graph (a) and (b): Example corrections to the soft factor with (a) a virtual gluon and (b) a real gluon connecting lines with equal rapidity.
Graph (c) and (d): Example corrections to the dTMD with (c) a virtual gluon and (d) a real gluon connecting lines with equal rapidity.

$\mathbf{v_A} = \mathbf{v_L}$ and $\mathbf{v_B} = \mathbf{v_R}$. This choice has for instance been made in [40]. Plugging this into eq. (6.35), we see that one soft factor is cancelled by its inverse. This leads to a simpler factorized form with only one soft factor, namely

$$\bar{F}^T_{\text{sub}} \cdot S(v_L, v_R) \cdot F_{\text{sub}} = \bar{F}^T_{\text{unsub}}(v_R) \cdot S^{-1}(v_L, v_R) \cdot F_{\text{unsub}}(v_L) \ . \tag{6.37}$$

We note that in the calculation of the soft factor and the dTMDs to $\mathcal{O}(\alpha_S)$, there would in principle be corrections with gluons connecting lines with equal rapidity as shown in figure 6.7. There are several problems with these graphs. On one hand, the graphs 6.7(b) and (d) are divergent, i.e. ill-defined when using spacelike auxiliary vectors $v^2_{L/R} < 0$ [43]. On the other hand, the more severe problem is that this kind of graphs should not have been part of the soft factor and the dTMDs in the first place. The graphs in figure 6.7 correspond to soft gluon exchange within one of the collinear factors, and should therefore be treated as part of it. The derivation of the emergence of Wilson lines in the dTMDs used that a gluon collinear to the momentum of the right-moving (left-moving) partons connects the collinear factor of the right-moving (left-moving) proton and an active quark or antiquark of the left-moving (right-moving) proton. However, graphs like 6.7(c) and (d) would correspond to a gluon coupling two quarks in the left-moving collinear factor. In the full expression of the cross section (6.37), these diagrams cancel among the dTMDs and the soft factor, but in the calculation of the individual factors they have to be excluded by hand.

Additional soft factors. This new, at first sight more complicated scheme has been proposed by Collins in chapter 13.7 of [5] and we will now generalise the concepts given there to the case of double parton scattering. For simplicity, we will do this for the case of two colored, scalar partons per target, given that the concepts immediately carry over to particles with spin, as this only introduces more algebra in the numerator. The starting point is the r.h.s. of eq. (6.37)

$$\bar{F}^T_{\text{unsub}}(v_R)\cdot S^{-1}(v_L,v_R)\cdot F_{\text{unsub}}(v_L)=\frac{F(x_i,\mathbf{k}_i,\mathbf{r},y_{v_R})\bar{F}(\bar{x}_i,\bar{\mathbf{k}}_i,\bar{\mathbf{r}},y_{v_L})}{S(\mathbf{k}_{S,j},y_{v_L},y_{v_R})}\,, \tag{6.38}$$

where for sake of brevity we have dropped the labels "unsub" for the dTMDs on the right hand side. We have included the dependence of the dTMDs and the soft factor on momenta and an appropriate momentum convolution as well as the correct order of multiplication as in eq. (6.37) is understood. Note that the combination of dTMDs and the soft factor in eq. (6.38) is, up to power corrections, independent of the rapidities y_{v_L} and y_{v_R} of the auxiliary vectors v_L and v_R.
The soft factor can be rewritten as

$$\begin{aligned}\frac{1}{S(\mathbf{k}_{S,j},y_{v_L},y_{v_R})}&=\frac{1}{\sqrt{S(\mathbf{k}_{S,j},y_{v_L},y_{v_R})}}\cdot\frac{1}{\sqrt{S(\mathbf{k}_{S,j},y_{v_L},y_{v_R})}}\\&=\frac{1}{\sqrt{S(\mathbf{k}_{S,j},y_{v_L},y_{v_R})}}\cdot\frac{\sqrt{S(\mathbf{k}_{S,j},y_{v_L},y_{n_R})S(\mathbf{k}_{S,j},y_{n_L},y_{v_R})}}{\sqrt{S(\mathbf{k}_{S,j},y_{v_L},y_{n_R})S(\mathbf{k}_{S,j},y_{n_L},y_{v_R})}}\\&\quad\cdot\frac{1}{\sqrt{S(\mathbf{k}_{S,j},y_{v_L},y_{v_R})}}\,,\end{aligned} \tag{6.39}$$

where we have introduced two new spacelike auxiliary vectors $n_L=(-e^{y_n},e^{-y_n},\mathbf{0})$ and $n_R=(e^{y_n},-e^{-y_n},\mathbf{0})$, which both have central rapidity y_n. Rearranging all these factors, (6.38) becomes

$$\begin{aligned}\frac{d\sigma}{\prod_{i=1}^2 dx_i d\bar{x}d^2\mathbf{q}_i}\propto&\left(F(x_i,\mathbf{k}_i,\mathbf{r},y_{v_L})\frac{\sqrt{S(\mathbf{k}_{S,j},y_{n_L},y_{v_R})}}{\sqrt{S(\mathbf{k}_{S,j},y_{v_L},y_{v_R})}\sqrt{S(\mathbf{k}_{S,j},y_{v_L},y_{n_R})}}\right)\\&\times\left(\frac{\sqrt{S(\mathbf{k}_{S,j},y_{v_L},y_{n_R})}}{\sqrt{S(\mathbf{k}_{S,j},y_{v_L},y_{v_R})}\sqrt{S(\mathbf{k}_{S,j},y_{n_L},y_{v_R})}}\bar{F}(\bar{x}_i,\bar{\mathbf{k}}_i,\bar{\mathbf{r}},y_{v_R})\right)\,.\end{aligned} \tag{6.40}$$

Being matrices in color space, it is not obvious that the soft factors in (6.40) commute and the rearrangement can be done. This can, however, be seen from the following discussion:
As is shown in chapter 3.3 of [9], the soft factors satisfy the following relation at one loop level, as long as the difference between the rapidities of the two Wilson lines Δy_{ij} is large, which we always require:

$$\frac{\partial S(y_i,y_j)}{\partial\Delta y_{ij}}=\mathbf{K}S(y_i,y_j)=[K_1\mathbb{1}+K_2\mathbf{A}+K_3\mathbf{B}]S(y_i,y_j) \tag{6.41}$$

where $\mathbf{K}$, $\mathbf{A}$ and $\mathbf{B}$ are matrices in color space and K_1, K_2 and K_3 are numbers. Therefore, the soft factors and their inverse can be written as

$$S(y_i,y_j)=S_0\text{exp}[\Delta y_{ij}\mathbf{K}]\,,\quad S^{-1}(y_i,y_j)=(S_0)^{-1}\,\text{exp}[-\Delta y_{ij}\mathbf{K}]\,. \tag{6.42}$$

From this form it can be seen, that soft factors with different rapidities commute. Moreover, the products of soft factors in (6.40) always combines to one effective soft factor, e.g.

$$\begin{aligned}\frac{\sqrt{S(y_{v_L}, y_{n_R})}}{\sqrt{S(y_{n_L}, y_{v_R})}\sqrt{S(y_{v_L}, y_{v_R})}} &= S_0 \exp[\tfrac{1}{2}(y_{v_L} - y_n - y_n + y_{v_R} - y_{v_L} + y_{v_R})\mathbf{K}] \\ &= S_0 \exp[\tfrac{1}{2}(2y_{v_R} - 2y_n)\mathbf{K}] \\ &= \frac{1}{\sqrt{S(2y_n, 2y_{v_R})}} \end{aligned} \tag{6.43}$$

which simplifies calculations considerably. In the combinations of dTMDs and soft factors denoted by the parentheses in (6.40), the limits $y_{v_L} \to -\infty$ and $y_{v_R} \to +\infty$ can be taken, because rapidity divergences cancel. In momentum space, the final definition for a subtracted dTMD is a complicated convolution of the unsubtracted dTMD and the soft factors, while in position space it is just a product of the individual factors. The definition for a quark-antiquark dTMD in this framework therefore reads

$$\begin{aligned} F(x_i, \mathbf{k}_i, \mathbf{r}) = \left[\prod_{i=1}^{2} \int \frac{dz_i^-}{2\pi} e^{ix_i z_i^- p^+} \int \frac{d^2\mathbf{z}_i}{(2\pi)^2} e^{-i\mathbf{z}_i\cdot\mathbf{k}_i}\right] 2p^+ \int dy^- d^2\mathbf{y} e^{i\mathbf{y}\cdot\mathbf{r}} \\ \times \langle p|\mathcal{O}^*(0, z_2; -\infty)\mathcal{O}(y, z_1; -\infty)|p\rangle \sqrt{\frac{S(\mathbf{z}_1, \mathbf{z}_2, \mathbf{y}; \infty, y_{n_R})}{S(\mathbf{z}_1, \mathbf{z}_2, \mathbf{y}; y_{n_L}, -\infty) S(\mathbf{z}_1, \mathbf{z}_2, \mathbf{y}; \infty, -\infty)}}\,, \end{aligned} \tag{6.44}$$

where $y_{n_L} = y_{n_R} = y_n$ is an intermediate rapidity, which is the only new parameter the dTMD depends on. The soft factors in (6.44) are defined by the following vacuum expectation value of Wilson lines

$$\begin{aligned} S(\mathbf{z}_1, \mathbf{z}_2, y; y_w, y_v) = \frac{1}{N^2} \langle 0| \Big(W_{kj}(\mathbf{y} + \tfrac{1}{2}\mathbf{z}_1; v) W^\dagger_{ji}(\mathbf{y} + \tfrac{1}{2}\mathbf{z}_1; w) W_{il}(\tfrac{1}{2}\mathbf{z}_2; w) W^\dagger_{lk}(\tfrac{1}{2}\mathbf{z}_2; v)\Big) \\ \times \Big(W^\dagger_{i'j'}(\mathbf{y} - \tfrac{1}{2}\mathbf{z}_1; w) W_{j'k'}(y - \tfrac{1}{2}\mathbf{z}_1; v) W^\dagger_{k'l'}(-\tfrac{1}{2}\mathbf{z}_2; v) W_{l'i'}(-\tfrac{1}{2}\mathbf{z}_2; w)\Big) |0\rangle \end{aligned} \tag{6.45}$$

where N is the number of colors. Note that the soft factors only depend on transverse position and that these transverse positions have to match the positions of the quark and antiquark fields. In momentum space, the soft factors therefore do not depend on longitudinal momenta, which are integrated out. The definition (6.44) has to be understood in the following manner: First, the limit of infinit rapidity is taken starting from spacelike Wilson lines. Therefore the gauge fields in the Wilson lines always are at spacelike separation and commute in the Feynman gauge we use. That means, that the path ordering in the Wilson lines does not contradict the time-ordering needed for the definition of Green functions [5]. This is in fact true for gauge fields originating from one Wilson line, but not necessarily for gauge fields coming from different Wilson lines. Therefore, this issue needs further investigation in the case of multiparton scattering [9]. Only after the infinit rapidity limit is taken, one can perform the UV subtractions and send the dimensional parameter ε to zero. The order of these limits is crucial since they do not commute [5].

We conclude this section by listing some very convenient features of the definition (6.44).

- All rapidity divergences cancel, which is essential for a valid definition of dTMDs.
- The three subtraction terms combine to one effective subtraction term, simplifying calculations considerably.
- The dTMDs depend on only one additional parameter y_n and the dependence on this parameter is governed by the modified Collins-Soper evolution equation [5]. Thus, predictive power is not compromised.
- The factorization formula is of the form $H \otimes F \otimes \bar{F}$ and contains no explicit soft factor. As the soft factors do not have a physical meaning on their own (they cannot be measured) but always appear multiplied with distribution functions, this definition makes comparison between theory and experiment much easier.
- Ill-defined diagrams, i.e. diagrams with real gluons connecting Wilson lines with equal rapidity [43], cancel, rendering every individual factor in the factorization formula gauge invariant. In a formalism using spacelike Wilson lines with a different subtraction method, these diagrams may have to be excluded from the individual factors by hand, making them gauge dependent [5].
- The definition is boost invariant.

6.4.3. Collins-Soper evolution

Cross sections with measured transverse momenta $|\boldsymbol{q}_i|$ that are much smaller than the largest scale of the process Q contain logarithms in $|\boldsymbol{q}_i|/Q$. These logarithms are large and therefore need to be summed to all orders in the strong coupling in order to have a perturbatively stable result. The method to resum these so-called Sudakov logarithms has been developed by Collins, Soper and Sterman (CSS) [44].
When adopting the scheme of regularizing the rapidity divergences of the dTMDs by taking the auxiliary vectors to be off the light cone, one introduces a dependence of the dTMDs on the rapidity of these auxiliary vectors. Looking for example at the dTMD for the right-moving proton, the distribution then depends on the rapidity of v_A via a parameter

$$\zeta^2 = \frac{(2pv_A)^2}{|v_A|^2}\,. \tag{6.46}$$

In the same way, the dTMD for the left-moving proton acquires a dependence on the rapidity of v_B via

$$\bar{\zeta}^2 = \frac{(2\bar{p}v_B)^2}{|v_B|^2}\,. \tag{6.47}$$

In both cases one gets large logarithms of the type $\log(\zeta^2/\Lambda^2)$ when calculating loop corrections to the dTMDs, which spoil the precision of fixed order perturbation theory. The dependence of the dTMDs on these parameters is governed by a generalized version of the Collins-Soper (CS) equation [45], whose solution resums these Sudakov logarithms to all orders and thereby greatly enhances the accuracy of fixed order perturbation theory. The original

version of the CS equation was developed for single parton scattering and its extension to double parton scattering is given in [9, chapter 3.4].
We conclude this section by noting that for the new scheme involving additional soft factors discussed above, both dTMDs only depend on only one additional parameter y_n, and only via the soft factors. The dependence on this parameter is then governed by a modified Collins-Soper equation in the case of single parton scattering [5, chapter 13]. The analog in double parton scattering has not been studied yet, as far as we know.

7. Proof of cancellation of Glauber gluon exchange at next to leading order

In this chapter we will demonstrate the absence of contributions from the Glauber region for single gluon exchange in two particular toy models, and subsequently also for the general case. In the following we will discuss two possible approaches.

7.1. Possible approaches to a proof at the one gluon exchange level

7.1.1. Comparison of the result of a direct calculation with the factorized form

The first possibility is to assume factorization and then to compare the result of a direct calculation of the full process with that of a calculation starting from the factorized form of the cross section. This involves calculating all the one gluon exchange diagrams of the dTMDs, the soft factors and the hard part. The diagrams one has to calculate are schematically shown in figure 7.1 for the double Drell-Yan process. Using this method, one has to show that both results are equal up to power corrections in Λ/Q, thereby a posteriori justifying the Grammer-Yennie approximations needed to establish the factorized form. This then implies, that there is no contribution from the Glauber region. This method has been used e.g. in [40] to prove factorization for SIDIS at low transverse momentum at the one gluon exchange level.

While this method is perfectly suitable for not too complicated processes at the parton level, the calculations can become very difficult and lengthy when considering more complicated diagrams. A good example for such complications is given by the double box graph in figure 7.7, where after the first few integrals the calculation produces in each intermediate step results which need several pages to print. Given that even the slightest mistake in any step of this calculation gives a result varying from the factorized one, it is obvious that this method is not best suited for proving factorization for higher orders.

7.1.2. Power counting

The second possibility is to not calculate all diagrams explicitly, but to instead use power counting and contour deformation arguments for a certain combination of the full diagram and Grammer-Yennie approximants. Given that factorization only breaks down when the integration contour is trapped in the Glauber region, one can restrict the analysis to that region. One thus applies the appropriate scaling properties given in eqs. (6.1) and (6.2) to each line and then is led to examine the pole structure of the integrand. Two possible situations are shown in figure 7.2.
When the integration contour is not pinched between two poles as shown in figure 7.2(a) one

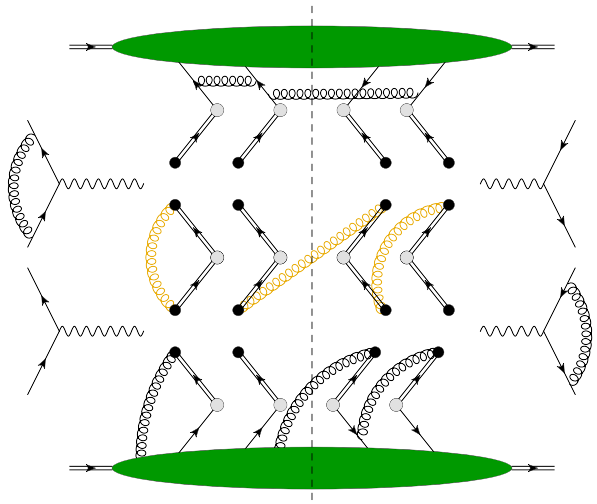

Figure 7.1.: Examples for corrections to the factorized form of the double Drell-Yan process

can always deform the integration contour away from the pole such that it does not give a leading contribution. This is not the case for the pole structure in figure 7.2(b), where we have a pinch of the integration contour near the origin.
Following the method outlined in [13, chapter 3.2] we take the auxiliary vectors in the Grammer-Yennie approximants for collinear gluons, (6.5) and (6.6), and for soft gluons, (6.19) and (6.20), to be the same, i.e. we choose $v_L = v_A$ and $v_R = v_B$. We then group the parton lines in each graph into subgraphs L and R, with L containing the lines above the vertices producing the gauge bosons and R containing the lines below. For a gluon connecting two active partons, the Grammer-Yennie approximation reads

$$R_\mu g^{\mu\alpha} \to R_\mu \frac{\ell^\mu v_R^\alpha}{\ell v_R - i\eta'}\,, \quad g^{\alpha\nu} L_\nu \to \frac{\ell^\nu v_L^\alpha}{\ell v_L + i\eta} L_\nu\,, \tag{7.1}$$

which is appropriate for a gluon flowing out of R and into L. Adopting the reasoning of R. Basu et al. [46], a potentially non factorizing remainder is then obtained by replacing

$$g^{\mu\nu} \to \left(g^{\mu\alpha} - \frac{\ell^\mu v_R^\alpha}{\ell v_R - i\eta'}\right)\left(g_\alpha{}^\nu - \frac{\ell^\nu v_{L\alpha}}{\ell v_L + i\eta}\right) \tag{7.2}$$

in the gluon propagator. Note that the replacement (7.2) is tantamount to the subtraction

$$\text{full graph} - (\text{collinear}_p + \text{collinear}_{\bar{p}} - \text{soft})\,. \tag{7.3}$$

If this combination does not get a leading contribution from the Glauber region for a specific graph, one can conclude that factorization does hold for the graph at hand. For this it is sufficient to show that the combination is power suppressed, i.e. suppressed by at least one power of Λ^2/Q^2. The great advantage of this method is that one can use power counting arguments instead of the explicit computation of possibly complicated loop integrals, and we will use it in our calculations in the sections below. If, however, this combination does receive a leading contribution from the Glauber region, one must check that this contribution cancels

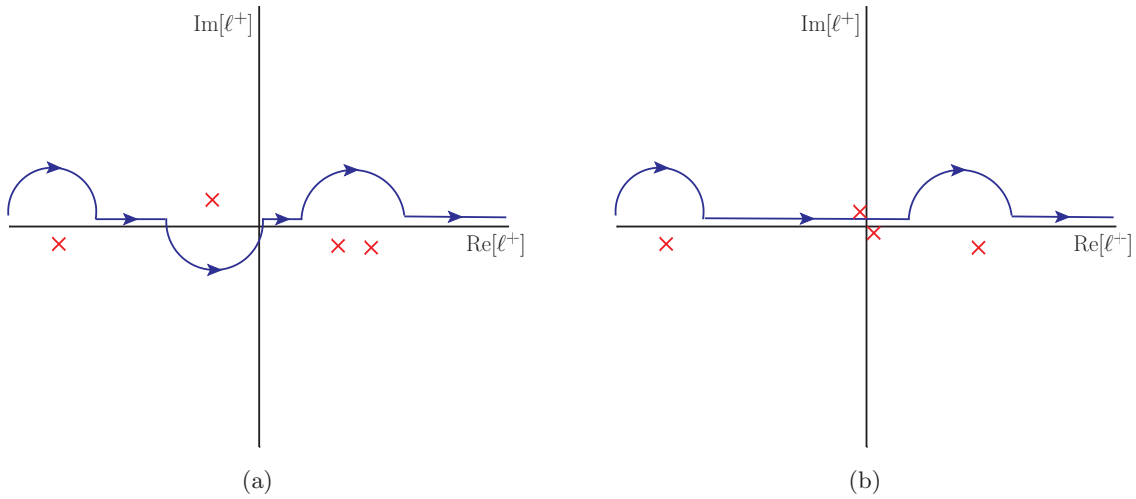

Figure 7.2.: Integration contour in the complex ℓ^+-plane. Poles of the integrand are indicated by the red crosses. In situation (a), all poles can be avoided by contour deformation. In the case of (b) the integration contour is trapped between two poles near the origin.

in the sum over all diagrams. Otherwise TMD factorization is broken for the process under consideration.

7.2. Model 1

We will first consider the most simple possible extension of the parton level single Drell-Yan process, where we have a right-moving, on-shell quark annihilating with a left-moving, on-shell antiquark. As a double parton scattering analog, we will study the valence quark double Drell-Yan production $\pi^+\pi^- \to \mu^+\mu^-$ in diagram 7.3(a). The momenta given there are chosen to be

$$\begin{aligned} p_1 &= (p_1^+, m_u^2/(2p_1^+), \mathbf{0}), \quad p_2 = (p_2^+, m_d^2/(2p_2^+), \mathbf{0}), \\ \bar{p}_1 &= (m_u^2/(2\bar{p}_1^-), \bar{p}_1^-, \mathbf{0}), \quad \bar{p}_2 = (m_d^2/(2\bar{p}_2^-), \bar{p}_2^-, \mathbf{0}), \end{aligned} \tag{7.4}$$

and they are all taken to be flowing into the vertices producing the gauge bosons. As pions are color singlet states, a factor of $\delta_{ij}\delta_{i'j'}\delta_{km}\delta_{k'm'}$ has to be incorporated into the expression for the diagram.

We will now study the possible one gluon corrections to this process. We use a finite gluon mass to regulate infrared divergences, given that this will turn out to be crucial in the following. The relevant diagrams are given in figure 7.3(b)–(d). Note that diagrams with a gluon exchange across the cut do not contribute to this order since the corresponding color factor is zero (one cannot form a color singlet state out of a gluon and two colorless gauge bosons). The gluon in the photon vertex correction 7.3(b) does not connect the two hard scattering processes. This graph is well known from single Drell-Yan and has been shown to factorize quite some time ago, see [39]. We will hence not discuss it in any further detail and instead turn to diagram 7.3(c), where the gluon does connect the two hard scatters.

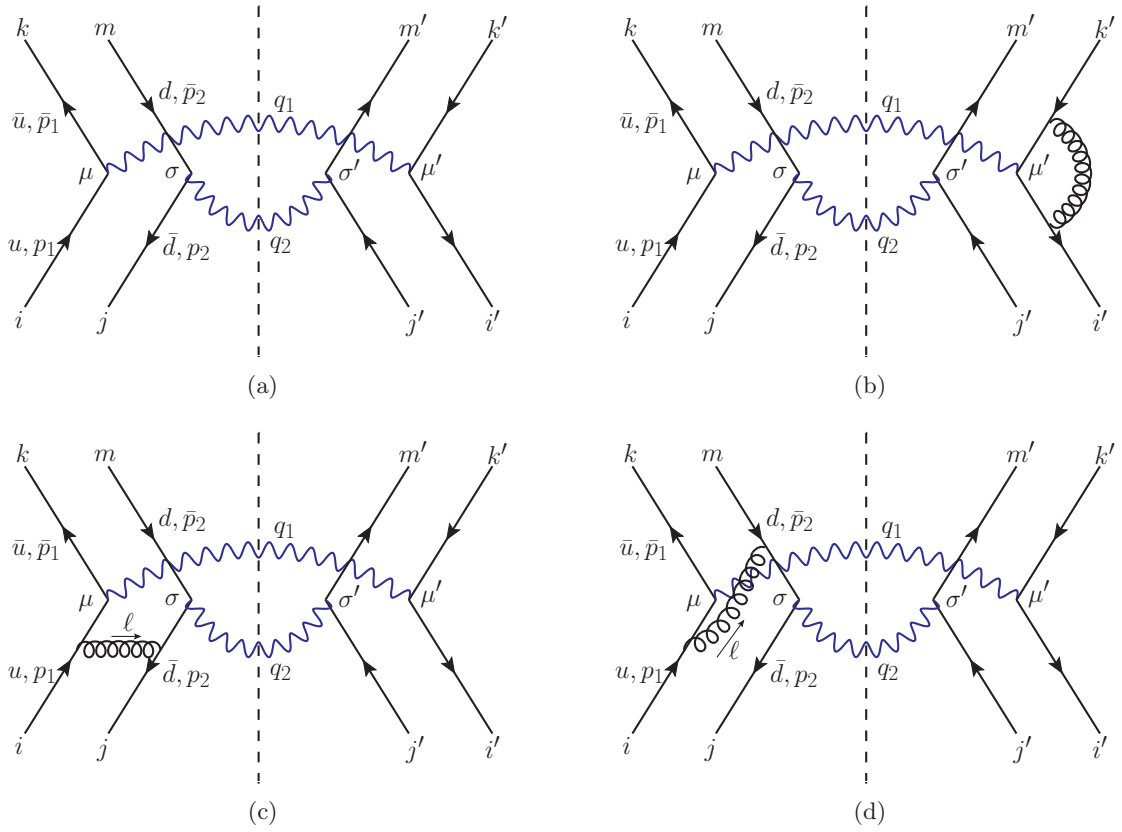

Figure 7.3.: (a) Tree level graph for the parton level double Drell-Yan process $\pi^+\pi^- \to \mu^+\mu^-$. The description of momenta and indices is given in the text. (b)-(d) One gluon exchange corrections to the tree level graph. Additional corrections obtained by mirroring at the photon vertices or complex conjugation as well as self energy diagrams and three more photon vertex corrections are not shown.

Momentum conservation implies $p_1 - \ell + \bar{p}_1 = q_1 = p_1 + \bar{p}_1$ and therefore $\ell = 0$ for that graph. This rather curious behaviour is due to the fact that we work in an oversimplified model where the on-shell quark lines are not allowed to exchange any momentum. This could for instance be cured by letting the quark and antiquark emerge from a point-like coupling through which momentum can be exchanged between the lines. We will now show that these contributions cancel adding their conjugate graphs.
The contribution from diagram 7.3(c) is proportional to

$$\begin{aligned}\frac{-i}{\ell^2 - \lambda^2 + i\epsilon} \operatorname{tr}\Big[(\not{p}_1 + m_u)\gamma^{\mu'}(\bar{\not{p}}_1 - m_u)\gamma^{\mu}(\not{p}_1 - \not{\ell} + m_u)\gamma^{\nu}\Big] \\ \times \operatorname{tr}\Big[(\not{p}_2 - m_d)\gamma_{\nu}(\not{p}_2 + \not{\ell} - m_d)\gamma^{\sigma}(\bar{\not{p}}_2 + m_d)\gamma^{\sigma'}\Big] \,. \end{aligned} \tag{7.5}$$

Next we consider the complex conjugate of diagram 7.3(c), which is proportional to

$$\begin{aligned}\frac{+i}{\ell^2 - \lambda^2 - i\epsilon} \operatorname{tr}\Big[(\not{p}_1 + m_u)\gamma^{\nu}(\bar{\not{p}}_1 - \not{\ell} + m_u)\gamma^{\mu'}(\not{p}_1 - m_u)\gamma^{\mu}\Big] \\ \times \operatorname{tr}\Big[(\not{p}_2 - m_d)\gamma^{\sigma}(\bar{\not{p}}_2 + m_d)\gamma^{\sigma'}(\bar{\not{p}}_2 + \not{\ell} - m_d)\gamma_{\nu}\Big] \,. \end{aligned} \tag{7.6}$$

When we now apply the momentum conservation constraint $\ell = 0$ to both (7.5) and (7.6) we see that both are equal but with opposite sign. This spurious soft divergence therefore cancels in the sum over diagrams. The preceding analysis can be repeated for the diagram in figure 7.3(d), and there we again find that these diagrams cancel.
The only remaining diagrams are the ones already familiar from single Drell-Yan and we therefore conclude that the double Drell-Yan process factorizes at next to leading order in this – admittedly oversimplified – model.

7.3. Model 2

We note that the calculations in the following section have been independently checked by Markus Diehl and Peter Plößl and have already been published [13].

7.3.1. Choice of model

Given that the model shown in the previous section led to very simple results due to a lack of correlation between the two hard scatters, we will now turn to a model that yields maximum correlation while simplifying several aspects of the calculation not needed for a proof of factorization.
A proof of factorization, i.e. a proof of the absence or cancellation of Glauber gluon contributions, only depends on the pole structure of loop integrands and therefore on the denominators. Including parton spin and color only introduces additional numerator algebra, i.e. potentially additional terms that only may cancel contributions from poles but never give additional ones. We therefore take a model with scalar partons that couple to each other via three- and four-point vertices. Gluons couple to the partons via the usual QCD-type vertices, see e.g. [47]. Some possible graphs of the double Drell-Yan process within this model are given in figure 7.4. One can immediately see that this kind of diagrams yields a maximum

amount of correlation between the two hard scatters as they are connected to one another.

We will first investigate where pinched poles in ℓ^+ or ℓ^- typically arise , taking the graph in figure 7.4(d) as an example. If ℓ is in the Glauber region we can neglect ℓ^- in the left-moving lines above the gauge boson vertices. It can also be neglected in the gluon propagator due to $|\boldsymbol{\ell}| \gg \ell^+, \ell^-$. The poles of the ℓ^--integration with small ℓ^- are therefore due to the propagator denominators

$$[(p-k_1+\ell)^2+i\epsilon]\,[(k_1-\ell)^2+i\epsilon] \approx [2(p-k_1)^+\ell^- + A + i\epsilon]\,[-2k_1^+\ell^- + B + i\epsilon]\,, \qquad (7.7)$$

where $A = 2(p-k_1)^+(p-k_1)^- - (\boldsymbol{p}-\boldsymbol{k}_1+\boldsymbol{\ell})^2$ and $B = 2k_1^+k_1^- - (\boldsymbol{k}_1-\boldsymbol{\ell})^2$ are both of order Λ^2. The ℓ^--integration contour is pinched near the origin, between a pair of poles with real parts of order Λ^2/Q. Note that the pole lies above the real axis when ℓ^- is routed against a large positive plus momentum (in this case k_1^+) and lies in the lower half plane when ℓ^- is routed along a large positive plus momentum (in this case $p^+ - k_1^+$).[1]
The same analysis can be done for the poles in ℓ^+, which can be neglected in the lines with large positive plus momentum, i.e. the lines below the gauge boson vertices, when ℓ is in the Glauber region. We then get the following poles in ℓ^+:

$$[(\bar{p}-\bar{k}_1+\ell)^2+i\epsilon]\,[(\bar{k}_1+\ell)^2+i\epsilon] \approx [2(\bar{p}-\bar{k}_1)^-\ell^+ + A + i\epsilon]\,[2\bar{k}_1^-\ell^+ + B + i\epsilon]\,, \qquad (7.8)$$

with $A = 2(\bar{p}-\bar{k}_1)^-(\bar{p}-\bar{k}_1)^+ - (\bar{\boldsymbol{p}}-\bar{\boldsymbol{k}}_1+\boldsymbol{\ell})^2$ and $B = 2\bar{k}_1^-\bar{k}_1^+ - (\bar{\boldsymbol{k}}_1+\boldsymbol{\ell})^2$. Now ℓ^+ is routed along both of the large positive minus momenta $(\bar{p}^- - \bar{k}_1^-)$ and $\bar{k}_1^-$, so that both poles are on the same side of the real axis. The integration contour of ℓ^+ can therefore be deformed out of the Glauber region and, e.g., into a region collinear to the right-moving particles. There, the approximations for collinear gluons stated in chapter 6 may be applied and factorization does hold.
Generally speaking, the integration contour of the integral over gluon longitudinal momenta is only pinched in the Glauber region, if both ℓ^+ and ℓ^- are trapped between coalescing poles in the Glauber region. For the graphs in figure 7.4, this is only the case for graph (f), because only there one always has to route ℓ^+ and ℓ^- along and against a large minus- or plus-momentum, respectively. We will further discuss this issue in section 7.3.5.
Before showing that there is no contribution from Glauber gluons in the sum over all possible graphs, we will perform explicit calculations for an even more simplified model in order to exhibit how the general power counting and contour deformation arguments work in a specific example. We therefore remove the spectator partons[2] and instead introduce a colourless scalar "hadron", to which a scalar parton pair attaches via a pointlike coupling. As a further simplification, we replace each electroweak gauge boson by a scalar particle with a pointlike momentum-independent coupling to two partons. This removes the dependence of the scattering amplitude on polarisation vectors or open Lorentz indices, without affecting the analytic structure of the graphs. The lowest order graph for double Drell-Yan within this model is shown in figure 7.5. We give a small mass m to the scalar partons in order to regulate collinear divergences and use a small gluon mass λ to regulate infrared divergences. The one-gluon exchange corrections to the basic graph are given in figure 7.6. Real gluon exchange does not contribute at this order, because one cannot form a color singlet state out

[1] We call ℓ to be routed along (against) a momentum k when the momentum of the line is $k+\ell$ ($k-\ell$).
[2] Active partons attach to a vertex producing an electroweak gauge boson, all other partons are spectators.

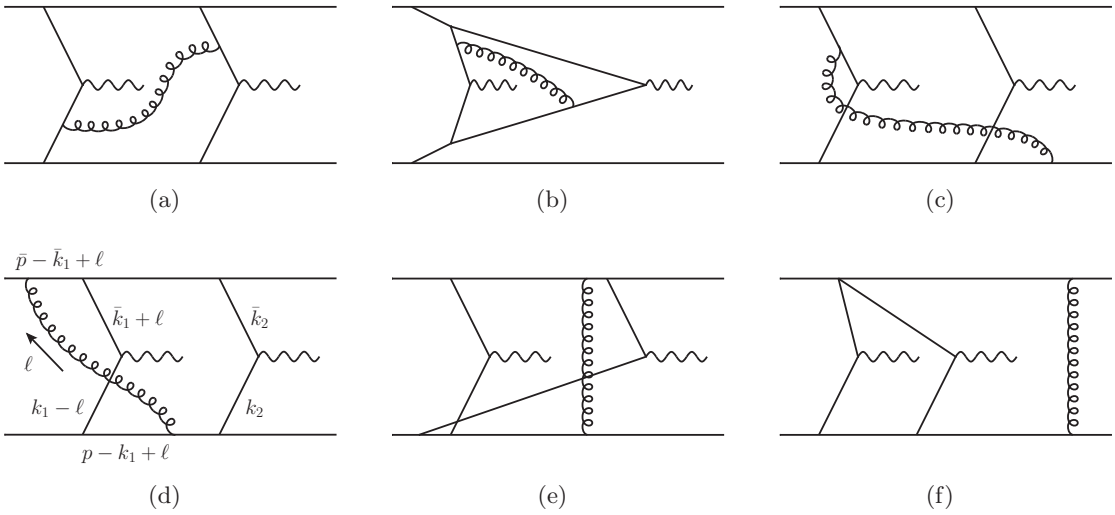

Figure 7.4.: Example graphs for the double Drell-Yan amplitude within the model used. In the physical process these graphs are embedded in graphs with further spectator lines and with a hadron entering each collinear subgraph.

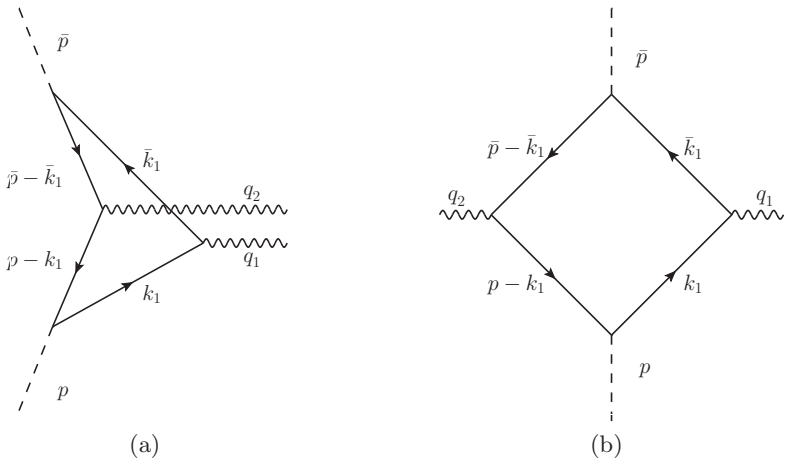

Figure 7.5.: (a) Double-Drell Yan graph for the simplified model described in section 7.3.1. The dashed lines are the incoming scalar hadrons, whilst the solid lines are scalar partons. (b) Redrawing of (a) used for better legibility. A second graph is obtained by reversing the arrows, which denote the flow of color charge.

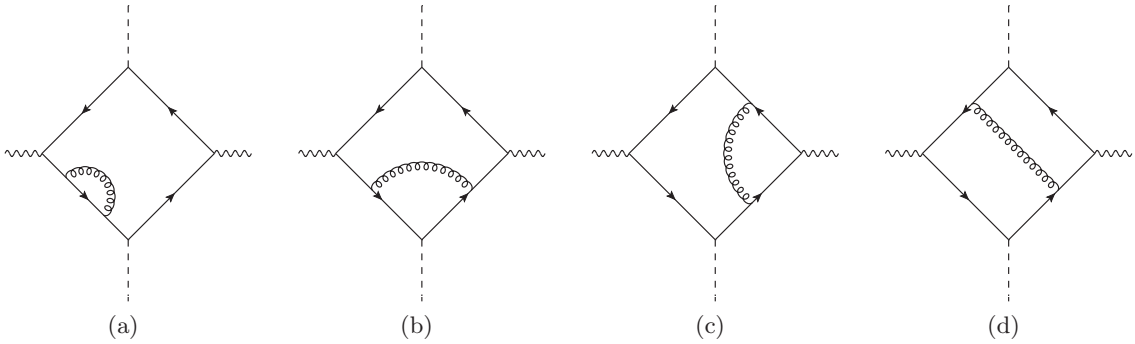

Figure 7.6.: One-gluon corrections to the double Drell-Yan amplitude in the model used: (a) parton self energy, (b) hadron vertex correction, (c) gauge boson vertex correction, (d) double box graph, where the gluon connects the two hard scatters.

of a gluon and two colorless gauge bosons. We will only consider the kinematical region where all parton lines in figure 7.5 have left or right-moving collinear momenta and thus transverse momenta of order $\Lambda \ll Q$, which is indeed the only leading momentum region of the graph due to the dimensionful, superrenormalizable hadron-parton-parton coupling. Therefore the problems mentioned in chapter 5 are not present in this case, while these problems do not interfere with the issue of Glauber gluon cancellation anyway.

7.3.2. Topologically factorizing corrections

We do not need to calculate the parton self energy and hadron vertex corrections shown in figure 7.6(a) and (b) explicitly, because these graphs are part of the one-loop expression of the collinear factor for the right-moving hadron and factorize topologically. Note that due to the presence of the $gg\phi\phi$ vertex there are additional gluon seagull diagrams. The contribution of these diagrams is proportional to

$$\int \mathrm{d}^{4-2\varepsilon}\ell \, \frac{1}{\ell^2 - \lambda^2 + i\varepsilon} \propto \lambda^{2-2\varepsilon} \,, \tag{7.9}$$

and therefore vanishes in the limit of zero gluon mass, which we take whenever possible.

7.3.3. Double box graph

We will start with the most complicated of all graphs, namely the double box graph shown in figure 7.7, as this calculation exhibits all the techniques needed. The gauge boson vertex correction graph in figure 7.6(c) will then be comparatively simple to calculate. The starting expression of the graph in figure 7.7 is, up to a constant, given by

$$\begin{aligned}\Gamma = \int \mathrm{d}\bar{k}_2^+ \, \mathrm{d}k_1^- \, \mathrm{d}^2\boldsymbol{k}_1 \int \frac{\mathrm{d}^4\ell}{\ell^2 - \lambda^2 + i\varepsilon} \, \frac{(2k_1 + \ell)_\mu \, g^{\mu\nu} (2\bar{k}_2 + \ell)_\nu}{[(\bar{k}_2 + \ell)^2 - m^2 + i\varepsilon]\,[(k_1 + \ell - p)^2 - m^2 + i\varepsilon]} \\ \times \frac{1}{[(k_1 + \ell)^2 - m^2 + i\varepsilon]\,[k_1^2 - m^2 + i\varepsilon]\,[(\bar{k}_2 - \bar{p})^2 - m^2 + i\varepsilon]\,[\bar{k}_2^2 - m^2 + i\varepsilon]} \,.\end{aligned} \tag{7.10}$$

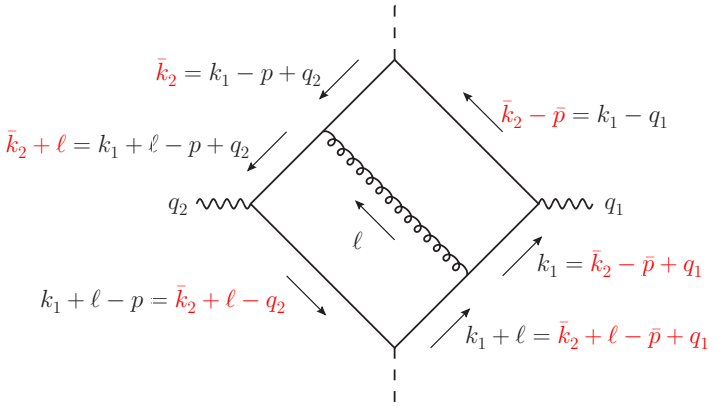

Figure 7.7.: Double box graph, showing momentum labellings and our routing of the extra loop momentum ℓ.

We can work in 4 spacetime dimensions, as this graph is not ultraviolet divergent. It is understood that $k_1 + \bar{k}_1 = q_1$, $k_2 + \bar{k}_2 = q_2$, $k_1 + k_2 = p$, $\bar{k}_1 + \bar{k}_2 = \bar{p}$ and $p + \bar{p} = q_1 + q_2$ by momentum conservation.
We choose a frame where the hadron with momentum p moves fast to the right and the hadron with momentum $\bar{p}$ fast to the left, with $\boldsymbol{p} = \bar{\boldsymbol{p}} = \mathbf{0}$. For k_i and $\bar{k}_i$ $(i = 1, 2)$ in the collinear region, the momentum components have typical size

$$q_i^{\pm} \sim p^+ \sim \bar{p}^- \sim Q\,, \qquad k_i^- \sim \bar{k}_i^+ \sim p^- \sim \bar{p}^+ \sim \Lambda^2/Q\,, \qquad |\boldsymbol{q}_i| \sim |\boldsymbol{k}_i| \sim |\bar{\boldsymbol{k}}_i| \sim \Lambda\,. \tag{7.11}$$

The choice of independent integration variables in (7.10) is appropriate for power counting since both $\bar{k}_2^+$ and k_1^- can freely vary over their natural range Λ^2/Q.
In the collinear momentum region, for the lowest order graph in figure 7.5 all four propagator denominators are of order Λ^2 and the integration volume is of order Λ^6/Q^2, giving an overall behaviour like $1/(\Lambda^2 Q^2)$. The Glauber region defined in (6.2) of ℓ contributes at the same order: The numerator factor $(2k_1 + \ell)(2\bar{k}_2 + \ell)$ is of order Q^2, the integration volume $\mathrm{d}^4\ell$ of order Λ^6/Q^2 and each of the three additional propagators of order $1/\Lambda^2$. Both k_1^- and ℓ^- can be of order Λ as long as $k_1^- + \ell^- \sim \Lambda^2/Q$, because this only carries the momentum k_1 off shell, which is compensated by a larger integration volume of ℓ^- compared with the Glauber region. Likewise, ℓ^+ can also be of order Λ.
As discussed in section 7.1.2, we replace

$$g^{\mu\nu} \to \left(g^{\mu\alpha} - \frac{\ell^\mu v_R^\alpha}{\ell v_R - i\eta'}\right)\left(g_\alpha{}^\nu - \frac{\ell^\nu v_{L\alpha}}{\ell v_L + i\eta}\right) \tag{7.12}$$

in the gluon propagator. Showing that this combination gives a power suppressed result is then tantamount to showing the validity of the Grammer-Yennie approximation and therefore the absence of a contribution from the Glauber region.

Lightlike Wilson lines

We will first consider the most simple case in which the soft and collinear Wilson lines are taken lightlike, with $v_R^+ = v_L^- = 1$ and $v_R^- = v_L^+ = 0$. The replacement in (7.12) then reads

$$\begin{aligned}(2k_1+\ell)_\mu g^{\mu\nu}(2\bar{k}_2+\ell)_\nu \;\to\; &\big[(2\boldsymbol{\ell}\boldsymbol{k}_1+\boldsymbol{\ell}^2)(2\boldsymbol{\ell}\bar{\boldsymbol{k}}_2+\boldsymbol{\ell}^2)\\ &- 2\ell^+k_1^-(2\boldsymbol{\ell}\bar{\boldsymbol{k}}_2+\boldsymbol{\ell}^2) - 2\ell^-\bar{k}_2^+(2\boldsymbol{\ell}\boldsymbol{k}_1+\boldsymbol{\ell}^2) - \ell^+\ell^-\big\{4(\boldsymbol{k}_1+\boldsymbol{\ell})(\bar{\boldsymbol{k}}_2+\boldsymbol{\ell}) - \boldsymbol{\ell}^2\big\}\\ &+ 2\ell^+\ell^-(2k_1^-+\ell^-)(2\bar{k}_2^++\ell^+)\big] \,/\, \big[(\ell^- - i\eta')(\ell^+ + i\eta)\big] \end{aligned} \tag{7.13}$$

in (7.10). The leading contribution on the l.h.s. of (7.13) is $4k_1^+\bar{k}_2^- \sim Q^2$, and therefore we only get a leading contribution on the r.h.s. from gluon momentum regions where this expression is also of order Q^2. When ℓ is soft $\sim(\Lambda,\Lambda,\Lambda)$ or collinear, the numerator of the right-hand-side is of order Λ^4 and the denominator of order Λ^2, giving a power-suppressed $\mathcal{O}(\Lambda^2)$ contribution overall. For the momentum scalings $\ell \sim (\Lambda^2/Q,\Lambda,\Lambda)$ and $\ell\sim(\Lambda,\Lambda^2/Q,\Lambda)$, the numerator remains of order Λ^4 whilst the denominator is reduced to order Λ^3/Q, which is however not enough to give a leading contribution. In the ultrasoft region of ℓ the denominator is of order Λ^4/Q^2 but the numerator shrinks to order Λ^6/Q^2, resulting again in a subleading contribution. Only when ℓ is in the Glauber region, where the numerator is of order Λ^4 and the denominator of order Λ^4/Q^2, one gets a leading contribution by power counting.
According to this power counting argument the r.h.s. can yield a leading contribution when the gluon momentum is in the Glauber region. We will therefore further investigate this case. For a gluon momentum in the Glauber region, we can neglect all terms in (7.13) that contain either ℓ^+ or ℓ^- (or both), because these terms are subleading compared to terms only containing transverse momenta.
We now use Feynman parameters (cf. appendix C) to combine all terms containing ℓ and get

$$I = \frac{3!N}{D}\int[\mathrm{d}^4\alpha]\int\frac{\mathrm{d}\ell^-}{\ell^- - i\eta'}\int\frac{\mathrm{d}\ell^+}{\ell^+ + i\eta}\,\frac{1}{[2\ell^+\ell^- + 2a^-\ell^+ + 2a^+\ell^- + A + i\varepsilon]^4}\,, \tag{7.14}$$

with

$$\begin{aligned} A &= 2(\alpha_3 q_1^+ - \alpha_2 q_2^+ - \alpha_3\bar{p}^+)k_1^- + 2\bar{k}_2^+(\alpha_1 q_2^- - \alpha_1 p^- - \alpha_2 p^-) + 2(1-\alpha_4)\bar{k}_2^+k_1^-\\ &\quad + 2\alpha_2 q_2^+ p^- - \alpha_1(\bar{\boldsymbol{k}}_2+\boldsymbol{\ell})^2 - (\alpha_2+\alpha_3)(\boldsymbol{k}_1+\boldsymbol{\ell})^2 - \alpha_4(\boldsymbol{\ell}^2+\lambda^2) - (1-\alpha_4)m^2\,,\\ a^+ &= \alpha_3 q_1^+ - \alpha_2 q_2^+ - \alpha_3\bar{p}^+ + (1-\alpha_4)\bar{k}_2^+\,,\\ a^- &= \alpha_1 q_2^- - (\alpha_1+\alpha_2)p^- + (1-\alpha_4)k_1^-\,,\\ N &= (2\boldsymbol{\ell}\boldsymbol{k}_1+\boldsymbol{\ell}^2)(2\boldsymbol{\ell}\bar{\boldsymbol{k}}_2+\boldsymbol{\ell}^2)\,,\\ D &= [k_1^2 - m^2 + i\varepsilon]\,[(\bar{k}_2-\bar{p})^2 - m^2 + i\varepsilon]\,[\bar{k}_2^2 - m^2 + i\varepsilon]\,. \end{aligned} \tag{7.15}$$

The integration measure for Feynman parameters is

$$[\mathrm{d}^n\alpha] = \mathrm{d}\alpha_1\cdots\mathrm{d}\alpha_n\;\delta(\alpha_1+\cdots+\alpha_n-1) \qquad \text{with } 0\le\alpha_i\le 1, \tag{7.16}$$

and it is understood that I is still to be integrated over k_1^-, $\bar{k}_2^+$, $\boldsymbol{k}_1$ and $\boldsymbol{\ell}$. The volume of this integration space is

$$\int \mathrm{d}k_1^-\mathrm{d}\bar{k}_2^+\mathrm{d}^2\boldsymbol{k}_1\mathrm{d}^2\boldsymbol{\ell} \sim \frac{\Lambda^2}{Q}\frac{\Lambda^2}{Q}\Lambda^2\Lambda^2 \sim \frac{\Lambda^8}{Q^2}\,. \tag{7.17}$$

The leading contribution to Γ is $\mathcal{O}[1/(\Lambda^2 Q^2)]$, and therefore the integral I has to be of order $1/\Lambda^{10}$ for a leading power contribution. On the other hand, showing that I is power suppressed compared to this leading power behaviour is tantamount to showing that the Grammer-Yennie approximations do indeed hold.
As appropriate for the Glauber region, we only consider the case $|\boldsymbol{\ell}| \sim \Lambda$ in the following. Power counting thus gives $A \sim \Lambda^2$ for any value of the Feynman parameters,[3] even if we take masses $\lambda, m \ll \Lambda$. This implies that regions where $\alpha_i \ll 1$ for one or several i are power suppressed: contributions from such regions are suppressed by the phase space $[\mathrm{d}^n\alpha]$ and cannot be enhanced by having a smaller denominator. Only the region where all Feynman parameters are of generic size can possibly give a contribution of order $1/\Lambda^{10}$ to I. We then have

$$A \sim \Lambda^2\,, \qquad\qquad a^+, a^- \sim Q\,, \qquad\qquad a^- > 0\,, \tag{7.18}$$

whereas a^+ can have either sign, depending on the relative size of $\alpha_3 q_1^+$ and $\alpha_2 q_2^+$.
We will now take a closer look at I. First, we perform the integral over ℓ^+ using Cauchy's theorem. We get a nonzero result only for $\ell^- + a^- < 0$ (otherwise the poles are on the same side of the real axis). Picking up the residue at $\ell^+ = -i\eta$ we get

$$I = -2\pi i\,\frac{3!N}{D}\int[\mathrm{d}^4\alpha]\int_{-\infty}^{-a^-}\frac{\mathrm{d}\ell^-}{\ell^- - i\eta'}\,\frac{1}{[2a^+\ell^- + A + i\varepsilon]^4}, \tag{7.19}$$

where we have dropped $i\eta$ in the last denominator, since it comes with the same sign as $i\varepsilon$ and thus does not change the position of the pole.
We note that the evaluation of Feynman integrals in light-cone coordinates has to be done with some care, because in some cases the naive application of Cauchy's theorem can lead to wrong results. In the case at hand we have cross checked our results with the method described in appendix D. As explained there, we could not have used Cauchy's theorem for the ℓ^+ integration in (7.14) if we had kept the full numerator of the graph given in (7.13), because terms with ℓ^+ or $(\ell^+)^2$ would have cancelled the denominator $\ell^+ + i\eta$. Using the method just mentioned, we have checked that these terms give a power suppressed contribution and can hence be discarded, as we argued on the basis of power counting before (7.14).
One can already see that due to $a^+ \sim Q$ and ℓ^- being at least of order Q in eq. (7.19), the last factor in (7.19) already gives a power suppressed result. This is in agreement with the observation that the integration contour of ℓ^- is far away from the poles in ℓ^-,

$$\ell_1^- = i\eta'\,, \qquad\qquad \ell_2^- = -A/(2a^+) - \mathrm{sgn}(a^+)\,i\varepsilon\,, \tag{7.20}$$

which are at small values of ℓ^-.

[3] This reflects the fact that the four propagators that have been combined into the term raised to the fourth power in (7.14) are each of order Λ^2 for $\ell^+ = \ell^- = 0$.

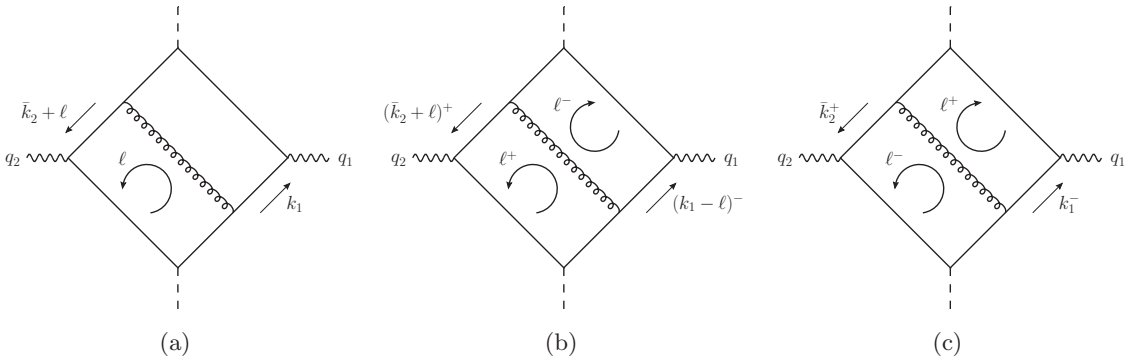

(a) (b) (c)

Figure 7.8.: Different momentum routings for the double box graph: (a) routing used in (7.10), where ℓ^- but not ℓ^+ is pinched in the Glauber region, (b) routing for which neither ℓ^+ nor ℓ^- is pinched in the Glauber region, (c) routing for which both ℓ^+ and ℓ^- are pinched in the Glauber region.

We nevertheless calculate (7.19) explicitly by partial fractioning and get

$$\begin{aligned} I = -2\pi i \frac{3!N}{D} \int [\mathrm{d}^4\alpha] \Bigg\{ & \frac{1}{(A+i\varepsilon)^4} \log\left|\frac{2a^+a^- - A}{2a^+a^-}\right| \\ & + \frac{i\pi}{(A+i\varepsilon)^4} \left[\Theta(2a^+a^- - A) + \Theta(a^-) - \Theta(a^+) - 1\right] \\ & - \frac{1}{(A+i\varepsilon)^3(A - 2a^+a^- + i\varepsilon)} - \frac{1}{2}\frac{1}{(A+i\varepsilon)^2(A - 2a^+a^- + i\varepsilon)^2} \\ & - \frac{1}{3}\frac{1}{(A+i\varepsilon)(A - 2a^+a^- + i\varepsilon)^3} \Bigg\}. \end{aligned} \tag{7.21}$$

Having $a^+a^- \sim Q^2$, we see that all terms containing at least one factor of $(A - 2a^+a^-)^{-1}$ are power suppressed. Also, the expansion of the logarithm

$$\log\left(\frac{Q^2 - \Lambda^2}{Q^2}\right) \approx -\frac{\Lambda^2}{Q^2} \tag{7.22}$$

gives a power suppressed contribution. The only potentially leading terms in eq. (7.21) are therefore the ones with Θ-functions. These terms do, however, cancel due to $a^- > 0$, which confirms the power counting argument for (7.19).

Alternative momentum routings

As we have already seen in section 7.3.1, the way in which ℓ^+ and ℓ^- are routed along or against the lines with large longitudinal momenta is decisive for whether these integration contours are pinched at small values of order Λ^2/Q or not. We will use the freedom of rerouting ℓ^+ and ℓ^- to study two additional momentum routings depicted in figure 7.8(b) and (c), while the routing in (a) has already been discussed in the last section. The routing in (b), which can be obtained by shifting $k_1^- \to k_1^- - \ell^-$, is chosen such that neither ℓ^+ nor ℓ^- are pinched in the Glauber region and one therefore immediately expect a power suppressed result. On the contrary, the routing in (c), which can be obtained by shifting $\bar{k}_2^+ \to \bar{k}_2^+ - \ell^+$,

is chosen such that both ℓ^+ and ℓ^- are pinched in the Glauber region and one could therefore expect that we get a leading contribution from the Glauber region. We will explicitly show that this is not the case for both routings in the following.
We start with the graph in figure 7.8(b). Using separate sets of Feynman parameters for combining the propagators containing ℓ^+ with the gluon propagator on one hand and for the propagators containing ℓ^- on the other hand, we get

$$I = 3!\,2!\,N \int [\mathrm{d}^4\alpha][\mathrm{d}^3\beta] \int \frac{\mathrm{d}\ell^-}{\ell^- - i\eta'} \int \frac{\mathrm{d}\ell^+}{\ell^+ + i\eta} \times \frac{1}{[2\alpha_4\,\ell^+\ell^- + 2a^-\ell^+ + A + i\varepsilon]^4\,[2b^+\ell^- + B + i\varepsilon]^3} \tag{7.23}$$

with A, a^- and N as in (7.15) and

$$\begin{aligned} B &= 2(\beta_1 q_1^+ - \beta_1\bar{p}^+ - \beta_2\bar{p}^+)\,k_1^- - 2\bar{k}_2^+(\beta_2 q_1^- - \beta_3 q_2^- + \beta_3 p^-) + 2\bar{k}_2^+ k_1^- \\ &\quad + 2\beta_2\bar{p}^+ q_1^- - \beta_1 \boldsymbol{k}_1^2 - (\beta_2+\beta_3)\bar{\boldsymbol{k}}_2^2 - m^2\,, \\ b^+ &= -\beta_1 q_1^+ + (\beta_1+\beta_2)\bar{p}^+ - \bar{k}_2^+\,. \end{aligned} \tag{7.24}$$

We see that $B \sim \Lambda^2$ for all values of the Feynman parameters (as is the case for A), even if m is neglected. Hence the regions with $\beta_i \ll 1$ cannot give a leading contribution to I due to the suppression from the integration volume $[\mathrm{d}^3\beta]$. In the generic region of Feynman parameters, we have

$$B \sim \Lambda^2\,, \qquad\qquad b^+ \sim Q\,, \qquad\qquad b^+ < 0\,. \tag{7.25}$$

Once again, we perform the ℓ^+ integral using Cauchy's theorem and obtain

$$I = -2\pi i\,3!\,2!\,N \int [\mathrm{d}^4\alpha][\mathrm{d}^3\beta] \int_{-\infty}^{-a^-/\alpha_4} \frac{\mathrm{d}\ell^-}{\ell^- - i\eta'}\, \frac{1}{[A+i\varepsilon]^4\,[2b^+\ell^- + B + i\varepsilon]^3}\,. \tag{7.26}$$

Just like in the case of eq. (7.19), ℓ^- is restricted to a region where it is at least of order Q due to $a^-/\alpha_4 \sim Q$. This constrains the term $2b^+\ell^- + B$ to be of order Q^2 or bigger and we see that we once again obtain a power suppressed result as before.
We now turn to the routing in figure 7.8(c), where both ℓ^+ and ℓ^- are pinched in the Glauber region. We once again combine the propagators containing ℓ^+ with the gluon propagator on one hand and the propagators containing ℓ^- on the other hand using Feynman parameters and get

$$I = 3!\,2!\,N \int [\mathrm{d}^4\alpha][\mathrm{d}^3\beta] \int \frac{\mathrm{d}\ell^-}{\ell^- - i\eta'} \int \frac{\mathrm{d}\ell^+}{\ell^+ + i\eta} \times \frac{1}{[2\alpha_4\,\ell^+\ell^- + 2a^+\ell^- + A + i\varepsilon]^4\,[2b^-\ell^+ + B + i\varepsilon]^3} \tag{7.27}$$

with A, a^+ and N as in (7.15), B as in (7.24) and

$$b^- = \beta_2 q_1^- - \beta_3 q_2^- + \beta_3\bar{p}^- - k_1^-\,. \tag{7.28}$$

In the generic region of Feynman parameters, both a^+ and b^- are of order Q but can have

either sign. We perform the ℓ^- integral using Cauchy's theorem and obtain

$$I = -2\pi i\, 3!\, 2!\, N \int [\mathrm{d}^4\alpha][\mathrm{d}^3\beta] \int_{-a^+/\alpha_4}^{\infty} \frac{\mathrm{d}\ell^+}{\ell^+ + i\eta} \frac{1}{[A+i\varepsilon]^4\,[2b^-\ell^+ + B + i\varepsilon]^3}\,. \tag{7.29}$$

Once again, the poles of the ℓ^+ integration are near zero. In contrast to the other two routings we have discussed, there may be poles near the integration contour, depending on the signs of a^+ and b^-. There are three different cases we need to discuss:

1. $a^+ < 0$ and b^- of either sign: both poles are far away from the integration region,
2. $a^+ > 0$ and $b^- > 0$: both poles are below the real axis,
3. $a^+ > 0$ and $b^- < 0$: the integration contour is pinched in the Glauber region.

In case 1, both poles are far away from the integration region and therefore we immediately get a power suppressed result. In case 2, both poles of the ℓ^+ integration are below the real axis and we can deform the integration contour into the upper half plane into a region where $2b^-\ell^+ \sim Q^2$, which is enough to obtain a power suppressed result.
In case 3, however, the contour is trapped in the Glauber region. We can make the same contour deformation as in case 2, but get an additional term picking up the residue of the eikonal propagator, which is proportional to $[A+i\varepsilon]^{-4}[B+i\varepsilon]^{-3}$ and would yield a leading power contribution to I. This additional contribution is, however, zero, which can be seen by integrating over either $\bar{k}_2^+$ or k_1^-:

$$\begin{aligned}[A+i\varepsilon]^{-4}\,[B+i\varepsilon]^{-3} = {}& [2a^+k_1^- + 2(\alpha_1 q_2^- - \alpha_1 p^- - \alpha_2 p^-)\,\bar{k}_2^+ + \cdots + i\varepsilon]^{-4} \\ & \times [2(\beta_1 q_1^+ - \beta_1 \bar{p}^+ - \beta_2 \bar{p}^+)\,k_1^- - 2b^-\bar{k}_2^+ + \cdots + i\varepsilon]^{-3}\,,\end{aligned} \tag{7.30}$$

where the ellipses denote terms independent of k_1^- and $\bar{k}_2^+$. We see that for $a^+ > 0$ the poles of (7.30) in k_1^- are on the same side of the real axis and thus give a zero integral (note that a^+ depends on $\bar{k}_2^+$ but not on k_1^-). The same result is obtained if one first integrates over $\bar{k}_2^+$ under the condition that $b^- < 0$. We have thus shown again that the Grammer-Yennie approximation works, but this required integration over several loop variables.

Wilson lines with finite rapidity

Taking Wilson lines with finite rapidity is one of the most prominent ways of regularizing rapidity divergences. Therefore, we will now study the double box graph again, but this time take v_R and v_L to have a finite rapidity.
As spacelike Wilson lines are known to admit the same contour deformations as in the original graph, we expect factorization to hold also for this case. Timelike Wilson lines do not necessarily admit these contour deformations and we will investigate how this affects the factorization properties of the double box graph explicitly.

Spacelike Wilson lines. We take spacelike Wilson lines with $v_R^+ = v_L^- = 1$ and $v_L^+ = v_R^- = -\delta^2$. As discussed in section 6.3, we must take v_R (v_L) to have large positive (negative) rapidity, of the same order as the appropriate collinear particles and therefore we count $\delta \sim \Lambda/Q$.

In the numerator of the right hand side of (7.13), replacing lightlike with spacelike Wilson lines only results in power-suppressed changes in the Glauber region, and the leading power term is still the one with only transverse components. In (7.14) we replace

$$\frac{1}{\ell^+ + i\eta} \to \frac{1}{\ell^+ - \delta^2\ell^- + i\eta}\,, \qquad \frac{1}{\ell^- - i\eta'} \to \frac{1}{\ell^- - \delta^2\ell^+ - i\eta'}\,. \tag{7.31}$$

The resulting new poles of the eikonal propagators are:

$$\ell^+_{\text{eik},1} = \delta^2\ell^- - i\eta\,, \qquad \ell^+_{\text{eik},2} = \delta^{-2}\ell^- - i\delta^{-2}\eta'\,. \tag{7.32}$$

The first pole reproduces the pole we already had in eq. (7.14) in the lightlike limit $\delta^2 \to 0$, whereas the second one has no counterpart in that equation. Both poles lie below the real axis, and therefore the contour deformations made to avoid the Glauber region in the lightlike case can also be done here. We therefore expect the Grammer-Yennie approximation to hold also in this case and will confirm this by further calculation. We only get a non-zero result from $\ell^- + a^- < 0$, because otherwise all poles in ℓ^+ are on the same side of the real axis. Using Cauchy's theorem to evaluate the integral over ℓ^+ and approximating $1 - \delta^4 \approx 1$ we obtain

$$\begin{aligned} I_{\text{SL}} = -2\pi i\,\frac{3!N}{D}\int[\mathrm{d}^3\alpha]\,\Bigg\{&\int_{-\infty}^{-a^-}\frac{\mathrm{d}\ell^-}{\ell^- - i\eta''}\,\frac{1}{[2\delta^2(\ell^-)^2 + 2\ell^-(a^+ + \delta^2 a^-) + A + i\varepsilon]^4} \\ &- \int_{-\infty}^{-a^-}\frac{\mathrm{d}\ell^-}{\ell^- - i\eta''}\,\frac{1}{[2\delta^{-2}(\ell^-)^2 + 2\ell^-(a^+ + \delta^{-2} a^-) + A + i\varepsilon]^4}\Bigg\} \end{aligned} \tag{7.33}$$

with $\eta'' = \eta' - \delta^2\eta$. We can once again limit ourselves to the generic region of Feynman parameters, as the arguments given above still hold. Power counting therefore gives

$$A \sim \Lambda^2\,, \qquad a^+, a^- \sim Q\,, \qquad a^- > 0\,. \tag{7.34}$$

Note that the ambiguous sign of η'' does not complicate further calculations, because the corresponding pole at $\ell^- = i\eta''$ is far away from the integration path as ℓ^- is restricted to the region smaller than $-Q$. This causes the integrand in (7.33) to be strongly power suppressed except for regions where the integration path is close to poles in ℓ^-. Using the power counting rules in (7.34), we find that the poles lie approximately at

$$\ell_1^- \approx -A/(2a^+) - \operatorname{sgn}(a^+)\,i\varepsilon\,, \qquad \ell_2^- \approx -\delta^{-2}a^+ + \operatorname{sgn}(a^+)\,i\varepsilon\,, \tag{7.35}$$

for the first term in (7.33) and at

$$\ell_3^- \approx -\delta^2 A/(2a^-) - i\varepsilon\,, \qquad \ell_4^- \approx -a^- - \delta^2 a^+ + i\varepsilon\,, \tag{7.36}$$

for the second term. With $A/(2a^+) \sim \Lambda^2/Q$ and $\delta^2 A/(2a^-) \sim \Lambda^4/Q^3$, the poles at ℓ_1^- and ℓ_3^- are close to zero. Hence they lie far away from the integration contour and cause no problem. We are now left to study the poles at ℓ_2^- and ℓ_4^-.
For $a^+ < 0$, ℓ_2^- has a huge positive real part of order Q^3/Λ^2 and is therefore far away from the integration region. For $a^+ > 0$ it lies near the integration path, but it can be avoided by contour deformation into the lower half plane. We therefore observe that the pole at ℓ_2^- does

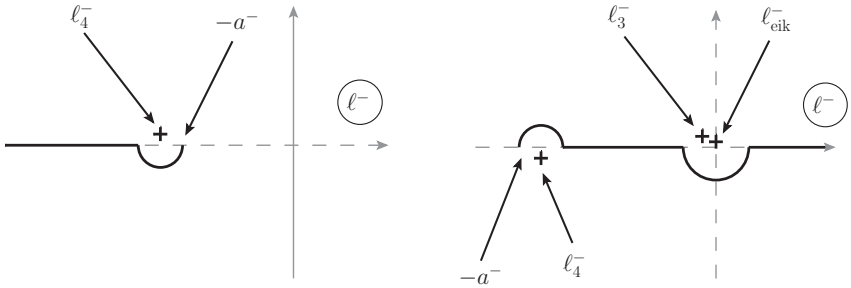

(a) (b)

Figure 7.9.: Integration paths and poles of the second integrals in (7.33)(a) and in (7.40)(b) for $a^+ > 0$.

not give rise to an enhancement of the integrand in (7.33).
The situation is different for the pole at ℓ_4^-, because it lies near the endpoint $-a^-$ of the ℓ^- integration for either sign of a^+. For $a^+ < 0$ we see that ℓ_4^- lies to the right of the endpoint within a distance $\delta^2 a^+ \sim \Lambda^2/Q$. An upper limit for the integrand in (7.33) is then given by the value at the endpoint, which is proportional to

$$[2\delta^{-2}(\ell^-)^2 + 2\ell^-(a^+ + \delta^{-2}a^-) + A]^{-4} = [-2a^+a^- + A]^{-4} \sim [Q^2]^{-4} \quad \text{for } \ell^- = -a^-\,, \quad (7.37)$$

We therefore get a strong suppression of the second integral in (7.33) in the case $a^+ < 0$.
If $a^+ > 0$, the pole at ℓ_4^- lies within a distance of Λ^2/Q to the left of the endpoint of the integration and therefore infinitesimally close to the integration path. There is, however, no second pole on the other side of the real axis which could obstruct a contour deformation into the lower half plane. A possible contour deformation for which the upper limit of the integrand as given in eq. (7.37) remains valid is a semi-circle around ℓ_4^- as shown in figure 7.9(a). We therefore also get a strongly power suppressed integral in this case.

Timelike Wilson lines. We will now examine the case when the Wilson lines are taken to be timelike. The leading numerator terms are once again given by N in (7.15). Taking timelike Wilson lines corresponds to the replacement

$$\frac{1}{\ell^+ + i\eta} \to \frac{1}{\ell^+ + \delta^2\ell^- + i\eta}\,, \qquad \frac{1}{\ell^- - i\eta'} \to \frac{1}{\ell^- + \delta^2\ell^+ - i\eta'} \quad (7.38)$$

in (7.14). Note that the ℓ^+ poles of the eikonal propagators

$$\ell^+_{\rm eik,1} = -\delta^2\ell^- - i\eta\,, \qquad \ell^+_{\rm eik,2} = -\delta^{-2}\ell^- + i\delta^{-2}\eta'\,, \quad (7.39)$$

are now on opposite sides of the real axis. As already mentioned, this may obstruct certain contour deformations needed to establish factorization and we will investigate the consequences in the following.
In order to evaluate the ℓ^+ integral, we close the integration contour in the lower half plane for $\ell^- + a^- < 0$ and take the residue at $\ell^+ = \ell^+_{\rm eik,1}$, whereas we close it in the upper half plane

for $\ell^- + a^- > 0$ and take the residue at $\ell^+ = \ell^+_{\text{eik},2}$. Approximating $(1-\delta^4) \approx 1$ we obtain

$$I_{\text{TL}} = -2\pi i \, \frac{3!N}{D} \int [\mathrm{d}^3\alpha] \left\{ \int_{-\infty}^{-a^-} \frac{\mathrm{d}\ell^-}{\ell^- - i\eta''} \, \frac{1}{[-2\delta^2(\ell^-)^2 + 2\ell^-(a^+ - \delta^2 a^-) + A + i\varepsilon]^4} \right.$$
$$\left. + \int_{-a^-}^{\infty} \frac{\mathrm{d}\ell^-}{\ell^- - i\eta''} \, \frac{1}{[-2\delta^{-2}(\ell^-)^2 + 2\ell^-(a^+ - \delta^{-2} a^-) + A + i\varepsilon]^4} \right\}. \tag{7.40}$$

In contrast to the spacelike case, the sign of $\eta'' = \eta' + \delta^2\eta$ now is unambiguous, which this time is important because the pole of the eikonal propagator

$$\ell^-_{\text{eik}} = i\eta'' \tag{7.41}$$

can now be near the integration contour. The remaining poles are

$$\ell^-_1 = -A/(2a^+) - \text{sgn}(a^+) i\varepsilon \,, \qquad \ell^-_2 = \delta^{-2} a^+ + \text{sgn}(a^+) i\varepsilon \tag{7.42}$$

for the first term in (7.40) and

$$\ell^-_3 = \delta^2 A/(2a^-) + i\varepsilon \,, \qquad \ell^-_4 = -a^- + \delta^2 a^+ - i\varepsilon \tag{7.43}$$

for the second term. For the first integral in (7.40), the situation is essentially identical to that for the first integral in (7.33) (except that ℓ^-_2 now has a negative real part for $a^+ < 0$ rather than $a^+ > 0$), and we can use the same strategy to avoid the poles.
In the second integral, the poles at ℓ^-_{eik} and ℓ^-_3 are both near the origin, but on the same side of the real axis. They can hence both be avoided by a contour deformation into the lower half plane as depicted in figure 7.9 (b). The pole at ℓ^-_4 lies near the endpoint of the integration, just like in the case of spacelike Wilson lines, and the same arguments as given in the treatment of the spacelike case apply here.
We therefore conclude that the result is power suppressed also in the case of timelike Wilson lines, in spite of the fact that contour deformations needed to establish factorization are much less straightforward in this case. Note that this is only an observation for the particular example at hand and we do not know whether timelike Wilson lines are generally suited for establishing factorization at higher orders in the strong coupling.

7.3.4. Gauge boson vertex correction

The gauge boson vertex correction depicted in figure 7.10 will now be comparatively easy to analyse. Note that neither ℓ^+ nor ℓ^- are routed in a way that they flow both against and along a line with large minus- or plus-momentum. We therefore expect the Grammer-Yennie approximations to be valid, because both longitudinal momenta can be freely deformed out of the Glauber region.
The starting expression for the gauge boson vertex correction is given by

$$\Gamma = \int \mathrm{d}\bar{k}_2^+ \, \mathrm{d}k_1^- \, \mathrm{d}^{2-2\epsilon}\boldsymbol{k}_1 \int \frac{\mathrm{d}^{4-2\epsilon}\ell}{\ell^2 - \lambda^2 + i\varepsilon} \, \frac{(2k_1 - \ell)_\mu g^{\mu\nu} (2\bar{k}_2 - 2\bar{p} - \ell)_\nu}{[(k_1 - \ell)^2 - m^2 + i\varepsilon][(\bar{k}_2 - \bar{p} - \ell)^2 - m^2 + i\varepsilon]}$$
$$\times \frac{1}{[k_1^2 - m^2 + i\varepsilon][(p - k_1)^2 - m^2 + i\varepsilon][\bar{k}_2^2 - m^2 + i\varepsilon][(\bar{p} - \bar{k}_2)^2 - m^2 + i\varepsilon]} \,. \tag{7.44}$$

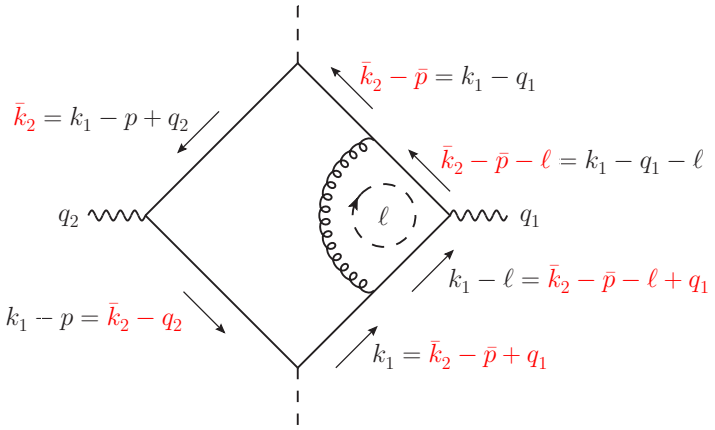

Figure 7.10.: Gauge boson vertex correction.

In contrast to the double box graph studied in the last section, the vertex correction is UV divergent and we therefore work in $4 - 2\epsilon$ spacetime dimensions. We once again make the replacement (7.12) in the gluon propagator. The resulting numerator is

$$\begin{aligned}(2k_1 - \ell)_\mu g^{\mu\nu}(2\bar{k}_2 - 2\bar{p} - \ell)_\nu \;\to\; &\big[(2\boldsymbol{\ell}\boldsymbol{k}_1 - \boldsymbol{\ell}^2)(2\boldsymbol{\ell}\bar{\boldsymbol{k}}_2 - \boldsymbol{\ell}^2) \\ &- 2\ell^+ k_1^-(2\boldsymbol{\ell}\bar{\boldsymbol{k}}_2 - \boldsymbol{\ell}^2) - 2\ell^-(\bar{k}_2^+ - \bar{p}^+)(2\boldsymbol{\ell}\boldsymbol{k}_1 - \boldsymbol{\ell}^2) - \ell^+\ell^-\big\{4(\boldsymbol{k}_1 - \boldsymbol{\ell})(\bar{\boldsymbol{k}}_2 - \boldsymbol{\ell}) - \boldsymbol{\ell}^2\big\} \\ &+ 2\ell^+\ell^-(2k_1^- - \ell^-)(2\bar{k}_2^+ - 2\bar{p}^+ - \ell^+)\big] \,/\, \big[(\ell^- - i\eta')(\ell^+ + i\eta)\big]\,. \end{aligned} \tag{7.45}$$

Considering only the Glauber region, the leading term on the right hand side of (7.45) is the one with only transverse components in the numerator just like before, and we omit all other terms.
We now use Feynman parameters to combine all propagator denominators except for the eikonal ones and obtain

$$I = \frac{2!N}{D}\int[\mathrm{d}^3\alpha]\int\frac{\mathrm{d}\ell^-}{\ell^- - i\eta'}\int\frac{\mathrm{d}\ell^+}{\ell^+ + i\eta}\,\frac{1}{[2\ell^+\ell^- + 2a^-\ell^+ + 2a^+\ell^- + A + i\varepsilon]^3}\,, \tag{7.46}$$

with

$$\begin{aligned} A &= 2(\alpha_1 q_1^+ - \alpha_1\bar{p}^+ - \alpha_2\bar{p}^+)\,k_1^- - 2\alpha_2\bar{k}_2^+ q_1^- + 2(\alpha_1+\alpha_2)\bar{k}_2^+ k_1^- + 2\alpha_2\bar{p}^+ q_1^- \\ &\quad - \alpha_1(\boldsymbol{k}_1 - \boldsymbol{\ell})^2 - \alpha_2(\bar{\boldsymbol{k}}_2 - \boldsymbol{\ell})^2 - \alpha_3(\boldsymbol{\ell}^2 + \lambda^2) - (\alpha_1+\alpha_2)m^2\,, \\ a^+ &= -\alpha_1 q_1^+ + (\alpha_1+\alpha_2)(\bar{p}^+ - \bar{k}_2^+)\,, \\ a^- &= \alpha_2 q_1^- - (\alpha_1+\alpha_2)k_1^-\,, \\ N &= (2\boldsymbol{\ell}\boldsymbol{k}_1 - \boldsymbol{\ell}^2)(2\boldsymbol{\ell}\bar{\boldsymbol{k}}_2 - \boldsymbol{\ell}^2)\,, \\ D &= [k_1^2 - m^2 + i\varepsilon][(p-k_1)^2 - m^2 + i\varepsilon][\bar{k}_2^2 - m^2 + i\varepsilon][(\bar{p} - \bar{k}_2)^2 - m^2 + i\varepsilon]\,. \end{aligned} \tag{7.47}$$

Note that this has exactly the same structure as the expression for the double box graph (7.14). One apparent difference is, that the denominator factor with A now appears to the third instead of the fourth power. This was, however, irrelevant for our arguments for power suppression of the integral. A less apparent difference is, that in this case we always have

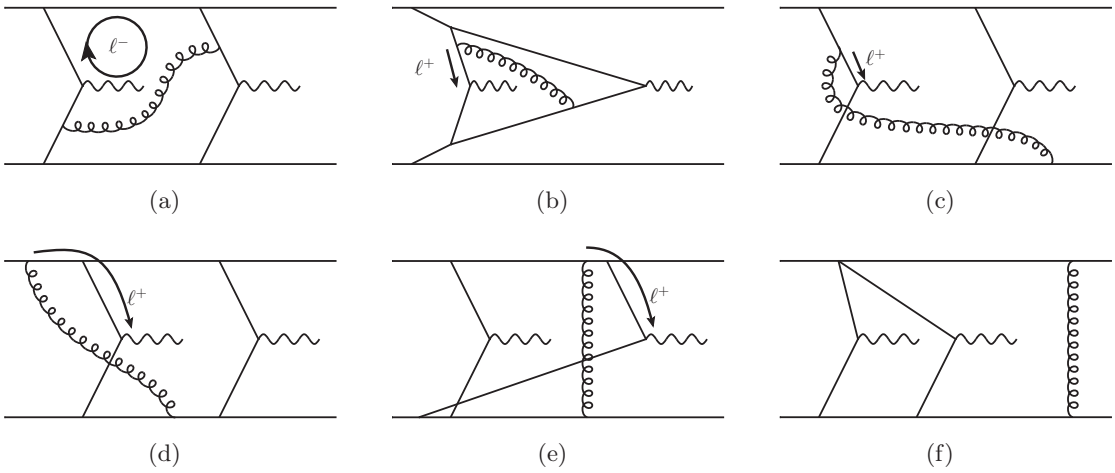

Figure 7.11.: Possible routings to avoid the Glauber region. No such routing is possible in (f).

$a^+ < 0$, which simplifies the discussion of the graph as one does not have to deal with different cases. All further arguments needed to show power suppression for the double box graph immediately carry over to the vertex correction graph and we conclude that we get a power suppressed result for this graph when using lightlike, spacelike or timelike Wilson lines.

7.3.5. Avoiding the Glauber region at one gluon exchange level

In the previous sections we have shown factorization at the one gluon exchange level in a specific, simplified setting. We have already stated in section 7.3.1 that in order to get a leading contribution from the Glauber region, both gluon longitudinal momenta have to be trapped between a pair of poles, which is only the case if both gluon longitudinal momenta are routed along and against lines with large longitudinal momentum. As we have seen for the double box graph in figure 7.8, it is enough that there exists such a routing, because even when choosing a routing where the gluon momentum seems to be trapped in the Glauber region on purpose we see that the result is still the same (albeit with some additional complications).
We now turn back to the more general graphs in figure 7.4, and we will, where possible, provide a routing of ℓ for each of them for which the gluon momentum is not pinched in the Glauber region, cf. figure 7.11. Bearing in mind that it is enough to be able to deform ℓ^+ or ℓ^-, we only give the routing of one component for each graph. For graphs (a) to (e), it is easy to find such a routing. For graph (f), however, it is impossible to find and indeed this graph gets a non-vanishing contribution from the Glauber region. This contribution vanishes after a sum over all possible final-state cuts in complete analogy to the single Drell-Yan process [39, 48]. One deforms the integration contour of either ℓ^+ or ℓ^- over the poles of the spectator lines and thereby picks up an additional contribution from the corresponding residue. After a sum over all cuts, these residues cancel due to unitarity. So even if there are non-vanishing contributions from the Glauber region in individual terms, they vanish in the sum over all. Therefore these graphs do not spoil the factorization of double Drell-Yan at the one gluon exchange level.

8. Example calculations at $\mathcal{O}(\alpha_S)$

In the last chapter we have proven the double Drell-Yan process to be factorizing at the level of a one gluon exchange. Therefore the dTMDs defined in section 4.1 are meaningful quantities beyond the tree level.
In this section we calculate some $\mathcal{O}(\alpha_S)$ corrections to the splitting contribution to a quark-antiquark dTMD shown in figure 8.1. This will demonstrate some of the techniques needed to evaluate such graphs and will exhibit some unique features of the new formalism proposed by Collins already discussed in section 6.4. In particular, we will see that the dTMDs defined in eq. (6.44) require a modified ultra-violet subtraction to render them finite. Moreover we will calculate the hard part of the process, as it is also modified in the new formalism. The convolution of the dTMDs with the hard part then gives the cross section of the double Drell-Yan process in the model under consideration.

8.1. One gluon corrections to dTMDs

We use the same model as we did for our explicit calculations in section 7.3, with some further simplifications. We now treat quarks and antiquarks as massless and in turn take the imcoming scalar "hadron" to be slightly off-shell with $p^2 < 0$ in order to regulate collinear divergences of the splitting. Working in $d = 4 - 2\varepsilon$ dimensions, we use dimensional regularization to regulate ultraviolet divergences and a nonzero gluon mass λ to regulate infrared divergences. We work in Feynman gauge throughout this section. First of all we calculate the tree level expression for the dTMD. The splitting contribution to the dTMD reads

$$\begin{aligned} F(x_i, \boldsymbol{k}_i, \boldsymbol{r})\Big|_{s\to q\bar{q}} = \frac{4\pi\alpha_G}{(2\pi)^5}(x_1p^+)(x_2p^+)2p^+ \int dk_1^- dk_2^- dr^- \\ \times \frac{\delta\left(p^- - (k_1^- - \frac{1}{2}r^-) - (k_2^- + \frac{1}{2}r^-)\right)\delta(p^+ - x_1p^+ - x_2p^+)}{[(k_1 - \frac{1}{2}r)^2 + i\varepsilon][(k_2 + \frac{1}{2}r)^2 + i\varepsilon][(k_1 + \frac{1}{2}r)^2 - i\varepsilon][(k_2 - \frac{1}{2}r)^2 - i\varepsilon]}\,, \end{aligned} \tag{8.1}$$

where α_G is the coupling factor of the two quarks to the "hadron". Using the abbreviations $k = k_1 - \frac{1}{2}r$ and $\kappa = k_1 + \frac{1}{2}r$ this becomes

$$\begin{aligned} F(x_i, \boldsymbol{k}_i, \boldsymbol{r})\Big|_{s\to q\bar{q}} = \frac{4\pi\alpha_G}{(2\pi)^5}\int dk^- d\kappa^- \frac{2\delta(1-x_1-x_2)}{[2x_1p^+k^- - \boldsymbol{k}^2 + i\varepsilon][2x_2p^+(p^- - k^-) - \boldsymbol{k}^2 + i\varepsilon]} \\ \times \frac{1}{[2x_1p^+\kappa^- - \boldsymbol{\kappa}^2 - i\varepsilon][2x_2p^+(p^- - \kappa^-) - \boldsymbol{\kappa}^2 - i\varepsilon]}\,. \end{aligned} \tag{8.2}$$

Both integrals can be evaluated employing Cauchy's theorem, and the final result reads

$$F(x_i, \boldsymbol{k}_i, \boldsymbol{r})\Big|_{s\to q\bar{q}} = \frac{\alpha_G}{4\pi^2}\delta(1-x_1-x_2)\frac{x_1x_2}{[\boldsymbol{k}^2 - x_1x_2p^2][\boldsymbol{\kappa}^2 - x_1x_2p^2]}\,. \tag{8.3}$$

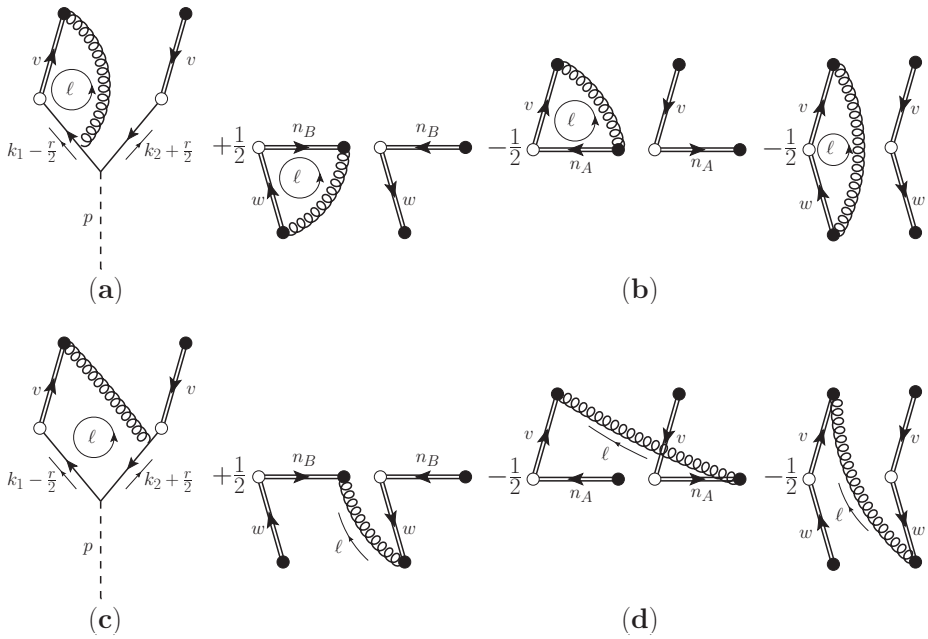

Figure 8.1.: Virtual corrections and subtraction terms: (a) Wilson line vertex correction; (b) soft subtraction terms to (a); (c) gluon connecting lines with different momentum fractions; (d) soft subtraction terms to (c). Only the part to the l.h.s. of the cut is shown.

We now turn to the one gluon corrections given in figure 8.1. The four directions of the Wilson lines are $v = (0, 1, \mathbf{0})$, $w = (1, 0, \mathbf{0})$, $n_A = (e^{y_n}, -e^{y_n}, \mathbf{0})$ and $n_B = (-e^{y_n}, e^{y_n}, \mathbf{0})$, where the lightlike vectors v and w are understood to be obtained as a limit from the spacelike region. The two vectors n_B and n_A, which both have rapidity y_n, represent left- and right-moving particles, respectively. The plus component of a right-moving particle is bigger than zero and therefore n_A is used for Wilson lines representing right-moving particles while n_B is used for left-moving ones.

In the new formalism by Collins discussed in section 6.4 one cannot treat the unsubtracted dTMD and the soft subtraction terms as independent quantities, as each of them is ill-defined taken on its own due to rapidity divergences, which only cancel in the sum of all terms. In the subtraction formula (6.44), the dTMD and the soft factors have to be taken at equal transverse position and we will use this to determine the structure of the soft subtraction terms in momentum space. In position space this is simply given by a product of the tree level dTMD $F^{(0)}$ and the $\mathcal{O}(\alpha_S)$ expansion of the corresponding combination of soft factors, which we will collectively denote by $S^{(1)}$ in the following. Looking at figure 8.1 (c) and (d), this reads

$$\begin{aligned} F^{(0)}(\boldsymbol{b}_1, \boldsymbol{b}_2, \boldsymbol{b}_2', \boldsymbol{b}_1') S^{(1)}(\boldsymbol{b}_1, \boldsymbol{b}_2, \boldsymbol{b}_2', \boldsymbol{b}_1') = \int d^2\boldsymbol{\kappa}_1 d^2\boldsymbol{\kappa}_2 d^2\boldsymbol{\kappa}_1' d^2\boldsymbol{\kappa}_2' d^2\boldsymbol{\ell}_s \; \delta^{(2)}(\boldsymbol{\kappa}_1 + \boldsymbol{\kappa}_2 - \boldsymbol{\kappa}_1' - \boldsymbol{\kappa}_2') \\ \times e^{-i\boldsymbol{\kappa}_1\boldsymbol{b}_1} e^{-i\boldsymbol{\kappa}_2\boldsymbol{b}_2} e^{i\boldsymbol{\kappa}_1'\boldsymbol{b}_1'} e^{i\boldsymbol{\kappa}_2'\boldsymbol{b}_2'} e^{-i\boldsymbol{\ell}_s(\boldsymbol{b}_1 - \boldsymbol{b}_2)} \times \\ \times F^{(0)}(\boldsymbol{\kappa}_1, \boldsymbol{\kappa}_2, \boldsymbol{\kappa}_2', \boldsymbol{\kappa}_1') S^{(1)}(\boldsymbol{\ell}_s, -\boldsymbol{\ell}_s, \mathbf{0}, \mathbf{0}) \end{aligned} \tag{8.4}$$

Note that we have ignored the dependence of the dTMD on the longitudinal momentum fractions x_1 and x_2, because this dependence is not needed for our argument. Moreover, note that by definition the soft factor does not depend on longitudinal momenta/positions. Fourier transforming this product back into momentum space, we get

$$\begin{aligned}
&\frac{1}{(2\pi)^8}\int d^2\boldsymbol{b}_1 d^2\boldsymbol{b}_2 d^2\boldsymbol{b}_1' d^2\boldsymbol{b}_2' \int d^2\boldsymbol{\kappa}_1 d^2\boldsymbol{\kappa}_2 d^2\boldsymbol{\kappa}_1' d^2\boldsymbol{\kappa}_2' d^2\boldsymbol{\ell}_s\ \delta^{(2)}(\boldsymbol{\kappa}_1+\boldsymbol{\kappa}_2-\boldsymbol{\kappa}_1'-\boldsymbol{\kappa}_2')\times\\
&\times e^{-i\boldsymbol{\kappa}_1\boldsymbol{b}_1}e^{-i\boldsymbol{\kappa}_2\boldsymbol{b}_2}e^{i\boldsymbol{\kappa}_1'\boldsymbol{b}_1'}e^{i\boldsymbol{\kappa}_2'\boldsymbol{b}_2'}e^{-i\boldsymbol{\ell}_s(\boldsymbol{b}_1-\boldsymbol{b}_2)}\times\\
&\times e^{+i\boldsymbol{k}\boldsymbol{b_1}}e^{+i\boldsymbol{\eta}\boldsymbol{b_2}}e^{-i\boldsymbol{k}'\boldsymbol{b_1}'}e^{-i\boldsymbol{\eta}'\boldsymbol{b_2}'}F^{(0)}(\boldsymbol{\kappa}_1,\boldsymbol{\kappa}_2,\boldsymbol{\kappa}_2',\boldsymbol{\kappa}_1')S^{(1)}(\boldsymbol{\ell}_s,-\boldsymbol{\ell}_s,\mathbf{0},\mathbf{0})\\
=&\int d^2\boldsymbol{\ell}_s F^{(0)}(\boldsymbol{k}-\boldsymbol{\ell}_s,\boldsymbol{\eta}+\boldsymbol{\ell}_s,\boldsymbol{\eta}',\boldsymbol{k}')S^{(1)}(\boldsymbol{\ell}_s,-\boldsymbol{\ell}_s,\mathbf{0},\mathbf{0})\delta^{(2)}(\boldsymbol{k}+\boldsymbol{\eta}-\boldsymbol{k}'-\boldsymbol{\eta}')
\end{aligned}\tag{8.5}$$

This means, that the subtraction terms for the dTMD are obtained as a transverse momentum convolution of the tree level dTMD and the $\mathcal{O}(\alpha_S)$ expansion of the combination of soft factors $S^{(1)}$, in contrast to the simple product we had in position space.

8.1.1. Wilson line vertex correction

We will now calculate the Wilson line vertex correction depicted in figure 8.1(a) and (b). The three Wilson lines combine to one effective subtraction term:

$$\begin{aligned}
&\frac{(-i)^3 i}{2}\left(\frac{e^{-y_n}}{[-\ell^-+i\epsilon][-\ell^- e^{y_n}+\ell^+e^{-y_n}+i\epsilon]}-\frac{e^{y_n}}{[\ell^++i\epsilon][-\ell^-e^{y_n}+\ell^+e^{-y_n}+i\epsilon]}\right.\\
&\qquad\left.-\frac{e^{y_n}}{[\ell^++i\epsilon][-\ell^-+i\epsilon]}\right)\\
=&-\frac{1}{2}\frac{e^{-y_n}\ell^+ + e^{y_n}\ell^- + \ell^- e^{y_n} - \ell^+e^{-y_n}}{[\ell^++i\epsilon][-\ell^-+i\epsilon][-\ell^-e^{y_n}+\ell^+e^{-y_n}+i\epsilon]}\\
=&\frac{1}{[\ell^++i\epsilon][-\ell^-+\ell^+e^{-2y_n}+i\epsilon]}\,.
\end{aligned}\tag{8.6}$$

We immediately see that the rapidity divergence at $\ell^-=0$ has cancelled. Calculating diagrams 8.1 (a) and (b), one has to keep in mind that only the sum of these diagrams is well-defined, while each of the summands is ill-defined taken on it's own. In this specific case where the extra gluon does not connect different quark lines, we can express the resulting correction to the dTMD as $I_{8.1(\mathrm{a})+(\mathrm{b})}\cdot F^{(0)}$, where in $I_{8.1(\mathrm{a})+(\mathrm{b})}$ we amputate all propagators that are not part of the gluon loop. Considering an incoming quark with momentum k, both diagrams together yield

$$\begin{aligned}
I_{8.1(\mathrm{a})+(\mathrm{b})} = \frac{4\pi i\alpha_S C_F\mu^{2\varepsilon}}{(2\pi)^{4-2\varepsilon}}\int d^{4-2\varepsilon}\ell\ \frac{1}{[\ell^2-\lambda^2+i\epsilon][\ell^++i\epsilon]}\times\\
\times\left[\frac{2k^+-\ell^+}{[(\ell-k)^2+i\epsilon]}-\frac{1}{[-\ell^-+\ell^+e^{-2y_n}+i\epsilon]}\right].
\end{aligned}\tag{8.7}$$

This can be calculated in the following way: First, we perform the ℓ^--integration using Cauchy's theorem (enclosing the pole of the gluon propagator). Then we perform the transverse $(2-2\varepsilon)$-dimensional integration and after substituting $x = \ell^+/k^+$ we get

$$\begin{aligned} I_{8.1\text{(a)+(b)}} = &-\frac{4\pi^2\alpha_S C_F \mu^{2\varepsilon}}{(2\pi)^{4-2\varepsilon}}\pi^{1-\varepsilon}\Gamma(\varepsilon)\int_0^1 \frac{dx}{x}\times \\ &\times\left[\frac{(2-x)}{[-x(1-x)k^2+(1-x)\lambda^2-i\epsilon]^\varepsilon} - \frac{2}{[-2x^2(k^+)^2e^{-2y_n}+\lambda^2-i\epsilon]^\varepsilon}\right] \\ &+\frac{8\pi^2\alpha_S C_F \mu^{2\varepsilon}}{(2\pi)^{4-2\varepsilon}}\pi^{1-\varepsilon}\Gamma(\varepsilon)\int_1^\infty \frac{dx}{x}\frac{1}{[-2x^2(k^+)^2e^{-2y_n}+\lambda^2-i\epsilon]^\varepsilon}\,, \end{aligned} \tag{8.8}$$

where we have split up the contribution of the second term in (8.6) into two terms, namely the second and third term in (8.8). The rapidity divergence at $x = 0$ cancels in (8.8), yielding a well-defined result. The third term in (8.8) gives a $1/\varepsilon^2$-pole and the gluon mass can be sent to zero due to $x > 1$. Abbreviating $\zeta^2 = 2(k^+)^2e^{-2y_n}$ the final result for diagrams 8.1 (a) and (b) is

$$\begin{aligned} I_{8.1\text{(a)+(b)}} = \frac{\alpha_S C_F}{4\pi}\Bigg[&\frac{1}{2}\log^2\left(\frac{-\zeta^2-i\epsilon}{\mu^2}\right) - \frac{1}{2}\log^2\left(\frac{-\zeta^2-i\epsilon}{\lambda^2}\right) + \log^2\left(\frac{-k^2+\lambda^2}{\lambda^2}\right) \\ &+\log\left(\frac{\mu^2}{-k^2+\lambda^2}\right) - \frac{\pi^2}{12} + \frac{1}{\varepsilon} - \gamma_E + \log(4\pi) + 2 \\ &+\frac{1}{\varepsilon^2} + \frac{1}{\varepsilon}\left(-\gamma_E + \log(4\pi) - \log\left(\frac{-\zeta^2-i\epsilon}{\mu^2}\right)\right) \\ &+\frac{1}{2}\left(-\gamma_E+\log(4\pi)\right)\left(-\gamma_E+\log(4\pi)-2\log\left(\frac{-\zeta^2-i\epsilon}{\mu^2}\right)\right)\Bigg] \end{aligned} \tag{8.9}$$

The $1/\varepsilon^2$ pole and the term $\sim 1/\varepsilon$ in the third line of (8.9) originate from the third term in (8.8), which is proportional to

$$\Gamma(\varepsilon)\int_1^\infty dx\ \frac{1}{x^{1+2\varepsilon}} = \frac{1}{2\varepsilon^2} + \frac{1}{2\varepsilon}\left(-\gamma_E + \frac{1}{2}\gamma_E^2\varepsilon + \frac{\pi^2}{12}\varepsilon\right)\,. \tag{8.10}$$

From (8.9) it can bee seen that TMDs calculated in this formalism require a modified UV subtraction to render them finite, cf. [5].

8.1.2. Four point correction

Before we move on the calculation of the four point correction to the dTMD depicted in figure 8.1 (c) and (d), we note that the following calculation has also been independently performed by Peter Plößl as a part of his master's thesis. The reason is that this calculation, though conceptually not too difficult and doable with the same techniques as used in the calculation of the Wilson line vertex correction, turns out to be rather long and even small mistakes can lead to vastly deviating results. The independent calculation therefore was deemed necessary to guarantee the correctness of the results.

We now calculate the four point correction shown in figure 8.1 (c) and (d). Once again the three soft subtraction terms combine to one effective subtraction term. In the following, we

will use the abbreviations $k = k_1 - r/2$ and $\eta = k_2 + r/2$. The sum of both diagrams (without the r.h.s. of the cut) reads

$$\begin{aligned} I_{8.1\text{(c)+(d)}} = &-\frac{4\pi i\alpha_S C_F}{(2\pi)^4}\mathcal{N}\int d^4\ell\ \frac{2\eta^+ + \ell^+}{\ell^+[\ell^2-\lambda^2+i\epsilon][(\ell-k)^2+i\epsilon][(\ell+\eta)^2+i\epsilon][\eta^2+i\epsilon]} \\ &-\frac{4\pi i\alpha_S C_F}{(2\pi)^4}\mathcal{N}\int d^4\ell\ \frac{1}{\ell^+[\ell^2-\lambda^2+i\epsilon][2k^+k^- - (\boldsymbol{\ell}-\boldsymbol{k})^2+i\epsilon]}\times \\ &\times\frac{1}{[2\eta^+\eta^- - (\boldsymbol{\ell}+\boldsymbol{\eta})^2+i\epsilon][\ell^- - \ell^+ e^{-2y_n} - i\epsilon]}\,, \end{aligned} \tag{8.11}$$

where

$$\mathcal{N} = \frac{4\pi\alpha_G}{(2\pi)^5}2p^+(x_1p^+)(x_2p^+)\int dk^-\ d\eta^-\delta(p^+ - x_1p^+ - x_2p^+)\delta^{(2)}(\boldsymbol{k}+\boldsymbol{\eta})\delta(p^- - k^- - \eta^-) \tag{8.12}$$

contains the normalization and momentum conservation factors and the additional integrals over η^- and k^-. Counting powers of ℓ we see that this graph is not UV divergent and, therefore, we send ε to zero. Just like in the case of the Wilson line vertex correction, we start with the ℓ^--integration using Cauchy's theorem.

Closing the integration contour in the lower half ℓ^--plane, we have the following poles contributing (the following poles are the zeros of the factors in the denominator in equation (8.11)).

ℓ^-	position of pole	momentum constraints term 1	momentum constraints term 2
ℓ_1^-	$\frac{\boldsymbol{\ell}^2+\lambda^2-i\epsilon}{2\ell^+}$	$\Theta(\ell^+)\Theta(k^+-\ell^+)$	$\Theta(\ell^+)$
ℓ_2^-	$-\eta^- + \frac{(\boldsymbol{\ell}-\boldsymbol{k})^2-i\epsilon}{2(\ell^++\eta^+)}$	$\Theta(\ell^++\eta^+)\Theta(k^+-\ell^+)$	does not contribute
ℓ_3^-	$k^- + \frac{(\boldsymbol{\ell}-\boldsymbol{k})^2-i\epsilon}{2(\ell^+-k^+)}$	$\Theta(\ell^+-k^+)\Theta(k^+-\ell^+)$	does not contribute

The momentum constraints apply to the first and second term in (8.11), respectively, where the constraint $\Theta(k^+ - \ell^+)$ comes from the fact, that all poles lie on the same side of the real axis for $\ell^+ > k^+$. As one can see from the table above, ℓ_3^- does not contribute due to the product of Θ-functions that is always zero and we get three contributions which, after substituting $x = \ell^+/p^+$, read

$$\begin{aligned} I_{8.1\text{(c)+(d)}} = &\ \alpha_S C_F\mathcal{N}\int d^2\boldsymbol{\ell} \\ &\times\left(-\int_0^{x_1} dx\ \frac{x+2x_2}{4\pi^2\left(2p^+k^-x(x-x_1)+\boldsymbol{\ell}^2(x_1-x)+(\boldsymbol{\ell}-\boldsymbol{k})^2x-\lambda^2x+\lambda^2x_1-ix_1\epsilon\right)}\right. \\ &\times\left.\frac{1}{(\boldsymbol{k}^2-2p^+\eta^-x_2-i\epsilon)\left(\boldsymbol{\ell}^2(x+x_2)-(\boldsymbol{\ell}-\boldsymbol{k})^2x+2p^+\eta^-x(x+x_2)+\lambda^2(x+x_2)-ix_2\epsilon\right)}\right. \end{aligned}$$

$$
\begin{aligned}
&+\int_0^\infty dx\ \frac{e^{2y_n}}{2\pi^2 x(-2k^- p^+ x_1+(\boldsymbol{\ell}-\boldsymbol{k})^2-i\epsilon)((\boldsymbol{\ell}-\boldsymbol{k})^2-2p^+\eta^- x_2-i\epsilon)}\\
&\times\frac{1}{\left(2p^{+2}x^2-e^{2y_n}(\lambda^2+\boldsymbol{\ell}^2-i\epsilon(2p^+x+1))\right)}\\
&+\int_{-x_2}^{x_1} dx\ \frac{(x+x_2)(x+2x_2)}{4\pi^2 x(2p^+(k^-+\eta^-)(x-x_1)(x+x_2)+(\boldsymbol{\ell}-\boldsymbol{k})^2(x_1+x_2)-i\epsilon(x_1+x_2))}\\
&\times\frac{1}{(\boldsymbol{k}^2-2p^+\eta^- x_2-i\epsilon)\left(\boldsymbol{\ell}^2(x+x_2)-(\boldsymbol{\ell}-\boldsymbol{k})^2 x+2p^+\eta^- x(x+x_2)+\lambda^2(x+x_2)-ix_2\epsilon\right)}\Bigg)
\end{aligned}
\tag{8.13}
$$

Now we use momentum conservation to substitute $k^- = p^- - \eta^-$ and perform the integration over η^- using Cauchy's theorem. Note that the position of the poles, i.e. whether they are located in the lower or upper η^- half plane, does not depend on any integration variables for the first two terms of (8.13), as for these two terms it holds $x \geq 0$. The third term in (8.13) gets another momentum contstraint, namely $\Theta(x)$ from the η^- integration, because for $x < 0$ all poles are on the same side of the real axis. The result is

$$
\begin{aligned}
I_{8.1\text{(c)+(d)}} &= \alpha_S C_F \mathcal{N}' \int d^2\boldsymbol{\ell}\\
&\times\Bigg(\int_0^{x_1} dx\ \frac{ix_2(x+2x_2)}{4\pi p^+(\boldsymbol{k}^2 x(x+x_2)+\boldsymbol{\ell}^2 x_2(x+x_2)-(\boldsymbol{\ell}-\boldsymbol{k})^2 x x_2+\lambda^2 x_2(x+x_2)-i\epsilon)}\\
&\times\frac{1}{(\boldsymbol{k}^2 x(x-x_1)+\boldsymbol{\ell}^2 x_2(x-x_1)-x x_2((\boldsymbol{\ell}-\boldsymbol{k})^2+p^2 x-p^2 x_1)+\lambda^2 x_2(x-x_1)+i\epsilon)}\\
&+\int_0^\infty dx\frac{i}{2\pi p^+ x\left(\lambda^2+\boldsymbol{\ell}^2-\zeta^2 x^2-i\epsilon\right)\left(-(\boldsymbol{\ell}-\boldsymbol{k})^2+p^2 x_1 x_2+i\epsilon\right)}\\
&+\int_0^{x_1} dx\ \frac{i(x+x_2)(x+2x_2)}{4\pi p^+ x((\boldsymbol{\ell}-\boldsymbol{k})^2+p^2(x-x_1)(x+x_2)-i\epsilon)}\\
&\times\frac{1}{(\boldsymbol{k}^2 x(x+x_2)+\boldsymbol{\ell}^2 x_2(x+x_2)-(\boldsymbol{\ell}-\boldsymbol{k})^2 x x_2+\lambda^2 x_2(x+x_2)-i\epsilon)}\Bigg)\,,
\end{aligned}
\tag{8.14}
$$

where we have substituted $\zeta^2 = 2(p^+)^2 e^{-2y_n}$ and

$$
\mathcal{N}' = \frac{4\pi\alpha_G}{(2\pi)^5} 2p^+(x_1 p^+)(x_2 p^+)\delta(p^+ - x_1 p^+ - x_2 p^+)\delta^{(2)}(\boldsymbol{k}+\boldsymbol{\eta})\,. \tag{8.15}
$$

Now we use Feynman parameters to combine the factors in the denominators, complete the square and perform the integration over the transverse gluon momentum. The calculation is done using the replacement $\zeta^2 \to -\zeta^2$ while keeping $\zeta^2 > 0$. This has the advantage that all denominators are positive definite and we can send the Feynman $i\epsilon$ to zero for the calculation. After we have obtained the final result, we can do the analytic continuation back to the original case (i.e. analytically continue from ζ^2 to $-\zeta^2 - i\epsilon$). This is possible, because we only used the approximation that the modulus of ζ^2 is large during the calculation. After

the transverse integral is performed, introducing $\bar{\alpha} = 1 - \alpha$ we get:

$$
\begin{aligned}
I_{8.1\text{(c)+(d)}} = \alpha_S C_F \mathcal{N}' \frac{1}{4p^+} \int_0^1 d\alpha \\
\Bigg(\int_0^{x_1} dx \, \frac{i x_1 (x - 2x_1 + 2)}{\left(-\bar{\alpha}\boldsymbol{k}^2 x (x(\alpha - x_2) + x_1 x_2) + x_1 \left(-\lambda^2 x_2 (x(\alpha - x_2) + x_1 x_2) - \bar{\alpha} p^2 x x_2^2 (x - x_1)\right)\right)} \\
- 2 \int_0^{\infty} dx \, \frac{i}{x \left(\alpha\lambda^2 + \alpha\bar{\alpha}\boldsymbol{k}^2 - \bar{\alpha} x_1 x_2 (p^2) + \alpha\zeta^2 x^2\right)} \\
+ \int_0^{x_1} dx \, \frac{i(x - 2x_1 + 2)}{x \left(\alpha(\lambda^2 + \bar{\alpha}\boldsymbol{k}^2 (x + x_2) - \lambda^2 x_1) - \bar{\alpha}(x - x_1) x_2^2 p^2\right)} \Bigg) \, .
\end{aligned} \tag{8.16}
$$

Note that the rapidity divergence at $x = 0$ cancels exactly between the second and third term. The easiest way to proceed is the following: Combine the second and third term, and do the integration over x first. After that, integrate out the Feynman parameter α. The first term is finite on its own and can therefore be treated separately. For this term, it is easier to first integrate over α and perform the integration over x afterwards. The rest of the calculation can now be performed using standard methods, but the intermediate steps become rather lengthy. Taking the limit $\zeta^2 \gg \lambda^2, p^2$ and incorporating the r.h.s. of the cut, the result for the correction to the dTMD is

$$
\begin{aligned}
F(x_i, \boldsymbol{k}, \boldsymbol{\kappa}, \zeta^2)_{8.1\text{(c)+(d)}} = \frac{\alpha_G \alpha_S C_F}{32\pi^3} \frac{x_1 x_2}{[\boldsymbol{k}^2 - x_1 x_2 p^2][\boldsymbol{\kappa}^2 - x_1 x_2 p^2]} \\
\times \Bigg[3\log^2(a_1) - \log^2(a_6) + \log^2(a_{13}) + 2\log(a_{12}) \log\left(\frac{a_2^2 a_4^2 a_6}{a_7^2 a_{13}}\right) \\
+ 2\log(a_7) \log\left(\frac{a_2^2 a_{10}}{a_3}\right) - \log(a_2 a_4) \log\left(\frac{a_2^5 a_4 a_9^2}{a_3^2}\right) + 2\log\left(\frac{a_5}{a_7}\right) \log\left(\frac{a_2 a_4 a_6}{a_7 a_{13}}\right) \\
+ 2\log(a_9) \log\left(\frac{a_7 a_9}{a_2 a_4 a_{10}}\right) - 2\log(a_1) \log\left(\frac{a_7^3 a_9^2 a_{13}}{a_3 a_4 a_5 a_6^2 a_{12}}\right) \\
- 2\mathrm{Li}_2\left(\frac{a_1 a_{14}}{a_{12}}\right) + 2\mathrm{Li}_2\left(\frac{a_3}{a_{13}}\right) - 4\mathrm{Li}_2\left(-\frac{a_1 a_3}{a_2 a_{13}}\right) - 2\mathrm{Li}_2\left(-\frac{a_{14}}{a_2 a_4}\right) \\
+ 2\mathrm{Li}_2\left(\frac{a_9}{a_1 a_2 a_4}\right) - 2\mathrm{Li}_2\left(\frac{a_{13}}{a_1 a_2 a_4}\right) + 2\mathrm{Li}_2\left(-\frac{a_{13} a_{14}}{a_2 a_4 a_{12}}\right) \\
- 2\mathrm{Li}_2\left(-\frac{a_3}{a_1 a_2 a_4}\right) + 2\mathrm{Li}_2\left(-\frac{a_1^2 a_5}{a_{13}}\right) + 4\mathrm{Li}_2\left(-\frac{a_3}{a_2 a_6}\right) - 2\mathrm{Li}_2\left(-\frac{a_{10}}{a_7}\right) \\
- 2\mathrm{Li}_2\left(-\frac{a_1^2 a_5}{a_6}\right) + 4\mathrm{Li}_2\left(-\frac{a_1 a_{14}}{a_2 a_7}\right) + 2\mathrm{Li}_2\left(-\frac{a_6}{a_7}\right) - 2\mathrm{Li}_2\left(-\frac{a_{13}}{a_8}\right) \\
+ 2\mathrm{Li}_2\left(\frac{a_1 a_2 a_4}{a_7}\right) + 2\mathrm{Li}_2\left(\frac{a_6}{a_7}\right) + 2\mathrm{Li}_2\left(\frac{a_1 a_7}{a_{12}}\right) + 2\mathrm{Li}_2\left(-\frac{a_1}{a_2}\right) \\
+ 2\mathrm{Li}_2\left(-\frac{a_1 a_6}{a_{12}}\right) + \frac{\pi^2}{3} \Bigg] \, ,
\end{aligned} \tag{8.17}
$$

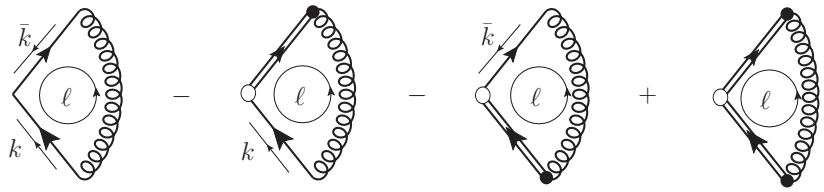

Figure 8.2.: Hard part of the cross section of double Drell-Yan for the parton lines with longitudinal momenta $k^+ = x_1 p^+$ and $\bar{k}^- = \bar{x}_1 \bar{p}^-$. Only the l.h.s. of the cut is shown.

where we have defined the following abbreviations:[1]

$$\begin{aligned}
a_1 &= x_1\,, & a_2 &= x_2\,, & a_3 &= \boldsymbol{k}^2\,,\\
a_4 &= -p^2\,, & a_5 &= -\zeta^2 - i\epsilon\,, & a_6 &= \lambda^2\,,\\
a_7 &= \boldsymbol{k}^2 - x_1 x_2 p^2\,, & a_9 &= \boldsymbol{k}^2 - x_1^2\zeta^2 - i\epsilon\,, & a_{10} &= -x_1^2\zeta^2 - i\epsilon\,,\\
a_{12} &= \boldsymbol{k}^2 + x_2\lambda^2\,, & a_{13} &= \boldsymbol{k}^2 + \lambda^2\,, & a_{14} &= \boldsymbol{k}^2 - x_2^2 p^2\,.
\end{aligned} \tag{8.18}$$

Given that this is a rather long result, we have performed two checks to verify its correctness. On one hand, the dTMD has to remain finite in the limit $\boldsymbol{k} \to \boldsymbol{0}$. We have checked that this is the case for (8.17). On the other hand, (8.17) seems to contain logarithms of dimensionful arguments. We have checked that this is not the case in the sum over all terms by replacing all dimensionful arguments m_i according to

$$\log\left(m_i^2\right) = \log\left(\omega_i^2\right) + \log\left(m^2\right)\,, \tag{8.19}$$

where ω_i has mass dimension 0 and m is a unit mass.

8.2. The hard part

As we have discussed in section 6.4.1, the approximator of each region has to be amended with suitable subtraction terms for smaller regions. In the case of the hard scattering part H, we have to subtract both collinear regions (each subtracted with the soft region) and the soft region. The approximations suitable for the hard region have to be applied to the subtraction terms, too. One has to set all masses as well as the transverse momenta equal to zero and apply the collinear approximation, i.e. $q_i^+ = x_i p^+$, $q_i^- = \bar{x}_i \bar{p}^-$ and $k_i^- = r^- = \bar{k}_i^+ = \bar{r}^+ = 0$. Moreover, one has to show that the hard part is free of soft divergences. The combination of diagrams from which the hard part is obtained is depicted in figure 8.2, and they give

[1] We have defined the abbreviations to be consistent with [50] for better comparability. We have, however taken the limit $\lambda^2 \to 0$ where appropriate, which then sets $a_7 = a_8$ and $a_9 = a_{11}$.

$$H_{8.2} = -\frac{4\pi i\alpha_S C_F \mu^{2\varepsilon}}{(2\pi)^{4-2\varepsilon}} \int d^{4-2\varepsilon}\ell \times \left[\frac{(2k-\ell)(2\bar{k}+\ell)}{[\ell^2+i\epsilon][\ell^2-2k^+\ell^-+i\epsilon][\ell^2+2\bar{k}^-\ell^++i\epsilon]} - \frac{2k^+-\ell^+}{[\ell^2+i\epsilon][\ell^2-2k^+\ell^-+i\epsilon][\ell^++i\epsilon]} - \frac{2\bar{k}^-+\ell^-}{[\ell^2+i\epsilon][\ell^2+2\bar{k}^-\ell^++i\epsilon][-\ell^-+i\epsilon]} + \frac{1}{[\ell^2+i\epsilon][\ell^++i\epsilon][-\ell^-+i\epsilon]} \right] . \tag{8.20}$$

The ℓ^--integral can be performed using Cauchy's theorem and after integrating over $d^{2-2\varepsilon}\boldsymbol{\ell}$ and substituting $x = \ell^+/k^+$ and $Q_1^2 = 2k^+\bar{k}^-$ we obtain

$$H_{8.2} = \frac{8\pi^2\alpha_S C_F \mu^{2\varepsilon}}{(2\pi)^{4-2\varepsilon}} \pi^{1-\varepsilon} \int_0^\infty dx \times \times \left[\Gamma(\varepsilon)\frac{1}{2x}\left(\Theta(1-x)[-Q_1^2x(1-x)-i\epsilon]^{-\varepsilon} - [-Q_1^2x-i\epsilon]^{-\varepsilon}\right) + \frac{\Gamma(2-\varepsilon)\Gamma(-1+\varepsilon)}{\Gamma(1-\varepsilon)}\frac{1}{2x^2Q_1^2}\left(\Theta(1-x)[-Q_1^2x(1-x)-i\epsilon]^{1-\varepsilon} - [-Q_1^2x-i\epsilon]^{1-\varepsilon}\right) \right] . \tag{8.21}$$

The divergence for $x \to 0$ cancels between the individual terms in the second and third line of (8.21), respectively. The integration over x can be carried out analytically and the final result is

$$H_{8.2} = \frac{\alpha_S C_F}{2\pi}\left[-\frac{1}{\varepsilon^2} - \frac{1}{2\varepsilon} - \frac{1}{\varepsilon}\left(-\gamma_E + \log(4\pi) - i\pi - \log\left(\frac{Q_1^2}{\mu^2}\right)\right)\right] + \text{finite terms} \tag{8.22}$$

where the finite terms only depend on Q_1^2 and μ^2 and not on the regulator ε. We will now compare this to the result of the vertex correction of the dTMDs (8.9). Adding the corresponding contribution for the left-moving particle to (8.9) we obtain

$$\frac{\alpha_S C_F}{4\pi}\left[\frac{2}{\varepsilon^2} + \frac{2}{\varepsilon} + \frac{1}{\varepsilon}\left(-2\gamma_E + 2\log(4\pi) - 2i\pi - \log\left(\frac{\zeta^2\bar{\zeta}^2}{(\mu^2)^2}\right)\right)\right] \tag{8.23}$$

for the UV divergent terms. It is easy to see that the poles $\sim 1/\varepsilon^2$ cancel in the combination $F\Big|_{8.1} \otimes \bar{F}\Big|_{8.1} \otimes H_{8.2}$. Using

$$\zeta^2\bar{\zeta}^2 = 2(k^+)^2 e^{-2y_n} 2(\bar{k}^-)^2 e^{2y_n} = (Q_1^2)^2 \tag{8.24}$$

this also becomes evident for the terms in parentheses proportional to $1/\varepsilon$. So all the additional poles that are not present in a direct calculation of the photon vertex correction cancel in the combination $F\Big|_{8.1} \otimes \bar{F}\Big|_{8.1} \otimes H_{8.2}$, as should be the case. The remaining UV divergent term is

$$\frac{\alpha_S C_F}{4\pi}\frac{1}{\varepsilon} , \tag{8.25}$$

which is exactly the pole term that is present in the calculation of the photon vertex correction. This can readily be seen from the UV behaviour of the first graph in figure 8.2:

$$\begin{aligned} I_{\text{phot.}}\Big|_{\text{UV}} &= -\frac{4\pi i\alpha_S C_F \mu^{2\varepsilon}}{(2\pi)^{4-2\varepsilon}} \int_{\text{UV}} d^{4-2\varepsilon}\ell \, \frac{(2k-\ell)(2\bar{k}+\ell)}{[\ell^2+i\epsilon][(\ell-k)^2+i\epsilon][(\ell+\bar{k})^2+i\epsilon]} \\ &= \frac{4\pi\alpha_S C_F \mu^{2\varepsilon}}{(2\pi)^{4-2\varepsilon}} \int_{\text{UV}} d^{4-2\varepsilon}\ell_E \, \frac{1}{[\ell_E^2]^2} \\ &= \frac{\alpha_S C_F}{4\pi} \left(\frac{1}{\varepsilon} + \text{finite} \right). \end{aligned} \tag{8.26}$$

The result for the hard part (8.22) also reveals another appealing feature of the new formalism. When regularizing the rapidity divergences by taking auxiliary vectors with finite rapidity, these auxiliary vectors also have to be employed when calculating the hard part. The lightlike vectors in figure 8.2 then have to be replaced with the corresponding vectors with finite rapidity, and the hard part then also depends on the rapidities of these vectors via the combination $|(v \cdot w)/(v^2 w^2)|$, see e.g. [40]. In the new formalism the only dependence on the rapidity of auxiliary vectors appears in the soft subtraction for the collinear factors, and only via one additional parameter y_n [5].

9. All-order proof of Glauber gluon cancellation

The methods used in the previous sections are clearly not suitable for an all-order proof of factorization of double Drell-Yan, as this would require an infinite amount of increasingly more difficult calculations. Instead, the methods used to demonstrate the all-order cancellation of Glauber gluon exchange for the single Drell-Yan process [5, 51] can be adapted and generalized to the case of double Drell-Yan. We will not present every step in detail, but instead outline the main ideas of the proof in the following.[1] We refer the reader to [13, chapter 4] for more detail, which we will follow closely below.

9.1. Light-cone perturbation theory

The methods to show factorization of double Drell-Yan to all orders in perturbation theory rely on the so-called light-cone perturbation theory (LCPT). It is similar to time ordered perturbation theory [4, 52], but instead of summing over all possible orderings of a graph in usual time $t = x^0$, one sums over all possible orderings in light-cone time x^+ or x^-. LCPT gives the same result as covariant perturbation theory and can be derived from it [5, 53]. We follow the conventions of [5] below.

1. The diagrams in LCPT are like the diagrams in covariant perturbation theory, except that vertices are ordered in the light-cone time x^+. We sum over all possible orderings in x^+ as well as all possible graphs. In diagrams we take x^+ to increase from left to right in the amplitude (i.e. to the left of the final state cut) and to decrease from left to right in the conjugate amplitude.

2. We assign each line L an on-shell four-momentum κ_L satisfying $\kappa_L^2 = m_L^2$. The plus and transverse components of these four-momenta are conserved at vertices, but the minus components are not – these are instead fixed by the on-shell condition, such that

$$\kappa_L = \left(\kappa_L^+, \kappa_L^- = \frac{\boldsymbol{\kappa}_L^2 + m_L^2}{2\kappa_L^+}, \boldsymbol{\kappa}_L\right) . \tag{9.1}$$

3. For each line L we include a factor $\frac{1}{2\kappa_L^+}\,\Theta(\kappa_L^+)$, where κ_L^+ flows in the future light-cone time direction.

4. For each loop, we integrate only over the plus and transverse components of the loop momentum with measure $(2\pi)^{1-d}\int \mathrm{d}\kappa^+ \mathrm{d}^{d-2}\,\boldsymbol{\kappa}$, where $d = 4 - 2\epsilon$.

[1] The calculations and results presented in the following were not part of the calculations for this thesis, but are included for the sake of completeness.

5. For each intermediate state ξ (that is, set of lines between two vertex positions in the light-cone time-ordering), we have a factor

$$\frac{i}{p^-_{\xi,\mathrm{inc}} - \sum\limits_{L\in\xi} \kappa^-_L + i\epsilon}\,, \tag{9.2}$$

where $p^-_{\xi,\mathrm{inc}}$ is the total external minus momentum entering the state from the left (i.e. from lower x^+) and κ^-_L is the on-shell minus momentum of a line L in ξ.

6. Coupling factors at vertices and symmetry factors are the same as in Feynman graphs.

For QCD there are more rules for the LCPT due to the presence of fermion and vector boson fields, which lead to extra vertices describing instantaneous particle exchanges with respect to the ordering in x^+, cf. [54, 55]. The precise structure of the vertices is, however, not important for the arguments given below. We will therefore not state these extra rules here.

9.2. Cancellation of Glauber gluon exchange in the double Drell-Yan process

We will now outline the main ideas behind the proof of cancellation of Glauber gluon exchange to all orders for the double Drell-Yan process. See [13, chapter 4.3] for a more detailed analysis. As we have already stated in section 6.4.1, a given graph can be decomposed into a sum over all possible approximants. For a given graph Γ, approximated for a region R, we will now consider the sum over all possible cuts. We partition the approximated graph into a collinear factor A and a remainder as shown in figure 9.1,

$$G_R = \sum_{\text{cuts}} \int \left[\prod_j \mathrm{d}^{4-2\varepsilon}\ell_j\right] A^{\mu_1\cdots\mu_n}(\tilde{\ell}_j) R_{\mu_1\cdots\mu_n}(\ell_j)\,, \tag{9.3}$$

with ℓ_j being soft momenta entering A from the soft subgraph. In the collinear factor A we can neglect the soft plus-momentum, indicated by $\tilde{\ell} = (0, \ell^-, \boldsymbol{\ell})$. Note that to conform with the original literature [5, 51] the remainder is called R, which must not be confused with the region R indicated by a subscript on G. Now let V denote the partitioning of the vertices where the soft gluons enter A between the amplitude and its conjugate. For a given V, the sum over cuts is then equivalent to a sum over a set $\mathcal{A}(V)$ of compatible cuts of A, and over a set $\mathcal{R}(V)$ of compatible cuts of R. The graph 9.1 can then be written as

$$\begin{aligned} G_R = {} & \int \frac{\mathrm{d}k_1^+\,\mathrm{d}^{d-2}\boldsymbol{k}_1}{(2\pi)^{d-1}} \frac{\mathrm{d}k_2^+\,\mathrm{d}^{d-2}\boldsymbol{k}_2}{(2\pi)^{d-1}} \frac{\mathrm{d}^{d-2}\boldsymbol{r}}{(2\pi)^{d-2}} \\ & \times \int \left[\prod_j \frac{\mathrm{d}\ell_j^-\,\mathrm{d}^{d-2}\boldsymbol{\ell}_j}{(2\pi)^{d-1}}\right] \sum_V \sum_{F_A\in\mathcal{A}(V)} \int \frac{\mathrm{d}k_1^-}{2\pi} \frac{\mathrm{d}k_2^-}{2\pi} \frac{\mathrm{d}r^-}{2\pi} A_{F_A}(k_1, k_2, r, \tilde{\ell}_j)\big|_{r^+=0} \\ & \times \sum_{F_R\in\mathcal{R}(V)} \int \left[\prod_j \frac{\mathrm{d}\ell_j^+}{2\pi}\right] R_{F_R}(k_1^+, \boldsymbol{k}_1, k_2^+, \boldsymbol{k}_2, -\boldsymbol{r}, \ell_j)\,, \end{aligned} \tag{9.4}$$

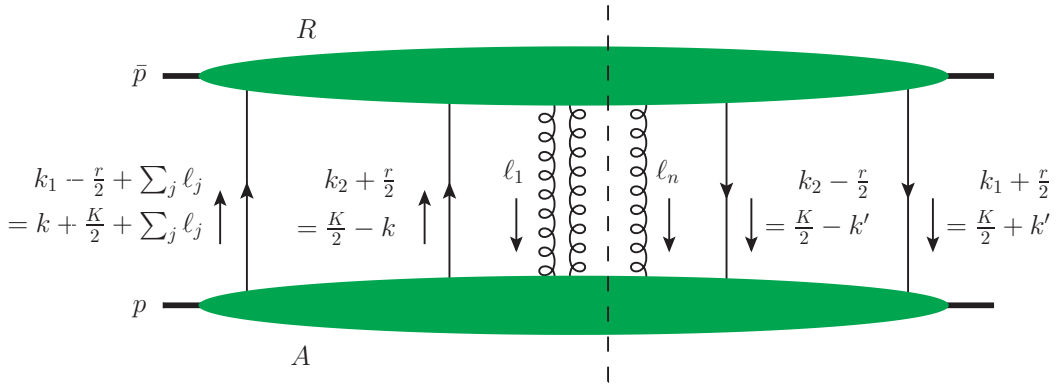

Figure 9.1.: Partitioning of a leading graph and region in double Drell-Yan production into a collinear factor A and the remainder R. There are exactly four physically polarized partons joining A to H, namely the quark lines.

where A_{F_A} (R_{F_R}) denotes A (R) with the cut F_A (F_R). Note that A is defined to include the propagators for the external collinear lines with momenta $k_1 - r/2 + \sum_j \ell_j$, $k_2 + r/2$, $k_2 - r/2$ and $k_1 + r/2$. On the other hand it is defined to exclude the propagators for the external soft lines with momenta ℓ_j, which are part of R. As is shown in [13, chapter 4.3.4], the factor in the last line of (9.4) is independent of the partitioning V. The sum over V then only applies to A and gives

$$\sum_V \sum_{F_A \in \mathcal{A}(V)} \int \frac{\mathrm{d}k_1^-}{2\pi} \frac{\mathrm{d}k_2^-}{2\pi} \frac{\mathrm{d}r^-}{2\pi} A_{F_A}(k_1, k_2, r, \tilde{\ell}_j) = \sum_{\text{all } F_A} \int \frac{\mathrm{d}k_1^-}{2\pi} \frac{\mathrm{d}k_2^-}{2\pi} \frac{\mathrm{d}r^-}{2\pi} A_{F_A}(k_1, k_2, r, \tilde{\ell}_j)\,. \tag{9.5}$$

This means, that one only has to consider the sum over all cuts of the collinear factor A. As it will turn out, there are no pinched poles in the Glauber region in this factor. As already mentioned, when considering A in LCPT, we treat the soft lines ℓ_j to be external, with an external momentum ℓ_j being injected at the vertex where the soft line couples to a collinear line. By contrast, we do include the propagators of the collinear lines, so we treat these as lines inside A that terminate on a two-point vertex H_i, whose other line is an external line that carries the collinear momentum away (and whose associated coupling constant is unity). These vertices participate in the light-cone time ordering in the same way as the other vertices in A. We call them "hard vertices" because in the graph for the physical process they are replaced by vertices at which the collinear lines enter the hard scattering.

In chapter 4.3.2 of [13] it is shown, that after a change of variables to k, k' and K as given in figure 9.1 and after an integral over the minus-momenta of k and k', one can attach the collinear lines to a common hard vertex H in the amplitude and to a common hard vertex H' in the conjugate. The result is shown in figure 9.2. The rest of the proof is then completely analog to the single Drell-Yan case. For a given time ordering T we now partition the states ξ according to whether they are before the hard vertex H in the amplitude, before the hard vertex H' in the conjugate amplitude, or in the "final state" between H or H' and the cut F_A. States before H go into the factor I_T, those before H' into I'_T, and those in the final

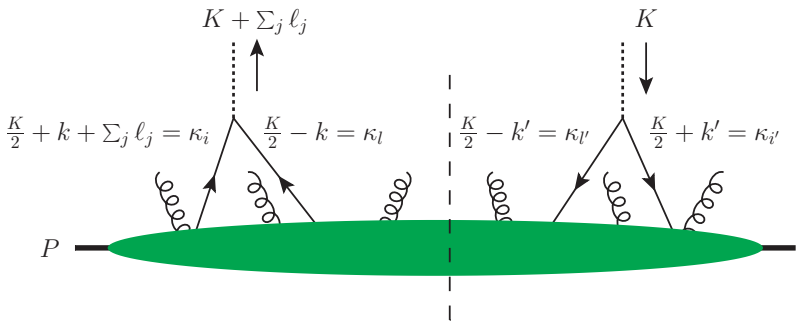

Figure 9.2.: LCPT picture for the collinear factor A in the double Drell-Yan process, with collinear lines in the amplitude or its conjugate attached together at three-point vertices. The dotted lines are external to the graph and carry away the combined momenta of the collinear partons, as explained in the text.

state into F_T:

$$\int \frac{\mathrm{d}K^-}{2\pi} A_{F_A}(K,\tilde{\ell}_j) = \int \frac{\mathrm{d}K^-}{2\pi} \sum_T I_T(\tilde{\ell}_j)\, F_T(K,\tilde{\ell}_j)\, I'_T(\tilde{\ell}_j) \times \text{numerator}\,. \tag{9.6}$$

The explicit expression for the "numerator" is not relevant for the following discussion. The individual factors in (9.6) read

$$I_T(\tilde{\ell}_j) = \prod_{\substack{\text{states } \xi \\ \xi<H}} \frac{1}{p^- + \sum\limits_{\substack{\text{vertices} j \\ j<\xi}} \ell_j^- - \sum\limits_{\substack{\text{lines } L \\ L\in\xi}} \kappa_L^- + i\epsilon}\,, \tag{9.7}$$

$$\begin{aligned} F_T(k,\tilde{\ell}_j) = {} & \prod_{\substack{\text{states } \xi \\ H<\xi<F_A}} \frac{1}{p^- - K^- - \sum\limits_{\substack{\text{vertices } j \\ j>\xi}} \ell_j^- - \sum\limits_{\substack{\text{lines } L \\ L\in\xi}} \kappa_L^- + i\epsilon} \\ & \times 2\pi\delta\Bigg(p^- - K^- - \sum_{\substack{\text{vertices } j \\ j>F_A}} \ell_j^- - \sum_{\substack{\text{lines } L \\ L\in F_A}} \kappa_L^-\Bigg) \\ & \times \prod_{\substack{\text{states } \xi \\ F_A<\xi<H'}} \frac{1}{p^- - K^- - \sum\limits_{\substack{\text{vertices } j \\ j>\xi}} \ell_j^- - \sum\limits_{\substack{\text{lines } L \\ L\in\xi}} \kappa_L^- - i\epsilon}\,, \end{aligned} \tag{9.8}$$

$$I'_T(\tilde{\ell}_j) = \prod_{\substack{\text{states } \xi \\ H'<\xi}} \frac{1}{p^- - \sum\limits_{\substack{\text{vertices } j \\ j>\xi}} \ell_j^- - \sum\limits_{\substack{\text{lines } L \\ L\in\xi}} \kappa_L^- - i\epsilon}\,, \tag{9.9}$$

where p is the proton momentum. One can immediately see that I_T and I'_T only have poles in the lower and upper half plane, respectively, and therefore these don't pose a problem.

Looking at F_T, however, there seem to be pinched ℓ_j^- poles. Abbreviating

$$D_f = \sum_{\substack{\text{lines } L \\ L \in \xi_f}} \kappa_L^- \,. \tag{9.10}$$

one can show (cf. [13, chapter 4.3.1]) that for the sum over cuts of F_T it holds

$$\sum_{F_A} F_T(K, \tilde{\ell}_j) = i \left[\prod_{f=1}^{N} \frac{1}{p^- - K^- - \sum\limits_{j>f} \ell_j^- - D_f + i\epsilon} - \prod_{f=1}^{N} \frac{1}{p^- - K^- - \sum\limits_{j>f} \ell_j^- - D_f - i\epsilon} \right], \tag{9.11}$$

where N is the number of states in F_T. Note that (9.11) is essentially the Cutkosky identity [23] in the LCPT formalism. Integrating (9.11) over K^-, it is easy to see that the integral vanishes if there is more than one state in F_T. For the case of exactly one state we simply get unity. Therefore the pinched poles in ℓ_j^- are now gone and one can deform the integration contour as needed for establishing factorization.
We conclude this section by noting that we have not treated additional longitudinally polarized gluon attachments between A and H, which one has to allow for to obtain a really complete proof. This additional complication is treated in [13, chapter 4.3.3].

10. Conclusion

A theoretical sound understanding of multiparton scattering in general and double parton scattering in particular may very well be needed if the search for new physics is to succeed, and this will require a substantial extension of calculational techniques. Among the most important of these techniques are the QCD factorization theorems, which allow for a precise calculation of cross sections. There has been promising progress in the extension of factorization techniques to multiparton scattering in the last few years for processes without color in the final state [9, 11, 13], while for processes with color in both the initial and final state there are severe problems even for single parton scattering [12].

In this thesis, we have revisited some of the building blocks for a theory of double parton interactions that have been developed already some years ago [9, 11]. Among these are double parton distributions, which exhibit a rich color and spin structure. For perturbatively large transverse momenta, we have calculated splitting contributions to these double parton distributions. These splitting contributions lead to a double counting between single and double parton scattering in graphs like figure 7.5 in QCD. The question how to seperate single and double parton scattering consistently has been discussed for a long time [9, 30, 31, 32, 33]. This is also one of the most important obstacles for establishing a complete proof of factorization of double Drell-Yan to all orders.

A proof of factorization always has to take corrections due to gluon exchange into account, and we have reviewed the analysis of one such coupling for the double Drell-Yan process in quite some detail [9]. In particular, we have discussed how the leading regions can be determined and how they lead to a modification of the factorized form of the cross section in tranverse momentum dependent factorization. We have used these results derived in [9] to then extend a new definition of TMDs involving extra soft factors proposed by Collins [5] to double TMDs. We have calculated several $\mathcal{O}(\alpha_S)$ corrections to these new dTMDs in a toy model and have thereby exhibited some unique features of this formalism.

One of the central parts of each factorization proof is to show that contributions from the Glauber region are either not present or cancel in the sum over all diagrams. We have shown that there is no such contribution for one extra gluon exchange in the double Drell-Yan process. We have shown this explicitly for two different models and have given an argument why this is always the case. In the last part of the thesis we have briefly reviewed the proof of cancellation of Glauber gluons to all orders [13]. Both proofs generalise to other double scattering processes with colorless particles in the final state and also to higher multiparton scattering.

Although the building blocks for establishing factorization of double Drell-Yan are provided and the cancellation of Glauber gluon exchange has been proven to all orders, there are still some gaps that prohibit a complete proof of all order factorization. One of these is the dou-

ble counting problem between single and double parton scattering already mentioned above. Another one is that the generalized Ward identities that are needed for both factorizing the collinear gluons from the hard part and for factorizing soft gluons from the collinear factors at an arbitrary order in the strong coupling have – to the best of our knowledge – not been established yet. So there is still some work to be done before arriving at a real proof of factorization of double Drell-Yan to all orders.

As we have seen, double-Drell-Yan serves as a perfect testing ground for the development of the theory due to its clean final state. The value for experimental studies is, however, rather limited due to the comparatively low rates of double Drell-Yan production. One of the long term goals surely is to extend the theory of multiparton scattering to more relevant processes, such as the production of double dijets. Before this can be done, however, one has to go back to single parton scattering and study the factorization properties of these processes within that framework first.

A. Feynman rules of QCD

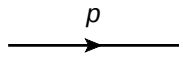

$$iS_F = i\frac{\not{p} + m}{p^2 - m^2 + i\epsilon}$$

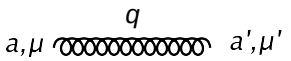

$$iG^{aa'}_{\mu\mu'} = -i\delta^{aa'}\frac{g_{\mu\mu'} - \dfrac{(1-c)q_\mu q_{\mu'}}{c(q^2+i\epsilon)}}{q^2+i\epsilon}$$

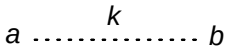

$$iD_F^{ab} = i\delta^{ab}\frac{1}{k^2+i\epsilon}$$

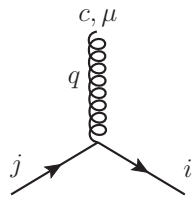

$$i\Gamma^\mu = -ig\gamma^\mu\left(t^c\right)_{ij}$$

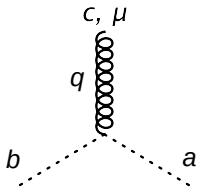

$$i\Gamma^\mu_{\text{ghost}} = -igf^{abc}q^\mu$$

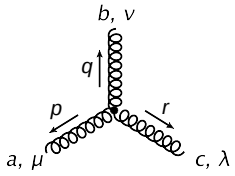

$$i\Gamma^{\mu\nu\lambda} = -gf^{abc}[g^{\nu\lambda}(r^\mu - q^\mu) + g^{\mu\lambda}(p^\nu - r^\nu) + g^{\nu\mu}(q^\lambda - q^\lambda)]$$

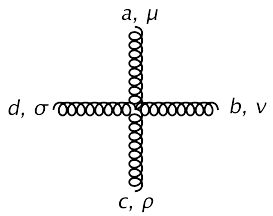

$$i\Gamma^{\mu\nu\rho\sigma} = -ig^2\left[f^{abe}f^{cde}(g_{\nu\sigma}g_{\rho\mu} - g_{\mu\sigma}g_{\rho\nu}) + f^{ace}f^{bed}(g_{\mu\sigma}g_{\rho\nu} - g_{\mu\nu}g_{\sigma\rho}) + f^{ade}f^{bce}(g_{\mu\nu}g_{\rho\sigma} - g_{\mu\rho}g_{\sigma\nu})\right]$$

B. SU(N) algebra

B.1. Identities and relations

In the fundamental representation of SU(N), the generators of SU(N) are represented by traceless, hermitian $N \times N$ matrices and satisify the commutation and anticommutation relations

$$\begin{aligned}[t^a, t^b] &= \frac{1}{N}\delta^{ab} + d^{abc}t^c \\ \{t^a, t^b\} &= if^{abc}t^c \,,\end{aligned} \tag{B.1}$$

where the tensors d^{abc} and f^{abc} are symmetric or antisymmetric in all indices, respectively, and the sum over equal indices $c = 1, \ldots, N^2 - 1$ is tacitly assumed. A product of two generators can be decomposed in the following way:

$$(t^a t^b)_{ij} = \frac{1}{2N}\delta^{ab}\delta_{ij} + \frac{1}{2}(if^{abc} + d^{abc})t^c_{ij} \,. \tag{B.2}$$

Due to $f^{aac} = 0$ and $d^{aac} = 0$, we then get

$$(t^a t^a)_{ij} = \frac{\delta^{aa}}{2N}\delta_{ij} = \frac{N^2 - 1}{2N}\delta_{ij} = C_F\delta_{ij} \,. \tag{B.3}$$

In the adjoint representation, the generators are represented by $(N^2 - 1) \times (N^2 - 1)$ matrices, which are definded by the structure constants f^{abc} via

$$(t^a)_{bc} = -if^{abc} \,. \tag{B.4}$$

B.2. Calculation of color factors in splitting diagrams

We will now give the explicit calculation of the color factors of the splitting contributions to dTMDs in chapter 5 and start with the splitting of a gluon into a quark-antiquark pair. The color factors are

$$\begin{aligned}{}^1F_{a_1,\bar{a}_2}(x_i, \boldsymbol{k}_i, \boldsymbol{r})\Big|_{g\to q\bar{q}} &\sim (t^a)_{ij}(t^{a'})_{j'i'}\delta_{ii'}\delta_{jj'} = \frac{1}{2}\delta^{aa'} \,, \\ {}^8F_{a_1,\bar{a}_2}(x_i, \boldsymbol{k}_i, \boldsymbol{r})\Big|_{g\to q\bar{q}} &\sim \frac{2N}{\sqrt{N^2-1}}(t^a)_{ij}(t^{a'})_{j'i'}(t^c)_{i'i}(t^c)_{jj'} = -\frac{1}{2\sqrt{N^2-1}}\delta^{aa'} \,,\end{aligned} \tag{B.5}$$

where a and a' are the color indices corresponding to the gluon on the l.h.s. and the r.h.s. of the cut, respectively. The color factors for the interference distributions are the same. We

now turn to the splitting of a quark into a quark and a gluon. The color factors are

$$
\begin{aligned}
{}^{1}F_{a_1,a_2}\Big|_{q\to gq} &\sim (t^a)_{jk}(t^{a'})_{k'j'}\delta^{aa'}\delta_{jj'} = C_F\delta_{kk'}\,,\\
{}^{A}F_{a_1,a_2}\Big|_{q\to gq} &\sim (t^a)_{jk}(t^{a'})_{k'j'}\sqrt{2}if^{aa'c}t^c_{j'j} = \frac{(N^2-1)\sqrt{N^2-4}}{2N\sqrt{2}}\delta_{kk'}\,,\\
{}^{S}F_{a_1,a_2}\Big|_{q\to gq} &\sim (t^a)_{jk}(t^{a'})_{k'j'}\sqrt{\frac{2N^2}{N^2-4}}d^{aa'c}(t^c)_{j'j} = -\frac{N^2-1}{2\sqrt{2}}\delta_{kk'}\,.
\end{aligned}
\tag{B.6}
$$

The last color factors we need to calculate are for the splitting of a gluon into two gluons. The singlet, symmetric octet and antisymmetric octet contributions can be calculated for any number of colors and read

$$
\begin{aligned}
{}^{1}F_{a_1,a_2}\Big|_{g\to gg} &\sim f^{abc}f^{a'b'c'}\delta^{aa'}\delta^{bb'} = N\delta^{cc'}\,,\\
{}^{A}F_{a_1,a_2}\Big|_{g\to gg} &\sim -f^{abc}f^{a'b'c'}\frac{\sqrt{N^2-1}}{N}f^{aa'e}f^{bb'e} = -\frac{1}{2}N\sqrt{N^2-1}\delta^{cc'}\,,\\
{}^{S}F_{a_1,a_2}\Big|_{g\to gg} &\sim f^{abc}f^{a'b'c'}\frac{N\sqrt{N^2-1}}{N^2-4}d^{aa'e}d^{bb'e} = \frac{1}{2}N\sqrt{N^2-1}\delta^{cc'}\,.
\end{aligned}
\tag{B.7}
$$

For SU(3) the color factors for the higher color representations are

$$
\begin{aligned}
{}^{10}F_{a_1,a_2}\Big|_{g\to gg} &\sim f^{abc}f^{a'b'c'}\frac{2}{\sqrt{10}}t^{aa',bb'}_{\overline{10}} = 0\,,\\
{}^{\overline{10}}F_{a_1,a_2}\Big|_{g\to gg} &\sim f^{abc}f^{a'b'c'}\frac{2}{\sqrt{10}}t^{aa',bb'}_{10} = 0\,,\\
{}^{27}F_{a_1,a_2}\Big|_{g\to gg} &\sim f^{abc}f^{a'b'c'}\frac{4}{\sqrt{27}}t^{aa',bb'}_{27} = -3\sqrt{3}\delta^{cc'}\,,
\end{aligned}
\tag{B.8}
$$

where the color projectors for 10, $\overline{10}$ and 27 are given by [25]

$$
\begin{aligned}
t^{aa',bb'}_{10} &= \delta^{ab}\delta^{a'b'} - \delta^{ab'}\delta^{a'b} - \tfrac{2}{3}f^{aa'c}f^{bb'c} - i(d^{abc}f^{a'b'c} + f^{abc}d^{a'b'c})\,,\\
t^{aa',bb'}_{\overline{10}} &= \delta^{ab}\delta^{a'b'} - \delta^{ab'}\delta^{a'b} - \tfrac{2}{3}f^{aa'c}f^{bb'c} + i(d^{abc}f^{a'b'c} + f^{abc}d^{a'b'c})\,,\\
t^{aa',bb'}_{27} &= \delta^{ab}\delta^{a'b'} + \delta^{ab'}\delta^{a'b} - \tfrac{1}{4}\delta^{aa'}\delta^{bb'} - \frac{6}{5}d^{aa'c}d^{bb'c}\,.
\end{aligned}
\tag{B.9}
$$

C. Feynman parameterization

In typical pQCD calculations, there are often several denominators depending on the gluon momentum. The method of Feynman parameterization is a convenient way to combine all of these denominators into one. The "standard" form of the Feynman parameterization is given by

$$\begin{aligned}\frac{1}{A_1^{\alpha_1}\cdots A_m^{\alpha_m}} &= \frac{\Gamma(\alpha_1+\ldots+\alpha_m)}{\Gamma(\alpha_1)\cdots\Gamma(\alpha_m)}\int_0^1 du_1\int_0^1 du_2\cdots\int_0^1 du_m\times \\ &\times\frac{u_1^{\alpha_1-1}u_2^{\alpha_2-1}\cdots u_m^{\alpha_m-1}\delta(1-\sum_{i=1}^m u_m)}{[u_1A_1+u_2A_2+\cdots+u_mA_m]^{\alpha_1+\alpha_2+\cdots+\alpha_m}}\ . \end{aligned} \tag{C.1}$$

D. Evaluation of Feynman integrals in light-cone coordinates

As mentioned in section 7.3.3 the evaluation of Feynman integrals in light-cone coordinates has to be done with some care. E.g. look at the integral

$$\int d^4\ell \, \frac{1}{[\ell_0^2 - \vec{\ell}^2 - M^2 + i\varepsilon]^6} = \int d\ell^+ \int d\ell^- \int d^2\boldsymbol{\ell} \, \frac{1}{[2\ell^+\ell^- - \boldsymbol{\ell}^2 - M^2 + i\varepsilon]^6} \, . \tag{D.1}$$

The integral on the l.h.s. of eq. (D.1) is obviously non-zero while a naive application of Cauchy's theorem to perform e.g. the ℓ^+ integration on the r.h.s. would yield zero. This seeming paradox is resolved by the fact that Cauchy's theorem is not applicable in this case, because for $\ell^- = 0$ the ℓ^+ integral is linearly divergent. This issue has been encountered in the past and in [56, 57] it was shown that the proper formula for such integrals reads

$$\int d\ell^+ \, \frac{1}{[2\ell^+\ell^- - M^2 + i\varepsilon]^n} = i\pi \frac{\delta(\ell^-)}{[n-1][M^2 - i\varepsilon]^{n-1}} \, . \tag{D.2}$$

This formula and the methods used to derive it can also be used to calculate the integral

$$I = \int \frac{d\ell^-}{[\ell^- - i\eta']} \int \frac{d\ell^+}{[\ell^+ + i\eta]} \frac{1}{[2\ell^+(\ell^- + a^-) + 2a^+\ell^- + B + i\varepsilon]^4} \tag{D.3}$$

that we have encountered in section 7.3.3. The first step is to shift integration variables according to $\ell^- \to \ell^- - a^-$, $\ell^+ \to \ell^+ - a^+$ and we get

$$I = \int \frac{d\ell^-}{[\ell^- - a^- - i\eta']} \int \frac{d\ell^+}{[\ell^+ - a^+ + i\eta]} \frac{1}{[2\ell^+\ell^- + B - 2a^+a^- + i\varepsilon]^4} \, . \tag{D.4}$$

The next step is partial fractioning with regards to ℓ^+, which after abbreviating $C = B - 2a^+a^-$ gives

$$I = \int d\ell^+ \, d\ell^- \frac{1}{[\ell^- - a^- - i\eta']} \left[-\sum_{n=1}^{4} \frac{2\ell^-}{[2\ell^+\ell^- + C + i\varepsilon]^n [2\ell^- a^+ + C + i\varepsilon]^{5-n}} + \frac{1}{[\ell^+ - a^+ + i\eta][2\ell^- a^+ + C + i\varepsilon]^4} \right] . \tag{D.5}$$

We first consider the terms with $n \geq 2$ in the sum in the first line of (D.5). We have to evaluate the integral

$$\begin{aligned}
&\int d\ell^+ \frac{2\ell^-}{[2\ell^+\ell^- + C + i\varepsilon]^n} = \lim_{\Lambda,\Lambda'\to\infty} \int_{-\Lambda'}^{\Lambda} d\ell^+ \frac{2\ell^-}{[2\ell^+\ell^- + C + i\varepsilon]^n} \\
&= -\frac{1}{n-1} \lim_{\Lambda,\Lambda'\to\infty} \left[\frac{1}{[2\Lambda\ell^- + C + i\varepsilon]^{n-1}} - \frac{1}{[-2\Lambda'\ell^- + C + i\varepsilon]^{n-1}} \right] \\
&= -\frac{1}{n-1} \lim_{\Lambda,\Lambda'\to\infty} \frac{d^{n-2}}{dC^{n-2}} (-1)^{n-2} \frac{1}{(n-2)!} \left[\frac{1}{[2\Lambda\ell^- + C + i\varepsilon]} - \frac{1}{[-2\Lambda'\ell^- + C + i\varepsilon]} \right] \\
&= -\frac{1}{n-1} \lim_{\Lambda,\Lambda'\to\infty} \frac{d^{n-2}}{dC^{n-2}} (-1)^{n-2} \frac{1}{(n-2)!} \frac{\ell^-}{[C + i\varepsilon]} \left[\frac{2\Lambda}{[2\Lambda\ell^- + C + i\varepsilon]} - \frac{2\Lambda'}{[2\Lambda'\ell^- - C - i\varepsilon]} \right] \\
&= -\frac{1}{n-1} \frac{\ell^-}{[C + i\varepsilon]^{n-1}} \left[\frac{1}{[\ell^- + i\varepsilon]} - \frac{1}{[\ell^- - i\varepsilon]} \right] \\
&= \frac{2\pi i}{n-1} \frac{\ell^-}{[C + i\varepsilon]^{n-1}} \delta(\ell^-) \,,
\end{aligned} \tag{D.6}$$

where we have used the identities

$$\begin{aligned}
\frac{1}{[\ell^- \pm i\varepsilon]} &= \mathrm{PV}\left(\frac{1}{\ell^-}\right) \mp i\pi\delta(\ell^-) \\
\left[\frac{1}{[2\Lambda\ell^- + C + i\varepsilon]} - \frac{1}{[-2\Lambda'\ell^- + C + i\varepsilon]} \right] &= \frac{\ell^-}{[C + i\varepsilon]} \left[\frac{2\Lambda}{[2\Lambda\ell^- + C + i\varepsilon]} - \frac{2\Lambda'}{[2\Lambda'\ell^- - C - i\varepsilon]} \right] .
\end{aligned} \tag{D.7}$$

From the last line of eq. (D.6) it can clearly be seen that the integral over ℓ^- vanishes for $n \geq 2$ and we therefore only have two terms left in eq. (D.5). The integral now reads

$$\begin{aligned}
I = \int \frac{d\ell^-}{[\ell^- - a^- - i\eta']} &\lim_{\Lambda,\Lambda'\to\infty} \int_{-\Lambda'}^{\Lambda} d\ell^+ \frac{1}{[2\ell^- a^+ + C + i\varepsilon]^4} \\
&\times \left[\frac{1}{[\ell^+ - a^+ + i\eta]} - \frac{2\ell^-}{[2\ell^+\ell^- + C + i\varepsilon]} \right] \\
= \int \frac{d\ell^-}{[\ell^- - a^- - i\eta']} &\frac{1}{[2\ell^- a^+ + C + i\varepsilon]^4} \lim_{\Lambda,\Lambda'\to\infty} \\
\times \left[\log(\Lambda - a^+ + i\eta) - \log(-\Lambda' - a^+ + i\eta) - \log(2\Lambda\ell^- + C + i\varepsilon) + \log(-2\Lambda'\ell^- + C + i\varepsilon) \right]
\end{aligned} \tag{D.8}$$

For $\ell^- > 0$ this is zero. For $\ell^- < 0$ we get an imaginary part of $-2\pi i$ from the logarithms and obtain

$$I = -2\pi i \int_{-\infty}^{0} d\ell^- \frac{1}{[\ell^- - a^- - i\eta'][2\ell^- a^+ + C + i\varepsilon]} \,. \tag{D.9}$$

After shifting $\ell^- \to \ell^- + a^-$ this reproduces the result we got in section 7.3.3 by using Cauchy's theorem. This is due to the fact that ℓ^- and $\ell^- + a^-$ can never go to zero at the same time in (D.3) for non-zero a^- and this is enough to resolve the potential issue at $\ell^- = -a^-$. Cauchy's theorem is, however, not applicable if one has additional powers of ℓ^+

and/or ℓ^- in the numerator. The method used above continues to work in this case and we have derived the relevant master intergrals, which we give in the following. When we have one additional factor of ℓ^- or ℓ^+ in the numerator, the relevant integrals read

$$\begin{aligned} I_1 &= \int d\ell^- \int d\ell^+ \, \frac{1}{[\ell^+ - a^+ + i\eta][2\ell^+\ell^- + C + i\varepsilon]^4} \\ &= \frac{1}{3}\pi i \frac{1}{[-a^+ + i\eta][C + i\varepsilon]^3} \end{aligned} \tag{D.10}$$

$$\begin{aligned} I_2 &= \int d\ell^+ \int \ell^+ \, \frac{1}{[\ell^- - a^- - i\eta'][2\ell^+\ell^- + C + i\varepsilon]^4} \\ &= \frac{1}{3}\pi i \frac{1}{[-a^- - i\eta'][C + i\varepsilon]^3} \, . \end{aligned} \tag{D.11}$$

For an additional factor of $(\ell^+\ell^-)^2$ we get

$$\begin{aligned} I_3 &= \int d\ell^- \int d\ell^+ \frac{\ell^+\ell^-}{[2\ell^+\ell^- + C + i\varepsilon]^4} \\ &= -\frac{1}{12}\pi i \frac{1}{[C + i\varepsilon]^2} \, . \end{aligned} \tag{D.12}$$

All other possible combinations of additional factors of ℓ^+ or ℓ^- are zero due to (D.2). Using these master integrals, we have checked that all contributions given by the additional terms in the numerator of (7.13) are power suppressed, as we expected from our power counting arguments.

Acknowledgements

First of all I want to thank my supervisor Prof. Dr. Andreas Schäfer for giving me the opportunity of writing this thesis and for all his patient and valuable support througout the years. I am indebted to Dr. Markus Diehl for the pleasant cooperation, numerous valuable discussions and helpful support in the course of writing this thesis. I would also like to thank Monika Maschek for her kind support.
I gratefully acknowledge discussions with Jonathan Gaunt, Tomas Kasemets, Philipp Wein, Michael Knödlseder, Michael Gruber and Peter Plößl. Special thanks go to Philipp Wein and Michael Gruber for their careful proofreading of the draft.
Some of the calculations for this work have been done using FORM [29] and the figures were produced with JaxoDraw [58]. This work has been supported by BMBF.

Bibliography

[1] ATLAS Collaboration, G. Aad et al., Phys. Lett. **B716** (2012) 1, [arXiv:1207.7214].

[2] CMS Collaboration, S. Chatrchyan et al., Phys. Lett. **B716** (2012) 30, [arXiv:1207.7235].

[3] J.C. Collins, D.E. Soper and G.F. Sterman, Adv. Ser. Direct. High Energy Phys. **5** (1989) 1, [hep-ph/0409313].

[4] G.F. Sterman (1996), [hep-ph/9606312].

[5] J.C. Collins, The Foundations of Perturbative QCD, Cambridge University Press, Cambridge (2011).

[6] CDF Collaboration, F. Abe et al., Phys. Rev. **D56** (1997) 3811.

[7] CMS Collaboration, P. Bartalini and L. Fano (2011), [arXiv:1103.6201 [hep-ex]].

[8] C.H. Kom, A. Kulesza and W.J. Stirling, [arXiv:1109.0309 [hep-ph]].

[9] M. Diehl, D. Ostermeier and A. Schäfer, JHEP **03** (2012) 089, [arXiv:1111.0910].

[10] S. Plätzer and M. Diehl (ed.), DOI: 10.3204/DESY-PROC-2012-03 (2012).

[11] A.V. Manohar and W.J. Waalewijn, Phys. Rev. **D85** (2012) 114009, [arXiv:1202.3794 [hep-ph]].

[12] Ted C. Rogers, Piet J. Mulders Phys. Rev. **D 81**: 094006 (2010), [hep-ph/1001.2977].

[13] M. Diehl, J.R. Gaunt, D. Ostermeier, P. Plößl and A. Schäfer, JHEP **01** (2016) 076, [hep-ph/1510.08696].

[14] M.E. Peskin and D.V. Schroeder, *An Introduction to Quantum Field Theory*, Addison-Wesley, Reading (1995).

[15] S. Weinberg, *The Quantum Theory Of Fields*, Cambridge University Press, Cambridge (2005).

[16] A. Schäfer, Lecture on Quantum Chromodynamics.

[17] A.A. Slavnov, Theor. Math. Phys. **10** (1972) 99.

[18] J.C. Taylor, Nucl. Phys. **B33** (1971) 436.

[19] C. Becchi, A. Rouet and R. Stora, Commun. Math. Phys. **42** (1975) 127.

[20] I.V. Tyutin (2008). [arXiv:0812.0580].

[21] W.A. Bardeen, A.J. Buras, D.W. Duke and T. Muta, Phys. Rev. **D18** (1978) 3998.

[22] Particle Data Group Collaboration, K.A. Olive et al., Chin. Phys. **C38** (2014) 090001.

[23] R.E. Cutkosky, J. Math. Phys. **1** (1960) 429.

[24] N. Paver and D. Treleani, Nuovo Cim. **A70** (1982) 215.

[25] M. Mekhfi, Phys. Rev. **D32** (1985) 2380.

[26] R.D. Tangerman and P.J. Mulders, Phys. Rev. **D51** (1995) 3357 [hep-ph/9403227].

[27] P.J. Mulders and J. Rodrigues, Phys. Rev. **D63** (2001) 094021, [hep-ph/0009343].

[28] C.H. Kom, A. Kulesza and W.J. Stirling, Phys. Rev. Lett. **107** (2011) 082002, [arXiv:1105.4186].

[29] J.A.M. Vermaseren (2000), [math-ph/0010025].

[30] J.R. Gaunt and W.J. Stirling (2012), [arXiv:1202.3056 [hep-ph]].

[31] J.R. Gaunt and W.J. Stirling JHEP **06** (2011) 048, [arXiv:1103.1888 [hep-ph]]

[32] M.G. Ryskin and A.M. Snigirev, Phys. Rev. **D83** (2011) 114047, [arXiv:1103.3495].

[33] M.G. Ryskin and A.M. Snigirev, Phys. Rev. **D86** (2012) 014018, [arXiv:1203.2330].

[34] M. Diehl, private communication.

[35] G.F. Sterman, Phys. Rev. **D17** (1978) 2773.

[36] S.B. Libby, G.F. Sterman, Phys. Rev. D **18** (1978) 4737.

[37] A.V. Belitsky, X. Ji and F. Yuan, Nucl. Phys. **B656** (2003) 165, [hep-ph/0208038].

[38] D. Boer, P.J. Mulders and F. Pijlman, Nucl. Phys. **B667** (2003) 201, [hep-ph/0303034].

[39] J.C. Collins, D.E. Soper and G. Sterman, Nuclear Physics **B223** (1983) 381.

[40] X. Ji, J.P. Ma and F. Juan, [arXiv:hep-ph/0404183].

[41] J.C. Collins and A. Metz, Phys. Rev. Lett. **93** (2004) 252001, [hep-ph/0408249].

[42] M.G. Echevarria, A. Idilbi and I. Scimemi JHEP **07** (2012) 002, [arXiv:1111.4996 [hep-ph]].

[43] A. Bacchetta, D. Boer, M. Diehl and P.J. Mulders, JHEP **08** (2008) 023, [arXiv:0803.0227].

[44] J.C. Collins, D.E. Soper and G.F. Sterman, Nucl. Phys. **B250** (1985) 199.

[45] J.C. Collins and D.E. Soper, Nucl. Phys. **B193** (1981) 381.

[46] R. Basu, A.J. Ramalho and G. Sterman, Nucl. Phys. **B244** (1984) 221.

[47] M. Srednicki, Quantum Field Theory, Cambridge University Press, Cambridge (2007).

[48] J.R. Gaunt, JHEP **07** (2014) 110, [arXiv:1405.2080 [hep-ph]].

[49] P.V. Landshoff, J.C. Polkinghorne, Phys. Rev. **D18** (1978) 3344.

[50] P. Plößl, Master's Thesis: Factorization for double Drell-Yan (2015).

[51] J.C. Collins, D.E. Soper and G. Sterman, Nucl. Phys. **B308** (1988) 833.

[52] G. Sterman, An Introduction to Quantum Field Theory, Cambridge University Press, Cambridge (1993).

[53] N.E. Ligterink and B.L.G. Bakker, Phys. Rev. **D52** (1995) 5954, [hep-ph/9412315].

[54] J.B. Kogut and D.E. Soper, Phys. Rev. **D1** (1970) 2901.

[55] S.J. Brodsky and G.P. Lepage, Adv. Ser. Direct. High Energy Phys. **5** (1989) 93.

[56] T.-M. Yan, Phys. Rev. **D7** (1973) 1780.

[57] T. Heinzl (2003), [hep-th/0310165].

[58] D. Binosi and L. Theussl, Comput. Phys. Commun. **161** (2004) 76, [hep-ph/0309015].